DETERMINATION OF HETEROGENEOUS PARAMETERS BY THE NEUTRON WAVE TECHNIQUE

By
EMILE ANTHONY BERNARD

UNIVERSITY OF FLORIDA
1968

To "B^4"

ACKNOWLEDGMENTS

The author wishes to express his thanks and appreciation to his supervisory committee, especially to its chairman, Dr. M. J. Ohanian, for their assistance and advice. Special thanks also go to Dr. R. B. Perez who was chairman prior to his departure from the University. Through his initial guidance and continued interest and assistance he has remained closely associated with the work of this dissertation. Appreciation is also extended to the Department of Nuclear Engineering Sciences and to the U. S. Atomic Energy Commission for their financial support of this dissertation.

Many other individuals rendered their time and services in support of this dissertation and the author wishes to give recognition to several of them. George Fogle gave invaluable assistance in the electronic and technical problems encountered with the experimental equipment. José Aldeanueva, Benny DuBois, Changmu Kang and Daniel Meade were constantly available to assist in the data acquisition. The competent assistance of Jim Burgess was very important in the development of the computer programs used for data analysis. Mrs. Edna Roberts was very helpful in the typing of the final manuscript.

The author wishes to thank especially his wife, Betty, who was always willing to do everything she could and assisted in many ways in the preparation of this dissertation.

TABLE OF CONTENTS

TABLE OF CONTENTS (cont'd)

LIST OF TABLES

LIST OF FIGURES

KEY TO SYMBOLS

A . . . . THERMAL NEUTRON ABSORPTION TERM

B_n . . . TRANSVERSE BUCKLING OF nth SPATIAL MODE

c_n . . . EXPANSION COEFFICIENT OF THERMAL NEUTRON FLUX AT $z = 0$

D . . . DIFFUSION COEFFICIENT

J_o . . . ZERO ORDER BESSEL FUNCTION

L^2 . . . DIFFUSION LENGTH SQUARED

L_s . . . SLOWING DOWN TIME FOR FISSION NEUTRONS

N . . . NORMALIZATION CONSTANT

P_n . . . EXPANSION COEFFICIENT OF RHO SQUARED IN POWER SERIES OF (Ls)

p . . . RESONANCE ESCAPE PROBABILITY

q . . . SLOWING DOWN DENSITY

R . . . EXTRAPOLATED RADIUS OF EXPERIMENTAL ASSEMBLY

r . . . RADIAL COORDINATE

r_o . . . RADIUS OF FUEL ROD

S . . . THERMAL NEUTRON SOURCE TERM

S_o . . . EXPANSION COEFFICIENT OF SOURCE AT $z = 0$

s . . . LAPLACE TRANSFORM PARAMETER WITH RESPECT TO AGE

t . . . TIME

u . . . LETHARGY

v . . . VELOCITY

z . . . AXIAL COORDINATE

α . . . REAL PART OF COMPLEX INVERSE RELAXATION LENGTH

δ . . . DIRAC DELTA FUNCTION

γ . . . FEINBERG-GALANIN CONSTANT

η . . . NEUTRONS PER THERMAL NEUTRON ABSORPTION IN FUEL

θ . . . FAST NEUTRON SLOWING DOWN DENSITY

ξ . . . IMAGINARY PART OF COMPLEX INVERSE RELAXATION LENGTH

ρ . . . COMPLEX INVERSE RELAXATION LENGTH AND LAPLACE
TRANSFORMATION PARAMETER WITH RESPECT TO z

Σ . . . MACROSCOPIC CROSS SECTION

τ . . . FERMI AGE

ϕ . . . NEUTRON FLUX

ω . . . FOURIER TRANSFORM PARAMETER WITH RESPECT TO TIME
AND THE RADIAN FREQUENCY

Abstract of Dissertation Presented to the Graduate Council
in Partial Fulfillment of the Requirements for
the Degree of Doctor of Philosophy

DETERMINATION OF HETEROGENEOUS PARAMETERS
BY THE NEUTRON WAVE TECHNIQUE

By

Emile Anthony Bernard

March 1968

Chairman: Dr. M. J. Ohanian
Major Department: Nuclear Engineering Sciences

The neutron wave technique has been used to study a heterogeneous
system consisting of a natural uranium rod surrounded by a moderator
of heavy water. By considering only a simple unit cell configuration,
the theoretical derivations are simplified and one can perform a
relatively simple and inexpensive experiment. The experimental
technique applied permits the measurement of several heterogeneous
parameters and can be used to study other fuel-moderator systems.

The Feinberg-Galanin Constant, γ, was measured. This measurement
was accomplished by first obtaining the experimental dispersion law
for the unit cell. Next, the theoretical dispersion law is computed
for various values of γ. The theoretical dispersion law best fitting,
the experimental one determines the value of γ.

The theoretical model used is the Age-Diffusion Model. By using
a series of transformations and an expansion in transverse eigen-

functions, the two coupled equations are solved for the thermal flux. Inversion of the solution yields the theoretical dispersion law. This dispersion law is interesting in that a critical frequency is pre - dicted at which the dispersion law for the unit cell is equal to that of the pure moderator. This intersection allows one to measure two other heterogeneous parameters of the group L_s, τ_{th}, η and p.

The thermal neutron pulse, as a function of axial position, was numerically transformed from the time to the frequency domain. The frequency dependent attenuation constants and phase shifts were then obtained and the experimental dispersion laws were determined.

The real and imaginary parts of the square of the complex inverse relaxation length were expanded in even and odd powers of the radian frequency. From the expansion coefficients γ was determined. However, it was found that more accurate results were obtainable when γ was de-termined from the dispersion law fit. The latter analysis yielded the result:

$$\gamma = 0.25 \pm .02 \text{ cm.}$$

The expansion coefficient analysis yielded the following results:

$$\gamma(P_0) = 0.29$$

and

$$\gamma(P_1) = 0.31 .$$

The dispersion law intersection was found to occur at

$$\alpha = -0.0532 \pm .0005 \text{ cm}^{-1}$$

$$\xi = -0.0586 \pm .0004 \text{ cm}^{-1}.$$

This corresponded to frequencies of 138 cps in the unit cell and 129 cps in the pure moderator dispersion laws. Evaluation of p and

τ_{th} results in unrealistic values for their quantities indicating that a more accurate model than Age-Diffusion Theory is required for this analysis. Furthermore it is necessary to eliminate variations in heavy water purity to improve the accuracy of the experimental data.

The analyses of this work have been conducted primarily in the ρ plane. It appears that more accurate and sensitive results are obtainable when the analyses are conducted in the ρ^2 plane. Data to aid this type of future studies have been included.

CHAPTER I

INTRODUCTION

Background

The Department of Nuclear Engineering Sciences at the University
of Florida has been engaged in an extensive research program in the
field of neutron wave propagation since 1960. The original studies
dealt with the theoretical (1) and experimental (2, 16) determina-
tion of the diffusion and thermalization parameters of homogeneous
moderating media. Successful results prompted studies of two region
moderating media (3), moderating media with localized absorbers (4),
a "homogenized" subcritical assembly (5, 6) and a reflected subcritical
assembly (7, 8, 11). The continued success of the neutron wave
technique has been demonstrated in recent conferences held at Karlsruhe
(9), Gainesville (10), San Diego (11) and Ann Arbor (12). Since past
endeavors have been successful it is of interest to investigate the
application of this technique to other systems.

In this work a heterogeneous moderator-fuel system will be investi-
gated using the neutron wave propagation technique. Cain (13) studied
the heterogeneous problem theoretically and computed the spatial and
frequency dependent neutron fluxes in various configurations. One of
the configurations consisted of two natural uranium fuel rods embedded
in a heavy water moderating medium. Calculation of the flux perturbation

showed no significant change due to the fuel rods. Experimental
measurements were predicted to be indeterminate unless enriched fuel
was used. Measurement of quantities other than the flux would have
to be made to obtain meaningful results with natural uranium fuel rods.

Corno (14) also studied heterogeneous systems theoretically and
proposed an experiment to study the heterogeneous characteristics of
a cylindrical fuel rod embedded in a moderating medium. The experi-
ment involved the use of a highly enriched driving shell surrounding
the fuel rod. By measuring the exponential attenuation of the
fundamental mode for different driving shells, γ and η can be determined.
γ is the Feinberg-Galanin Constant (15) and η is the number of neutrons
produced per thermal neutron absorption in the fuel. The technical
problems involved in designing and using such a driving shell make a
simpler experimental configuration desirable.

Booth, Perez and Hartley (16) have developed a procedure for
neutron wave propagation experiments. This procedure is a general one,
applicable to almost any system. The experimental quantity measured
is the complex inverse relaxation length, ρ, as a function of frequency
where

$$\rho = \alpha + i\xi,$$

α is the amplitude attenuation per unit length and ξ is the phase
shift per unit length. By measuring ρ it is then possible to obtain
the dispersion law, i.e., ξ versus α with frequency as the parameter.
Analysis of the complex inverse relaxation length allows the experi-
mental determination of the Feinberg-Galanin Constant for the fuel rod
in the system. A comparison between the dispersion law predicted by
theory and the experimental dispersion law can also be made. This

method of analysis will be employed to study the heterogeneous system.

Scope and Objectives

The neutron wave technique has been used successfully to study several systems. It has not been used experimentally to study heterogeneous moderator-fuel systems and the question of its practicality in such cases remains unresolved. This study will investigate the use of the technique on a system other than those already considered. The scope of the neutron wave technique is to be extended experimentally to include a method for investigating the heterogeneous moderator-fuel system. The system is to be as simple as possible. Heterogeneous parameters and their sensitivity to the neutron wave parameters will be determined. In particular, the Feinberg-Galanin Constant, γ, will be measured. One natural uranium fuel rod embedded in a moderating medium of heavy water, as shown in Figure 1., will be used to illustrate the method.

Two other heterogeneous parameters of the group η, p, τ_{th} and L_s can also be measured. Their measurements are made possible by the intersection of the dispersion laws of the moderator only and the moderator-fuel systems.

A review of the literature failed to show the existence of an established experimental method to measure γ directly. γ is usually computed but complex designs often call for approximations which lead to uncertainties in the results. The method presented here allows the measurement of γ to be made in a simple and inexpensive way using one fuel rod.
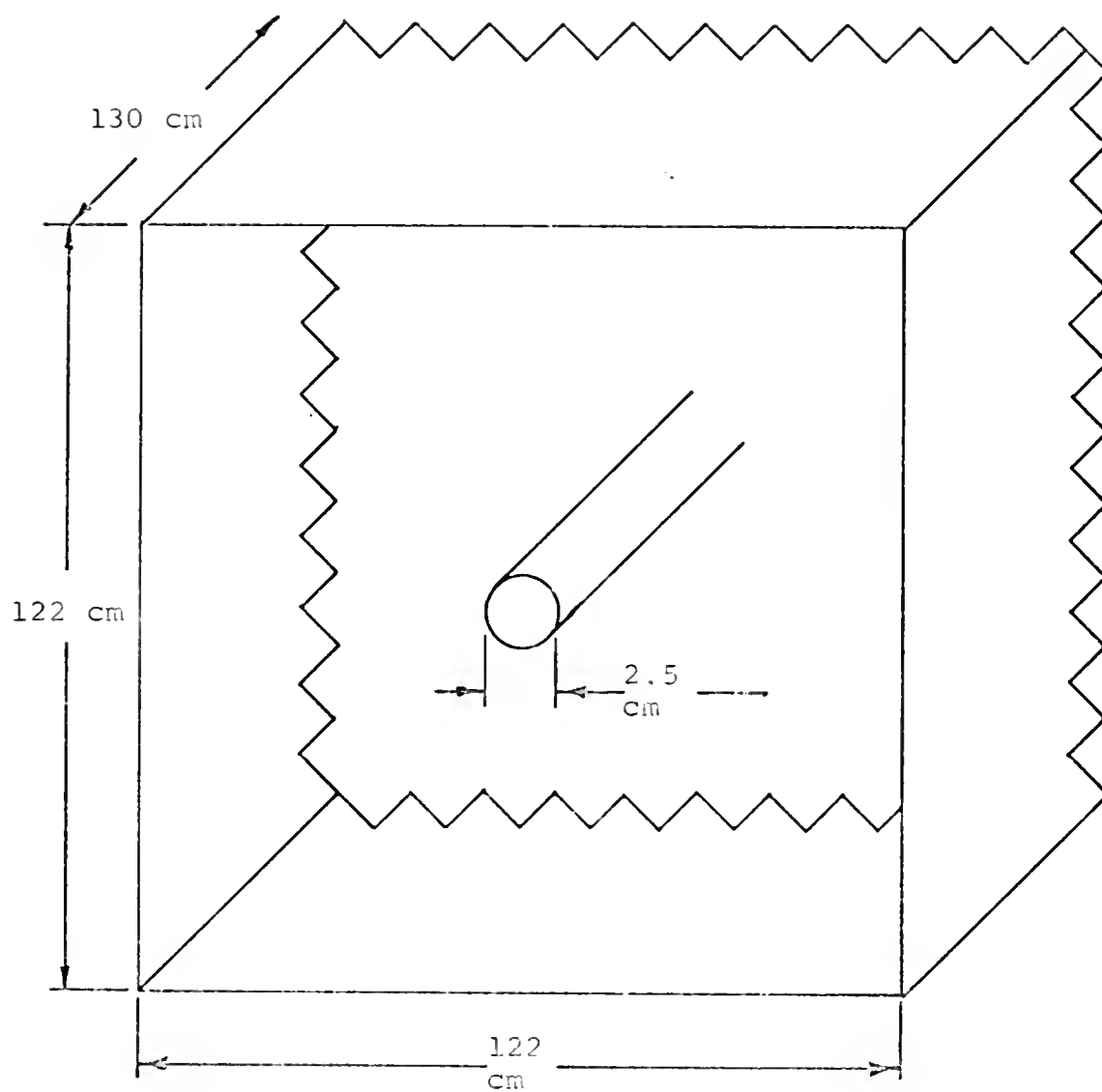
FIGURE 1.

A SCHEMATIC VIEW OF THE
HETEROGENEOUS SYSTEM

The effect on γ when a lattice is considered needs to be examined. Direct extrapolation from the one fuel rod case to that of a complex lattice must be demonstrated experimentally. In the absence of such data an extrapolation to the simple lattice configuration used by Dunlap (5) will be investigated. If lattice effects are significant the experimental method must be modified to make the measurement of γ a valid one.

The potential of the method will be investigated and its extension to determine other heterogeneous effects, such as interaction and shadowing effects, will be considered. Versatility of the method will also be discussed.

CHAPTER II

THEORY

Introduction

The theoretical model used in this analysis is the Age-
Diffusion Model. Although this is a simplified approach it is
sufficient to exhibit the characteristics to be expected from a
more refined analysis. To be more accurate, thermalization
effects should be considered. However, Dunlap (6) found that ex-
perimental results for the subcritical assembly agreed, within
several percent, with Age-Diffusion Theory for frequencies up to
330 cps. As will be seen in the development of this chapter,
the theoretical basis for the experimental method is established
by considering frequencies less than 330 cps. Therefore the
Age-Diffusion Model will be used.

The purpose of the theoretical model, in this case, is to
predict values for parameters which are to be measured experi-
mentally. Age-Diffusion Theory, since it does ignore thermaliza-
tion effects, can not be expected to predict accurate values.
However, these predictions are sufficient to verify the practicality
of the experiment and do offer a comparison with the experimental
results. Better comparisons will be obtained with more accurate
theoretical models.

An important number associated with heterogeneous calculations is the Feinberg-Galanin Constant, γ (15). This constant is defined as the ratio of the net current of neutrons into a fuel rod divided by the neutron flux on the surface of the rod. The value of γ is determined by two methods. The first method is to fit the experimental dispersion law, using γ as the fitting parameter. The second method is based on expanding ρ^2 in the dispersion law in a power series of $i\omega$ and equating coefficients of like powers. The first two expansion coefficients will be related to γ. The results of the two methods will be compared.

In the theoretical development of this chapter it will be shown that the dispersion laws for the moderator only and the moderator-fuel rod intersect. The frequency of the moderator-fuel rod dispersion law at which the intersection occurs is designated the critical frequency, ω_c. Experimentally this is important. By setting the real and imaginary parts of the moderator-fuel rod dispersion law equal to those of the moderator dispersion law and substituting the value of the measured critical frequency and α and ξ measured at the critical frequency, two heterogeneous parameters can be determined. Further detail is presented later in this chapter.

The Theoretical Model

Two equations make up the Age-Diffusion Model. The time dependent fast flux, ϕ (x, u, t), in terms of lethargy, u, is described by the equation

$$-D(u) \nabla^2 \phi(x, u, t) + \Sigma_a(u) \phi(x, u, t) =$$

$$- \frac{1}{v(u)} \frac{\partial \phi(x, u, t)}{\partial t} + S(x, u, t) - \frac{\partial q(x, u, t)}{\partial u}$$

[2.1]

and the associated equation for the thermal flux, $\phi^{th}(x,t)$ is

$$- D^{th} \nabla^2 \phi^{th}(x,t) + \Sigma_a^{th} \phi^{th}(x,t) =$$

$$- \frac{1}{v_{th}} \frac{\partial \phi^{th}}{\partial t} + q(x,u_{th},t) - A(x,t)$$

[2.2]

where

D = the diffusion constant [cm]

Σ_a = the macroscopic absorption cross section [cm^{-1}]

v = velocity [cm sec^{-1}]

q = slowing down density [neutrons cm^{-3} sec^{-1}]

S = source of neutrons due to the fuel rod [neutrons cm^{-3} sec^{-1}]

A = absorption of thermal neutrons in the fuel rod [neutrons $cm^{-3}sec^{-1}$]

Since cylindrical geometry will be considered,

$$x = x(r,z)$$

in both equations.

Solution of Equation For Fast Neutrons   The time dependence in

equation [2.1] is removed with a Fourier Transformation with respect

to t.   Since the flux results from the pulsed neutron source which is

assumed to start at zero time

$$\phi(x,u,t) = 0; \quad t < 0.$$

Under this condition the Fourier Transform of equation [2.1] is

$$- D(u) \nabla^2 \phi(x,u,\omega) + \Sigma_a(u) \phi(x,u,\omega) =$$

$$- \frac{i\omega}{v(u)} \phi(x,u,\omega) + S(x,u,\omega) - \frac{\partial q(x,u,\omega)}{\partial u}$$

[2.3]

where ω is the transform parameter.

The source term, $S(x,u,\omega)$, represents the fission neutrons produced by thermal neutron absorption in the fuel rod. It is assumed that these source neutrons appear with lethargy zero, at the surface of the fuel rod. The explicit form of the source term is then

$$S(x,u,\omega) = \delta(u) \frac{\Sigma_s(o)}{\Sigma_t(o)} \eta \gamma \frac{\delta(r - r_o)}{2 \pi r} \phi^{th}(x,\omega)$$

where

r_o = radius of the fuel rod [cm]

$\dfrac{\Sigma_s(o)}{\Sigma_t(o)}$ = the probability of a neutron entering the slowing down process

η = the neutron yeild per thermal neutron absorption

γ = $\dfrac{\text{net thermal neutron current into the rod}}{\text{thermal neutron flux at the surface of the rod}}$ [cm]

δ = the Dirac Delta Function.

It is convenient to write equation [2.3] in terms of the slowing down density, $q(x,u,\omega)$. The infinite medium relation,

$$q(x,u,\omega) = \xi \, \Sigma_t(u) \, \phi(x,u,\omega),$$

is assumed since measurements were made in heavy water which is a weak absorber of neutrons. Substituting for $\phi(x,u,\omega)$ and $S(x,u,\omega)$ equation [2.3] becomes

$$\{ - D(u) \nabla^2 + \Sigma_a(u) + \frac{i\omega}{v(u)} \} \frac{q(x,u,\omega)}{\xi \, \Sigma_t(u)} =$$

$$- \frac{\partial q(x,u,\omega)}{\partial u} + \delta(u) \frac{\Sigma_s(o)}{\Sigma_t(o)} \eta \gamma \frac{\delta(r - r_o)}{2 \pi r} \phi^{th}(x,\omega) .$$

[2.4]

A change of variables is now made from lethargy, u, to age, τ, using the definition

$$\frac{d\tau}{du} \equiv \frac{D(u)}{\xi\ \Sigma_t(u)} = \frac{D(\tau)}{\xi\ \Sigma_t(\tau)}$$

and the relations

$$\frac{\partial}{\partial u} = \frac{D(\tau)}{\xi\ \Sigma_t(\tau)}\ \frac{\partial}{\partial\tau}$$

$$\delta(u) = \frac{D(\tau)}{\xi\ \Sigma_t(\tau)}\ \delta(\tau)$$

equation [2.4] becomes

$$\{ -\nabla^2 + \beta(\tau,\omega)\}\ q(x,\tau,\omega) = -\frac{\partial q(x,\tau,\omega)}{\partial\tau}$$
$$+ \delta(\tau)\ \frac{\Sigma_s(o)}{\Sigma_t(o)}\ \eta\ \gamma\ \frac{\delta(r-r_o)}{2\pi r}\ \phi^{th}(x,\omega) \qquad [2.5]$$

where

$$\beta(\tau,\omega) = \frac{\Sigma_a(\tau) + \frac{i\omega}{v(\tau)}}{D(\tau)}\ .$$

By multiplying equation [2.5] by the integrating factor

$$e^{\int_o^\tau \beta(\tau',\omega)\ d\tau'} = \frac{1}{p(\tau,\omega)} = \frac{1}{p\ e^{i\omega L_s}}$$

where L_s is the slowing down time and p is the resonance escape probability and recognizing that

$$\frac{\partial}{\partial\tau}\ \{\frac{q(x,\tau,\omega)}{p(\tau,\omega)}\} = \frac{1}{p(\tau,\omega)}\ \frac{\partial q(x,\tau,\omega)}{\partial\tau} + \frac{q(x,\tau,\omega)}{p(\tau,\omega)}\ \beta(\tau,\omega),$$

$$\{-\nabla^2 + \frac{\partial}{\partial \tau}\} \; \Theta(x,\tau,\omega) = \delta(\tau) \frac{\Sigma_s(o)}{\Sigma_t(o)} \frac{\eta \gamma}{p(\tau,\omega)} \frac{\delta(r - r_o)}{2 \pi r} \phi^{th}(x,\omega) \quad [2.6]$$

where
$$\Theta(x,\tau,\omega) = \frac{q(x,\tau,\omega)}{p(\tau,\omega)}.$$

Equation [2.6] compares with equation [8.2.9a] of Beckurts and
Wirtz (17).

The next step is to remove the age dependence in equation [2.6]
using a Laplace Transformation with respect to τ. The boundary
conditions
$$\Theta(x,\tau=o,\omega) = 0$$

and
$$p(\tau=o,\omega) = 1$$

apply since no neutrons slow down past age zero and the resonance
escape probability at age zero is one. The former condition holds be-
cause the source neutrons are taken into account by the source term
in equation [2.6]. The Laplace Transformation of equation [2.6] is

$$\nabla^2 \Theta(x,s,\omega) - s\Theta(x,s,\omega) = -\frac{\Sigma_s(o)}{\Sigma_t(o)} \; \eta \gamma \; \frac{\delta(r - r_o)}{2 \pi r} \phi^{th}(x,\omega) \quad [2.7]$$

where s is the transform parameter.

At this point the dependent variables, $\Theta(x,s,\omega)$ and $\phi^{th}(x,\omega)$,
are expanded in terms of the radial eigenfunctions, $J_o(B_n r_o)$, given
by the solution of the Helmholtz equation,

$$(\nabla_r^2 + B_n^2) \; J_o(B_n r) = 0.$$

The orthogonality condition is

$$\int_o^R J_o(B_n r) \; J_o(B_p r) \; 2 \pi r \; dr = N_p \; \delta_{np}$$

where N_p is the normalization constant and δ_{np} is the Kronecker delta.
R, the extrapolated boundary, is such that

$$J_o(B_n R) = 0.$$

The expansions are

$$\Theta(x,s,\omega) = \sum_n \Theta_n(z,s,\omega) \; J_o(B_n r)$$

and

$$\phi^{th}(x,\omega) = \sum_n \phi_n^{th}(z,\omega) \; J_o(B_n r).$$

By noting that

$$\nabla_r^2 J_o(B_n r) = - B_n^2 \; J_o(B_n r),$$

multiplying by

$$2 \pi r \; J_o(B_p r),$$

integrating and applying the orthogonality condition, equation [2.7]
is reduced to the following equation for the expansion coefficients:

$$\frac{\partial^2 \Theta_p(z,s,\omega)}{\partial z^2} - (B_p^2 + s) \; \Theta_p(z,s,\omega) =$$

[2.8]

$$- \frac{\Sigma_s(o)}{\Sigma_t(o)} \; \frac{\eta \, \gamma}{N_p} \; \sum_n \phi_n^{th}(z,\omega) \; J_o(B_n r_o) \; J_o(B_p r_o).$$

The last step in the solution to the fast flux equation is to re-
move the spatial dependency by a second Laplace Transformation, this
time with respect to z. The Laplace Transformation of equation [2.8]
is

$$\rho^2 \, \Theta_p(\rho, S, \omega) - (B_p^2 + s) \, \Theta_p(\rho, s, \omega) =$$

$$- \frac{\Sigma_s(o)}{\Sigma_t(o)} \frac{\eta \, \gamma}{N_p} \sum_n \phi_n^{th}(\rho, \omega) \, J_o(B_n r_o) \, J_o(B_p r_o)$$

where ρ is the transform parameter and the boundary conditions are taken to be

$$\Theta_p(z=o, s, \omega) = \frac{d\Theta_p(z=o, s, \omega)}{dz} = 0$$

which neglects the gradient at $z=o$ because the dispersion law is independent of its presence. The solution for the fast flux expansion coefficients is

[2.9]

$$\Theta_p(\rho, s, \omega) = \frac{1}{s + (B_p^2 - \rho^2)} \frac{\Sigma_s(o)}{\Sigma_t(o)} \frac{\eta \, \gamma}{N_p} \sum_n \phi_n^{th}(\rho, \omega) \, J_o(B_n r_o) \, J_o(B_p r_o).$$

In order that the solution may be of use in solving for the thermal flux, it is necessary to transform from the s domain back to the τ domain. The inverse transformation of equation [2.9] is

$$\Theta_p(\rho, \tau, \omega) = e^{-(B_p^2 - \rho^2)\tau} \frac{\Sigma_s(o)}{\Sigma_t(o)} \frac{\eta \, \gamma}{N_p} \sum_n \phi_n^{th}(\rho, \omega) \, J_o(B_n r_o) \, J_o(B_p r_o)$$

$$n, p = 1, 2, \ldots k.$$

Solution of Equation for Thermal Neutrons It is also necessary to solve the thermal flux equation, equation [2.2]. The procedure is similar to that used to solve the fast flux equation. The order of transformation is changed so that the boundary conditions may be more readily applied. Before solving equation [2.2] it is noted that

$$A(x,t) = \gamma \frac{\delta(r - r_o)}{2 \pi r} \phi^{th}(x,t)$$

which represents the absorption of neutrons in the fuel rod as losses occurring at the surface of the fuel rod. By representing the absorptions in this manner and the source term in the manner described in the previous section, the problem is reduced to a one region problem with a source and absorber of neutrons.

Equation [2.2] is Laplace Transformed with respect to the z variable:

$$\{-D^{th}\rho^2 - D^{th} \nabla_r^2 + \Sigma_a^{th}\} \phi^{th}(r,\rho,t) + D^{th}\rho \phi^{th}(r,z=0,t)$$

$$+ D^{th} \frac{\partial \phi^{th}}{\partial t}(r,z=0,t) = \frac{1}{v_{th}} \frac{\partial \phi^{th}}{\partial t}(r,\rho,t) + q(r,\rho,\tau_{th},t) \qquad [2.10]$$

$$- \gamma \phi^{th}(r,\rho,t) \frac{\delta(r - r_o)}{2 \pi r}$$

where ρ is the transform parameter. In this case neither the thermal flux nor its derivative is zero at the origin. These terms are expressed as

$$\frac{\partial \phi^{th}}{\partial z}(r,z=0,t) = \frac{S_o(r,t)}{2} = S_o(t) J_o(B_1 r)$$

and

$$\phi^{th}(r,z=0,t) = \sum_n c_n(t) J_o(B_n r).$$

Making these substitutions, using the eigenfunction expansions and invoking the orthogonality condition as was done in the solution of the equation for the fast neutrons equation [2.10] becomes

$$\{-D^{th}\rho^2 + D^{th}B_p^2 + \Sigma_a^{th}\}\phi_p^{th}(\rho,t) + D_\rho^{th}c_p(t) + D^{th}S_o(t)\delta_{p1}$$

$$= -\frac{1}{v_{th}} \frac{\partial\phi_p^{th}}{\partial t}(\rho,t) + q_p(\rho,\tau_{th},t)$$

$$- \frac{\gamma}{N_p} \sum_n \phi_n^{th}(\rho,t) J_o(B_n r_o) J_o(B_p r_o)$$

where

$$q(\tau,\rho,\tau_{th},t) = \sum_n q_n(\rho,\tau_{th},t) J_o(B_n \tau).$$

The time dependence is transformed out by a Fourier Transformation, again using ω as the transform parameter. The result is

$$\{-\rho^2 + B_p^2 + \frac{\Sigma_a^{th} + \frac{i\omega}{v_{th}}}{D^{th}}\} \phi_p^{th}(\rho,\omega) + \rho\, c_p(\omega) + S_o(\omega)\, \delta_{p1}$$

$$= \frac{-\gamma}{D^{th}N_p} \sum_n \phi_n^{th}(\rho,\omega) J_o(B_n r_o) J_o(B_p r_o) + \frac{p(\tau_{th},\omega)}{D^{th}} \phi_p(\rho,\tau_{th},\omega)$$

where

$$q_p(\rho,\tau_{th},\omega) = p(\tau_{th},\omega)\, \phi_p(\rho,\tau_{th},\omega).$$

Combination of Fast and Thermal Neutron Solutions   The solution for
the thermal flux expansion coefficients is

$$\left\{ -(B_p^2 - \rho^2) - \frac{1}{L_{th}^2} - \frac{i\omega}{D_o^{th}} \right\} \phi_p^{th}(\rho,\omega)$$

$$+ \quad \frac{\gamma}{D^{th}N_p} \left\{ \eta \, p(\tau_{th},\omega) \quad \frac{\Sigma_s(o)}{\Sigma_t(o)} \; e^{-(B_p^2 - \rho^2)\tau_{th}} - 1 \right\}$$

[2.11]

$$X \sum_n \phi_n^{th}(\rho,\omega) J_o(B_n r_o) J_o(B_p r_o) = \rho \, c_p(\omega) + S_o(\omega) \, \delta_{p1}$$

$$n,p = 1,2, \ldots k$$

where the solution obtained for the fast flux expansion coefficients
has been substituted,

$$\frac{\Sigma_a^{th}}{D^{th}} = \frac{1}{L_{th}^2}$$

and

$$D^{th} v_{th} = D_o^{th} .$$

Since the moderator to fuel ratio considered is large, the probability
of a source neutron being absorbed on its first collision is very
small.   Therefore, the approximation

$$\frac{\Sigma_s(o)}{\Sigma_t(o)} = 1$$

is made.

Numerical Solution

Two cases of the solution will now be considered, $n,p = 1$ and $n,p = 1$ and 2. The former case represents the solution for the fundamental spatial mode while the latter illustrates the case which includes the first spatial harmonic as well as the fundamental solutions. The latter was used in all the computations. The importance of the first harmonic will be examined.

In both cases an inverse Laplace Transformation is required in order to obtain the solution in z space. To simplify the inverse transformation the poles of the transformed solution can be computed. The solution in z space is then of the form

$$\phi_p^{th}(z,\omega) = \sum_i G_i(\omega) e^{\rho_i(\omega)z}$$

where $G_i(\omega)$ is a constant, depending on the pole $\rho_i(\omega)$. The final solution in terms of z will not be computed. Instead, the poles of the transformed solution are computed, yielding the dispersion law.

For $n,p = 1$, ρ^2 is computed from the equation

$$\left\{ -(\beta_1^2 - \rho^2) - \frac{1}{L_{th}^2} - \frac{i\omega}{D_o^{th}} \right.$$

$$+ \frac{\gamma}{D^{th}N_1} \int \eta p e^{-(\beta_1^2 - \rho^2)\tau_{th} - i\omega L_s} - 1 \left. \right\} J_o^2(\beta_1 r_o) = 0 \qquad [2.12]$$

For $n,p = 1$ and 2, ρ^2 is computed by setting the determinant of a 2×2 matrix equal to zero. The elements of the matrix are

$$A_{11} = -B_1^2 + \rho^2 - \frac{1}{L_{th}^2} - \frac{i\omega}{D_o^{th}}$$

$$+ \frac{\gamma}{D^{th}N_1} \left\{ \eta p e^{-(B_1^2 - \rho^2)\tau_{th} - i\omega L_s} - 1 \right\} J_o^2(B_1 r_o),$$

$$A_{12} = \frac{\gamma}{D^{th}N_1} \left\{ \eta p e^{-(B_1^2 - \rho^2)\tau_{th} - i\omega L_s} - 1 \right\} J_o(B_1 r_o) J_o(B_2 r_o),$$

$$A_{21} = \frac{\gamma}{D^{th}N_2} \left\{ \eta p e^{-(B_2^2 - \rho^2)\tau_{th} - i\omega L_s} - 1 \right\} J_o(B_2 r_o) J_o(B_1 r_o),$$

$$A_{22} = -B_2^2 + \rho^2 - \frac{1}{L_{th}^2} - \frac{i\omega}{D_o^{th}}$$

$$+ \frac{\gamma}{D^{th}N_2} \left\{ \eta p e^{-(B_2^2 - \rho^2)\tau_{th} - i\omega L_s} - 1 \right\} J_o^2(B_2 r_o) .$$

In each case solutions were obtained using the FERVE2 Code (See Appendix D).

Results of the computation for selected frequencies are given in Table 1. The fundamental eigenvalues changed in the fourth significant digit from the one term $(n,p = 1)$ to the two term $(n,p = 1$ and $2)$ cases. Computations were also made for a ten term expansion (21) and the fundamental eigenvalues differed by less than 0.5% from those of the one term case. In the two term case the eigenvalues of the first harmonic mode are of the same order of magnitude as the fundamental

TABLE 1.

COMPUTATION OF ALPHA AND XI
AND CONTAMINATION BY FIRST SPATIAL HARMONIC

FREQUENCY	FUNDAMENTAL MODE ONE TERM EXPANSION		FUNDAMENTAL MODE TWO TERM EXPANSION		FIRST HARMONIC MODE TWO TERM EXPANSION		CONTAMINATION BY FIRST HARMONIC[1]	
	ALPHA	XI	ALPHA	XI	ALPHA	XI	Z=40CM	Z=50CM
0.	-0.03789	-0.0	-0.03789	-0.0	-0.08196	-0.0	2.9%	1.9%
50.	-0.04213	-0.01818	-0.04213	-0.01817	-0.08249	-0.00910	2.9%	1.9%
100.	-0.04921	-0.03114	-0.04921	-0.03113	-0.08399	-0.01789	2.9%	1.9%
150.	-0.05607	-0.04101	-0.05608	-0.04100	-0.08624	-0.02614	2.9%	1.9%
200.	-0.06241	-0.04916	-0.06242	-0.04914	-0.08902	-0.03379	2.9%	1.9%
250.	-0.06825	-0.05622	-0.06827	-0.05621	-0.09219	-0.04085	2.9%	1.9%
300.	-0.07369	-0.06254	-0.07371	-0.06253	-0.09542	-0.04737	2.9%	1.9%

1. BASED ON EXPERIMENTAL DATA

eigenvalues. However, the experimental source was found to contain a low percentage of first harmonic contamination.[1] These results are included in Table 1. In this case only the fundamental mode is significant.

γ Analysis

Using equation [2.12] it is possible to analyze γ. γ is varied parametrically and the resulting dispersion law is computed and compared with the experimental one. The best comparison represents the measured value of γ within the limitations of the theoretical model.

If ρ^2 in equation [2.12] is expanded in a power series of the form

$$\rho^2 = \sum_n P_n (i\omega)^n$$

and coefficients of like powers are equated, still another method of determining γ is available. The first two coefficients of the expansion are related to γ as follows

$$P_0 = B_1^2 + \frac{\dfrac{1}{L_{th}^2} + \gamma X(1 - \eta p)}{1 + \eta p \gamma X \tau_{th}} \qquad [2.13]$$

---

1. These results were obtained from the expansion coefficients of the transverse continuous mode data at $z = 40$ cm. The UFNLLS Code (20) was used to fit the data to the fundamental and first harmonic modes. Contamination at $z = 50$ cm, the first data point analyzed, was determined by evaluating the exponential attenuation of each mode and computing the percent contributions. The percentages are based on maximum amplitudes and represent maximum contamination.

and

$$P_1 = \frac{\dfrac{1}{D_o^{th}} + \gamma X(\eta p L_s(1 - B_1^2 \tau_{th} + P_0 \tau_{th}))}{1 + p\gamma X \tau_{th}(1 - B_1^2 \tau_{th} + P_0 \tau_{th})} \qquad [2.14]$$

where

$$X = \frac{J_o^2(B_1 r_o)}{D^{th} N_1}.$$

These expressions were obtained by separating the exponential term into frequency dependent and independent terms, expressing the result as a product of exponentials and expanding each product in a MacLaurin Series.

The sensitivity of P_0 and P_1 to γ was found to be

$$\frac{\partial P_0}{\partial \gamma} \sim 3.3 \times 10^{-4}$$

and

$$\frac{\partial P_1}{\partial \gamma} \sim 3.1 \times 10^{-7},$$

both P_0 and P_1 changing about the same amount in the second significant digit with respect to γ, yielding a 25% change in P_0 and 7% change in P_1.

Comparison of the two γ analyses with the experimental results will be made in Chapter IV.

The Critical Frequency

To investigate the critical frequency equation [2.12] is again considered, both for the moderator only and the moderator-fuel rod systems. The right hand sides of both equations are zero so the left hand sides can be equated. L_{th}^2 and D^{th} are constants of the moderator but D_o^{th} differs between the two systems because v^{th} is different. However, this difference is small [2] and they are assumed to be equal. It is now assumed that the dispersion laws intersect

---

2. Subsequent analysis showed the difference in v^{th} to be less than 2%.

so that the two ρ's are equal. The relation is then obtained:

$$-\frac{i\omega_c}{D_o^{th}} + \frac{\gamma J_o^2(B_1 r_o)}{D^{th} N_1} \left\{ \eta p e^{-(B_1^2 - \rho_c^2)\tau_{th} - i\omega_c L_s} - 1 \right\} \qquad [2.15]$$

$$= \frac{-i\omega_m}{D_o^{th}}$$

where ω_m is the frequency of the moderator only dispersion law asso-
ciated with the intersection and

$$\rho_c = \alpha_c + i\xi_c$$

is the value of ρ at the intersection. ω_c is the critical frequency
of the moderator-fuel rod dispersion law at the intersection. The
dispersion laws intersect at the same values of α and ξ but the
associated frequencies are different. By equating real and imaginary
parts of equation [2.15] the two equations

$$\eta\, p\, \cos\, (2\alpha_c \xi_c \tau_{th} - \omega_c L_s) e^{-\{B_1^2 - (\alpha_c^2 - \xi_c^2)\}\tau_{th}} = 1$$

and

$$\eta\, p\, \sin(2\alpha_c \xi_c \tau_{th} - \omega_c L_s) e^{-\{B_1^2 - (\alpha_c^2 - \xi_c^2)\}\tau_{th}} = \frac{\omega_c - \omega_m}{D_o^{th}} \frac{D^{th} N_1}{\gamma J_o^2 (B_1 r_o)}$$

are obtained. Computations performed for many conditions of inter-
section showed that $\omega_c > \omega_m$. Therefore, the sine and cosine must be
positive for a solution to exist because all the other quantities in
both equations are positive. The angle

$$2\alpha_c \xi_c \tau_{th} - \omega_c L_s$$

must be in the first quadrant. If these two equations are divided, one by the other, the result is

$$\tan (2\alpha_c \xi_c \tau_{th} - \omega_c L_s) = \frac{\omega_c - \omega_m}{D_o^{th}} \frac{D^{th} N_1}{\gamma J_o^2 (B_1 r_o)} . \qquad [2.16]$$

By determining the experimental intersection and computing N_1 and $J_o^2 (B_1 r_o)$ the right hand side of equation [2.16] can be evaluated, if v^{th} and γ are known. The argument of the left hand side can then be determined. This allows either τ_{th} or L_s to be evaluated in terms of the remaining parameters. Once the argument is found, either of the two original equations can be used to solve for η or p in terms of the other. The experimental results will be discussed in Chapter IV.

The intersection of the dispersion laws is illustrated in Table 2. and shown in Figure 2., where they are plotted for $\gamma = 0.0$ (pure moderator) and $\gamma = 0.6$. These values were selected to give a qualitative description of the intersection. Based on Cain's results (13), the value of γ was expected to be in this range.

The sensitivity of ω_c to γ was investigated by using the two term expansion of equation [2.12]. It was found that a change of 0.1 in γ produced a 2 cps change in ω_c.

TABLE 2.

NUMERICAL ILLUSTRATION OF
INTERSECTION OF DISPERSION LAWS

GAMMA = 0.0				GAMMA = 0.6		
FREQUENCY (CPS)	ALPHA (CM^{-1})	XI_1 (CM^{-1})		FREQUENCY (CPS)	ALPHA (CM^{-1})	XI_1 (CM^{-1})
294.0	-0.07326	-0.06260		305.0	-0.07331	-0.00626
295.0	-0.07337	-0.06272		306.0	-0.07341	-0.06278
296.0	-0.07347	-0.06284	**	306.5	-0.07347	-0.06284
297.0	-0.07357	-0.06296		307.0	-0.07352	-0.06289
298.0	-0.07368	-0.06309		308.0	-0.07363	-0.06301

** INTERSECTION
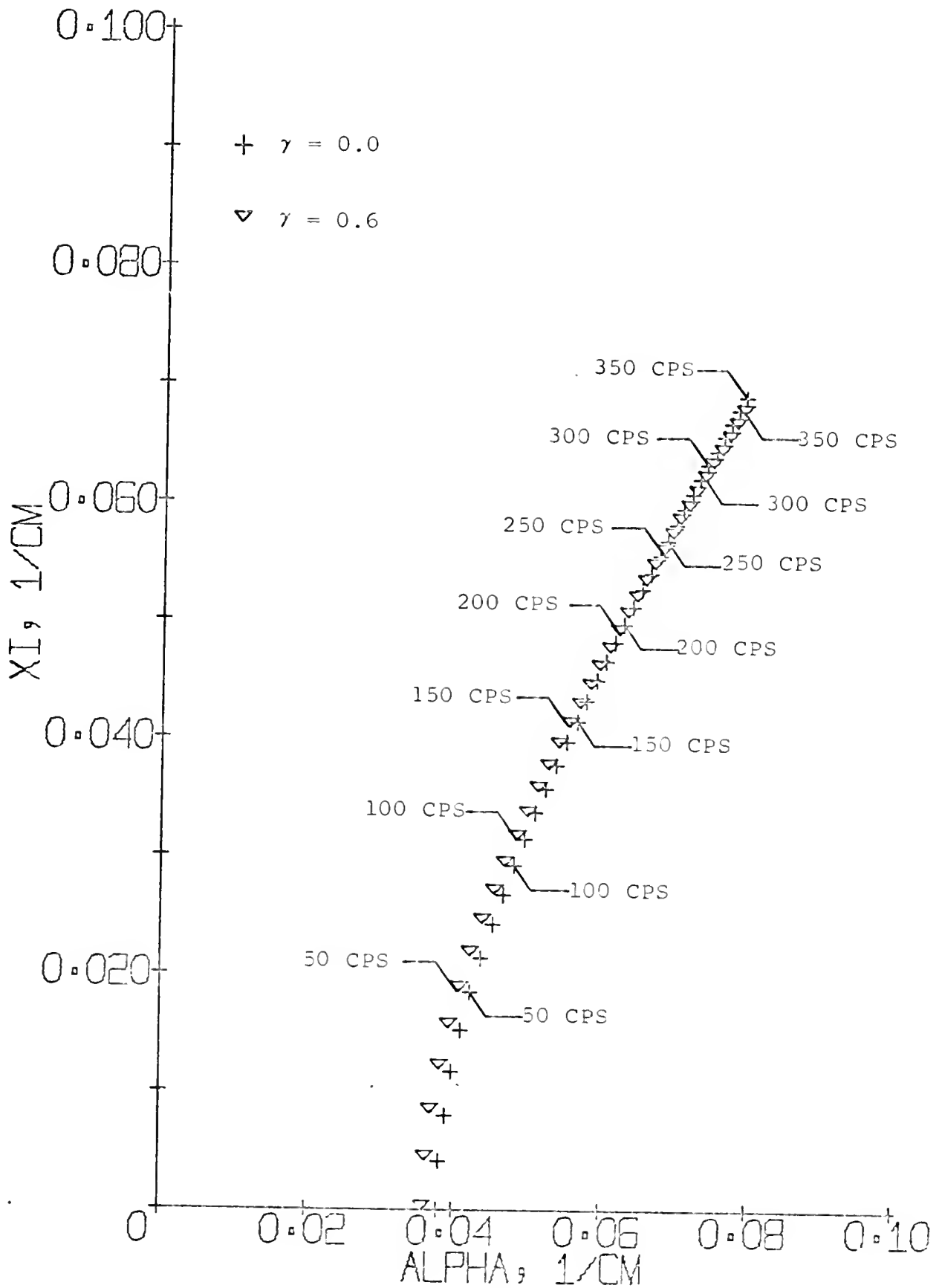
FIGURE 2.

ILLUSTRATION OF DISPERSION
LAW INTERSECTION

CHAPTER III

EXPERIMENTAL METHOD

Introduction

Two experiments were conducted. The first was in a pure moderating medium of heavy water. The second was in the same system with one fuel rod inserted as shown in Figure 1. The experimental dispersion laws for both systems were determined using the pulse propagation technique (16) and converting the data into the frequency domain in the usual way. A Texas Nuclear Corporation Neutron Generator (Model 9505) was used as the source. The system in which the measurements were made and the neutron generator which was used have been described in detail by Dunlap (5, 6). The 17 inch graphite stack between the light water thermalizing tank and the heavy water tank was removed. This was done to reduce the width of the thermal neutron pulse and thus increase the high frequency content.

Two data acquisition systems were used, one having a movable detector which was used for measurements along the axial length of the assembly and the other being the reference detector which was used for normalization purposes. The reference detector was moved to a position adjacent to the graphite in the thermalizing assembly.

This was done to reduce the effects of source anisotropy.[1] A brief
sketch of the set up is shown in Figure 3. Each detector system
contains basically the same components with the following exceptions:

(a)   The movable detector system has a 12 inch He3
       detector and the reference detector system has
       a 6 inch He3 detector

(b)   The movable detection system has additional
       components for data acquisition and analysis
       of the neutron pulse in time.

The two detection systems are shown in Figures 4. and 5.

Considerable time was spent in becoming familiar with each
and every component. This step can not be overemphasized in im-
portance for it proved invaluable in the immediate identification
of equipment failures. Several failures occurred and data acquisi-
tion was terminated with a minimum collection of faulty data. The
use of oscilloscopes was likewise important in the verification of
proper pulses, monitoring signals and general trouble shooting.

Light water contamination in the heavy water moderator changed
between the two experiments. The first experiment was conducted at
99.5% purity while the second one was conducted at 99.0% purity.
The decrease in purity was caused by the several transfers of the
moderator that took place between the performance of the two
experiments.

_____

1.   The angular distribution of neutrons was found to be de-
pendent on the amplitude of the target current. Experimental data
showed that the variation of anisotropy for the range of target
current amplitudes used was reduced to less than 1% when the reference
detector was positioned adjacent to the graphite.
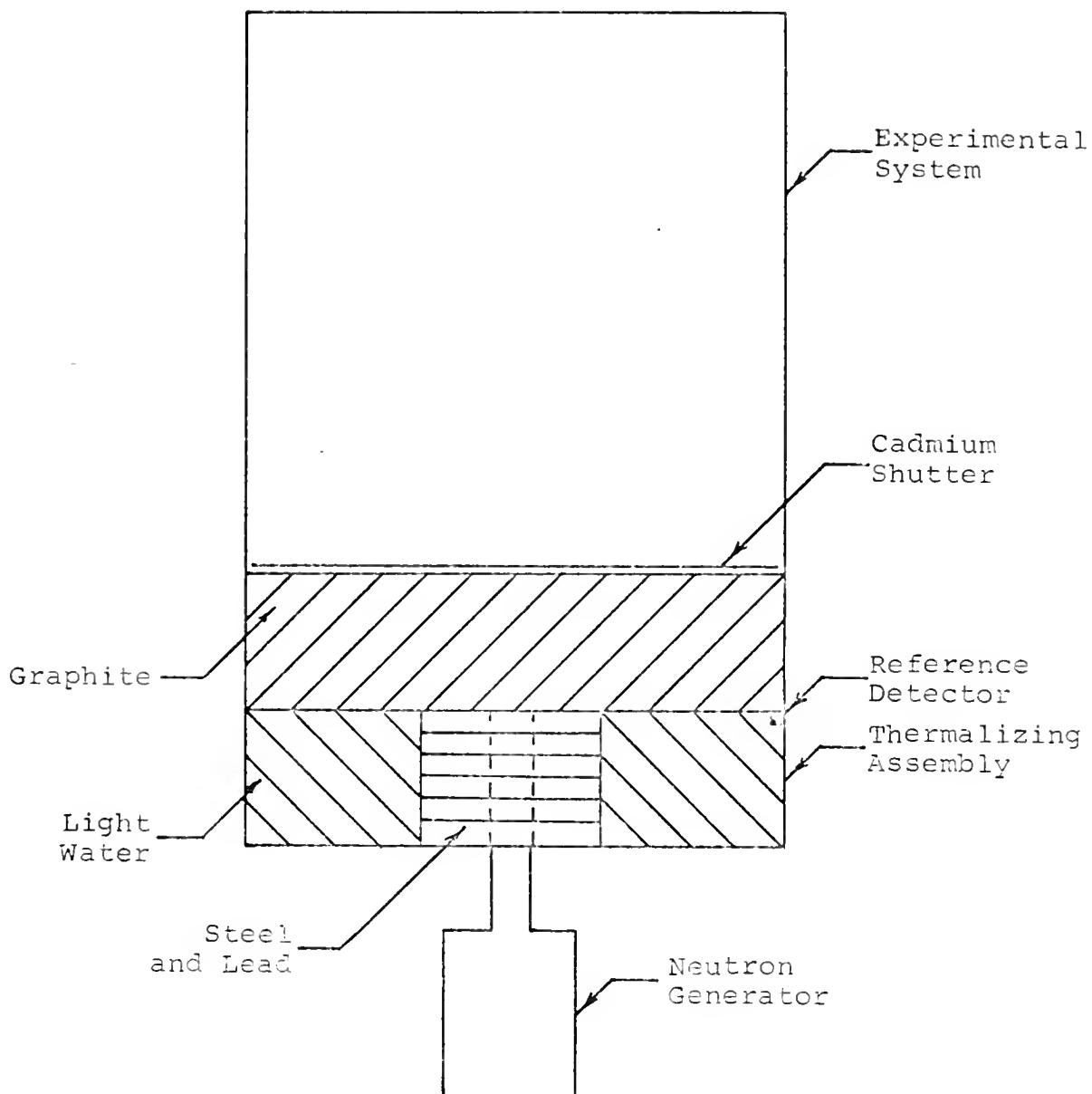
FIGURE 3.

EXPERIMENTAL ASSEMBLY
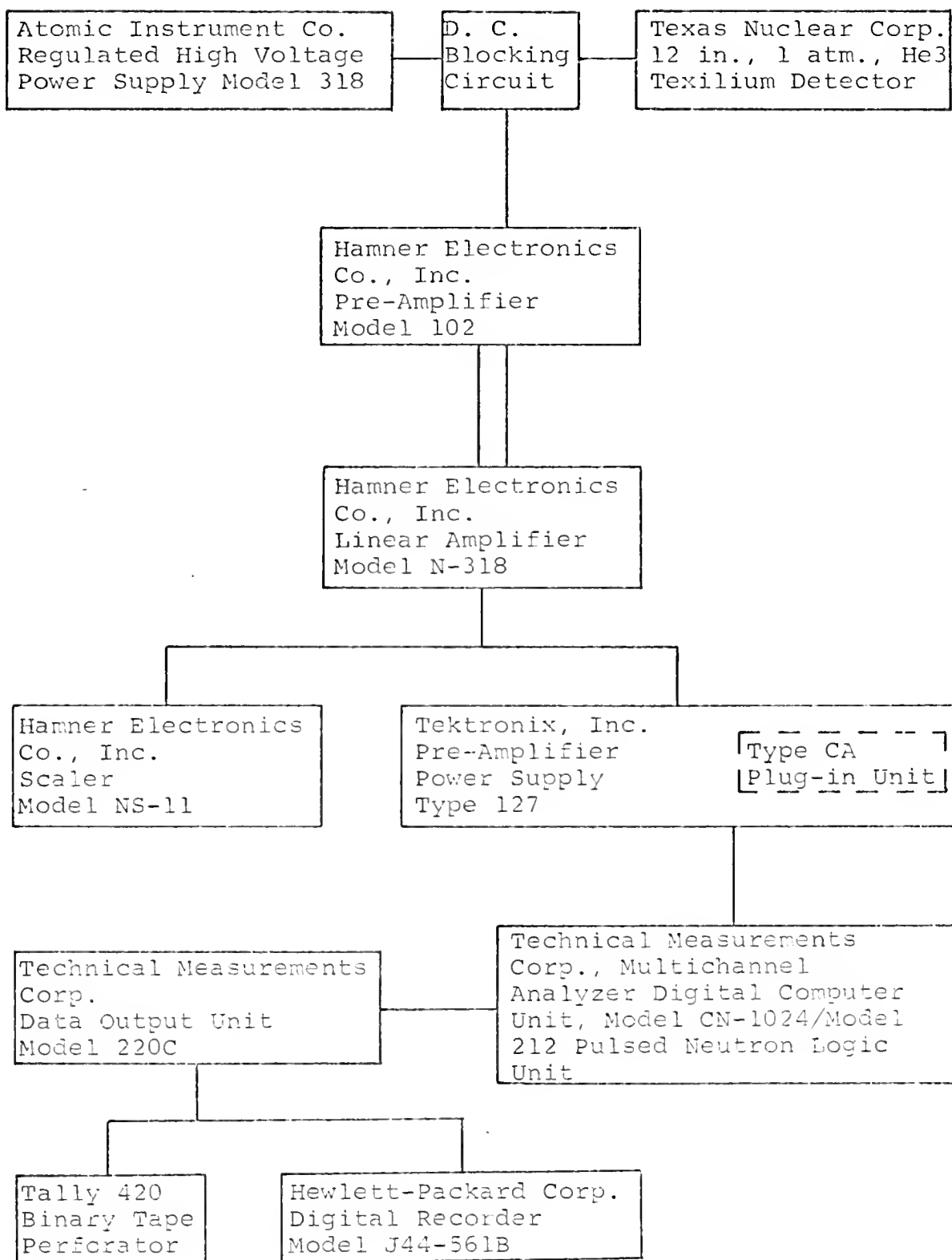
FIGURE 4.

MOVABLE DETECTOR COUNTING SYSTEM

```
┌────────────────────────┐  ┌──────────┐  ┌────────────────────────┐
│ Atomic Instrument Co.  │  │ D. C.    │  │ Texas Nuclear Corp.    │
│ Super Stable High      │──│ Blocking │──│ 6 in., 1 atm., He3     │
│ Voltage Power Supply   │  │ Circuit  │  │ Texilium Detector      │
│ Model 312              │  └────┬─────┘  └────────────────────────┘
└────────────────────────┘       │
                                 │
                         ┌───────┴─────────┐
                         │ Hamner Electronics │
                         │ Co., Inc.          │
                         │ Pre-Amplifier      │
                         │ Model 102          │
                         └───────┬─────────┘
                                 │
                         ┌───────┴─────────┐
                         │ Hamner Electronics │
                         │ Co., Inc.          │
                         │ Linear Amplifier   │
                         │ Model N318         │
                         └───────┬─────────┘
                                 │
                         ┌───────┴─────────┐
                         │ Hamner Electronics │
                         │ Co., Inc.          │
                         │ Scaler, Model NS-11│
                         └─────────────────┘
```
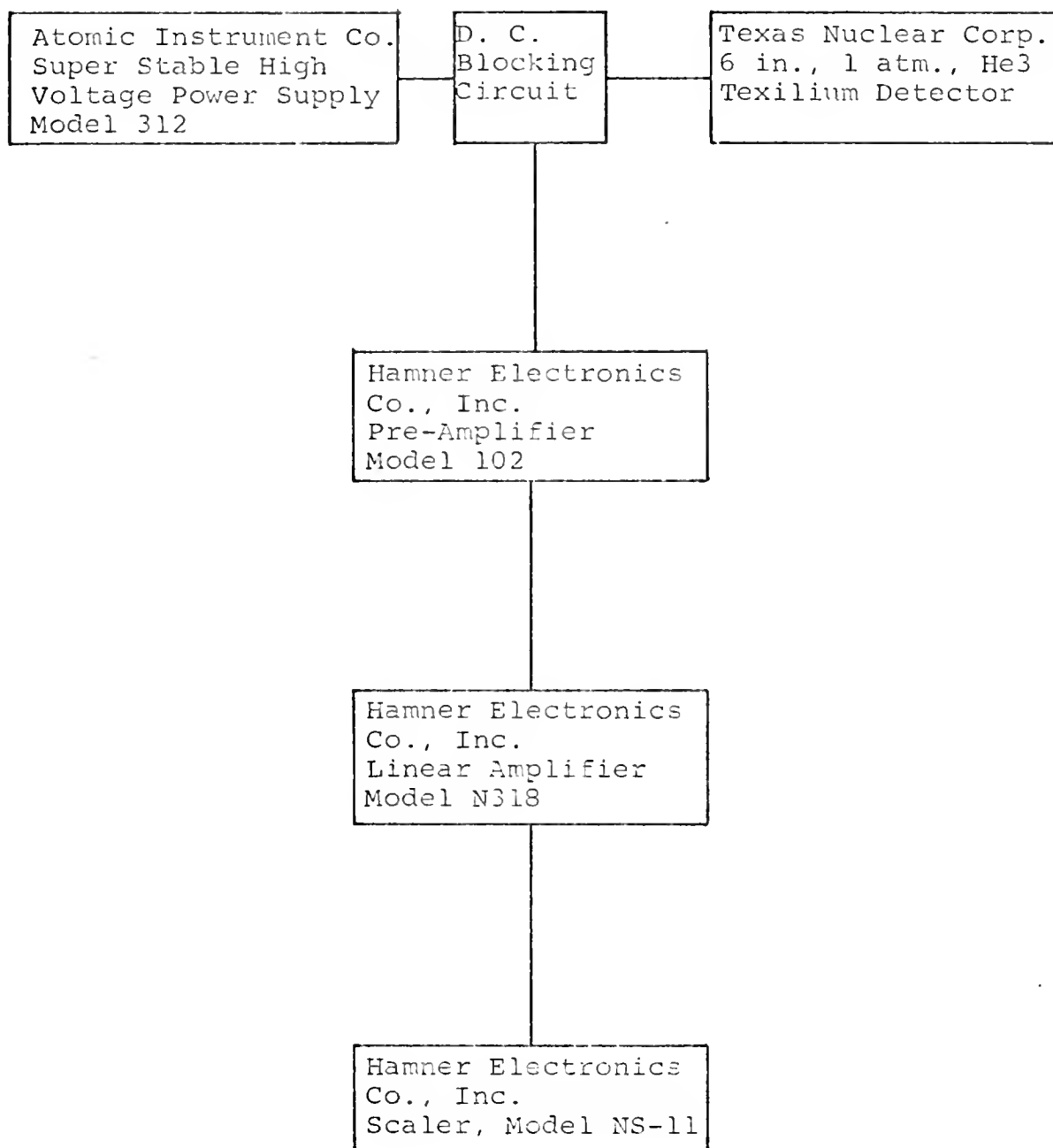
FIGURE 5.

REFERENCE DETECTOR COUNTING SYSTEM

31

Preliminary Procedures

Before any data were taken the following pre-operational checks and tests were performed on the counting systems:

(a) compatability of output-input signals between components

(b) detector plateau determination

(c) chi-squared checks

(d) resolution time determination

(e) gamma ray discrimination checks

(f) minimizing of internal noise

(g) reverification of plateaus, chi-squared check and resolution time.

Step (g) is necessary to assure that changes made in the system in the preceding steps have not affected the counting characteristics of the systems. Adequate guidance in the completion of most steps is easily obtained from the appropriate technical manuals and any Nuclear Engineering laboratory manual. Resolution time determination is described in Appendix A.

The last task to be accomplished before the actual experiment is begun is the selection of the target current pulse width and repetition rate for the neutron generator. Coincident with this is the selection of a compatible channel width for the multichannel analyzer. This procedure is described in Appendix B.

In the course of checking out the detector systems a limiting count rate was observed. Increased source intensity produced no increased scaler count rate at approximately 200,000 and 250,000 counts per second for the reference and movable detector amplifiers

respectively. All data were checked to insure that the maximum count rate during the neutron pulse peak did not approach the saturation rates.

Experimental Procedure

In order to obtain the thermal neutron pulse propagation characteristics through the assembly the cadmium difference technique was employed (16), using the cadmium shutter located at the forward edge of the assembly. The epicadmium contribution of the source was thereby eliminated.

Normally a completed neutron wave experiment consumes days and even weeks. During this time components may change enough to affect the data significantly. In order that one may have a standard of comparison for reproducibility purposes a continuous mode run was made at all the axial positions. These data can be acquired in several hours, a period in which variations are negligible. If necessary, normalization for minor variations of the systems can then be made.

The continuous mode experiment corresponds to the zero frequency component of the neutron pulse in that the amplitude attenuation per unit length are the same (16). If minor anomalies occur in the zero frequency component of the pulsed data, the data can be easily normalized to the continuous mode data. In this manner, small changes due to day-to-day variations of the source, e.g., angular distributions, and counting systems, e.g., shifts in detector plateaus, can be eliminated. In this series of experiments, no normalization was required.

The continuous mode data which were recorded at each position for both the cadmium shutter up and down runs included:

    (a)   run time

    (b)   reference detector scaler counts

    (c)   movable detector scaler counts.

After the continuous mode experiments were completed, the pulsed experiments were conducted. At this point the multichannel analyzer which was set up in accordance with Appendix B was used. Once the pulsed mode has been established, one proceeds to examine the propagation of the thermal neutron pulses through the assembly, employing the same cadmium difference technique used in the continuous mode case.

The pulsed mode data which were acquired for each run included:

    (a)   run time

    (b)   number of triggers

    (c)   reference detector scaler counts

    (d)   movable detector scaler counts

    (e)   multichannel analyzer printed output

    (f)   multichannel analyzer binary tape output.

Verification checks which were performed as soon as the data were recorded are described in Appendix C.

During each run, two signals were continuously monitored with oscilloscopes. One was the target current of the neutron gun. The other was the input to the amplifiers of the movable detector systems. Thus, two visual presentations were available to assure proper pulsed operation. A secondary purpose of monitoring the amplifier input signal was to measure the effective counting time of the movable detector. The effective counting time is discussed in Appendix C.

In both cadmium covered and bare pulsed runs, a minumum of 64,000 counts were accumulated in the peak channel of the multichannel analyzer. This sets the time required for each run. Data were acquired every 5 cms from 50 through 90 cms. These limits are based on the continuous mode analysis which showed definite deviations from a simple exponential decay with distance for positions outside this region. Deviation at the lower end was caused by the source while end effects were significant at the higher end. The procedure employed in determining the appropriate heterogeneous parameters is outlined in Figure 6. The data analysis is described in Chapter IV.
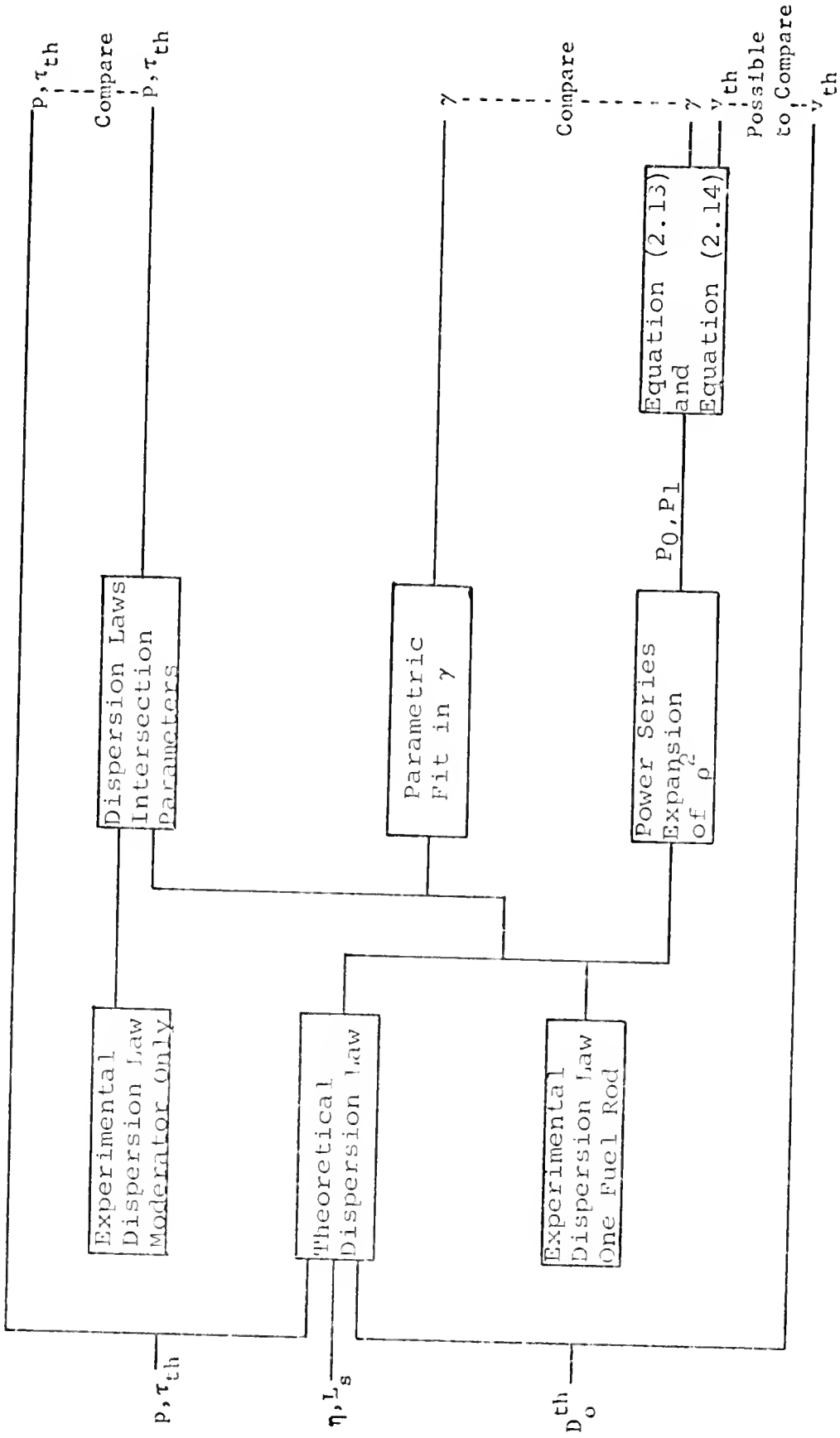
FIGURE 6.

METHOD OF ANALYSIS

CHAPTER IV

DATA ANALYSIS AND RESULTS

.General

Data analysis was accomplished with a modified version of the

Moore Moments Code (6) and a series of supplemental programs

written for the IBM-1800. By using the 1800 the direct interface

capability between the paper tape data and the computer could be

utilized. A flow chart of the computer programs is shown in

Figure 7., while more detailed descriptions are given in Appendix D.

Purity of the heavy water was estimated to be $99.5 \pm .2\%$ for

the moderator only experiment and $99.0 \pm .2\%$ for the one fuel rod

experiment. The 99.5% purity was based on the theoretical model

and the experimental data. This purity yielded the experimentally

observed values of α and ξ at near zero frequencies, where better

agreement exists between theory and experiment, when α and ξ were

computed from equation [2.12]. The 99.0% purity is based on the

difference of 0.5% purity in samples from the two experiments which

were analyzed by the Department of Chemistry. Purities were re-

ported to be $99.3 \pm .05\%$ and $98.8 \pm .05\%$ for the two experiments (18).

In both experiments the heavy water temperature was $21 \pm 2^\circ C$.

Experimental errors in measuring α and ξ were computed based on

the mean square deviation of the data points from the computed least

squares fit. Errors ranged from 0.3% to 2.0% and the latter was

taken as the experimental error for all determinations of α and ξ.

Resolution time measurements were conducted as described in

Appendix A. The subsequent analysis showed this method to be in
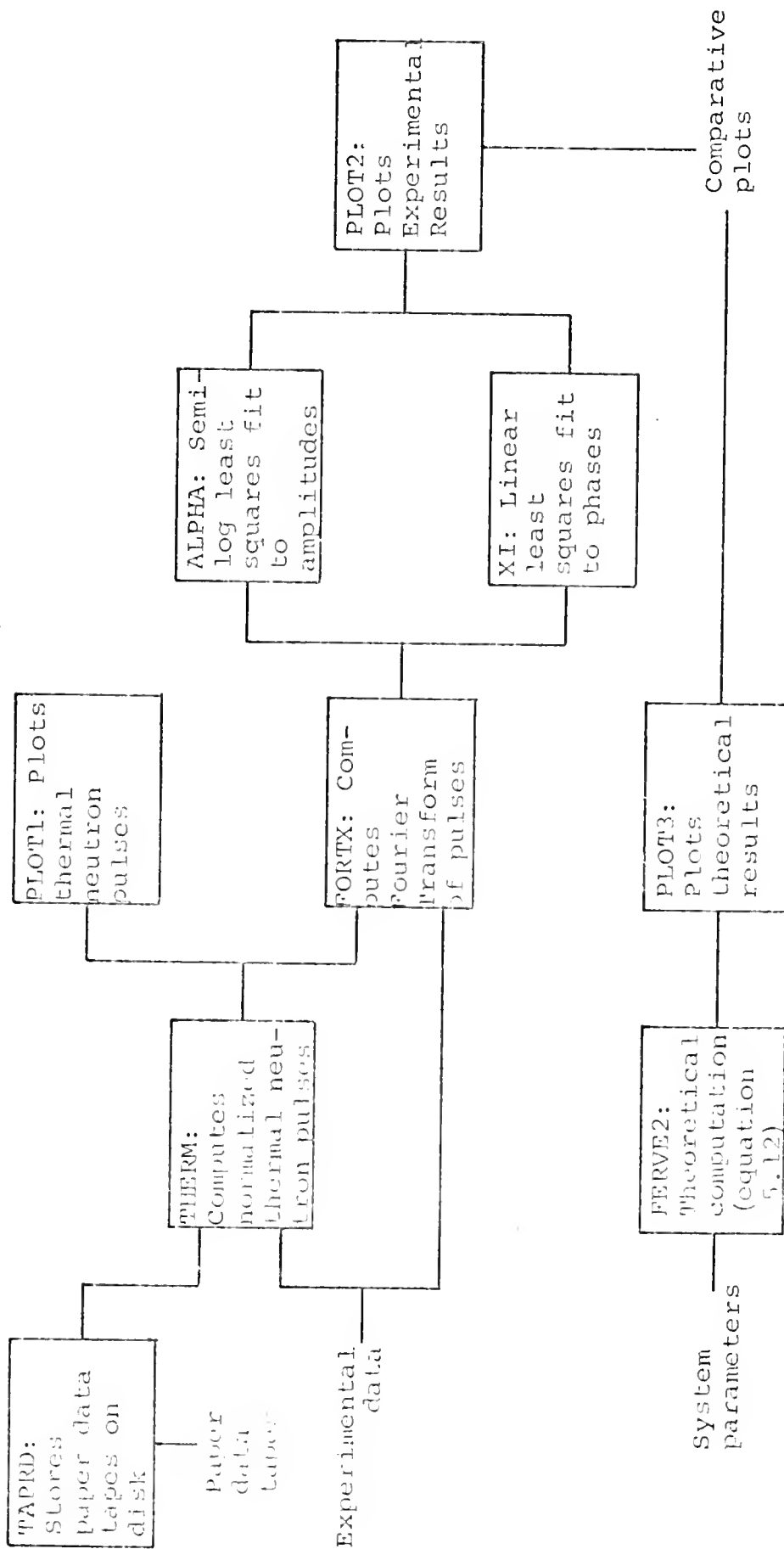
FIGURE 7.

INTERRELATION OF COMPUTER PROGRAMS

error and a discussion of the error is also included in Appendix A.
DuBois (7) measured the resolution times of the two detector systems
just prior to this series of experiments. Resolutions times were
determined to be 1.42 and 1.77 microseconds for the movable and
reference detector systems respectively. Since the components of the
systems had not been changed, these resolutions times were used in
this analysis.

As was mentioned in Chapter III, the 17 inch graphite stack
that had been located between the thermalizing and subcritical
assemblies was removed to obtain higher frequency content in the data.
There being less moderation, the asymptotic region of the assembly was
smaller. Dunlap (5) found the region to begin at 25 cms. Without
the graphite stack the asymptotic region began at 50 cms.

The asymptotic region was established by scanning[1] the data.
The undesirable characteristics of higher spatial and energy modes at
axial positions near the source and end effects at positions far from
the source tend to increase the computed values of α and ξ. In regions
where neither effect is significant minimum values of α and ξ are
computed. These minimum values were determined by computing α and ξ
using a four point scan of the data. Then a five point scan was used
and the minima were compared with the previous ones. If they differed
by less than 1% the additional data point was considered to be in the
asymptotic region. Progressively higher point scans were used until
the minimal differences exceeded 1%. The data point producing this

---

1. See the Special Controls Section of The ALPHA program des-
cription in Appendix D.

deviation was excluded. The 1% criterion is based on the results of Booth, Perez and Hartley (16) who found a 1% tolerance in the measurement of α and ξ. A consistent asymptotic range, for all frequencies in both experiments, was found to be 50-75 cms. The end point was the same as that determined by Dunlap (6).

In some cases deviating trends in the amplitudes and phases were obviously present. Deviations at a given axial position increased or decreased with increased frequency. In these cases the data points were eliminated, beginning at certain frequencies. The criteria for elimination were:

a)   the obvious deviating trend at maximum frequency

b)   the existence of a $0.25\%^2$ difference in α and ξ between the least squares computations which included and excluded the data point in question.

Once a 0.25% deviation was observed the data for higher frequencies at the given position were also eliminated.

In both experiments an expansion of the real and imaginary components of the experimental ρ^2 in powers of ω(rad/sec) was made. The expansions are:

$$\alpha^2 - \xi^2 = P_0 + P_2\omega^2 + P_4\omega^4$$

---

2.   Deviations greater than 0.25% produced significant discontinuities in α and ξ when subsequent data points were eliminated.

and

$$2\alpha\xi = P_1\omega + P_3\omega^3.$$

The P's were determined by using the UFNLLS Code (20). Data above
300 cps were excluded in the polynomial fitting because statistical
fluctuations were deemed too significant.

Perez, Ohanian and Dunlap (19) have found that greater sensitivity
of the dispersion law to thermalization and diffusion parameters
exists when it is considered in the ρ^2 plane rather than in the ρ plane.
No analysis will be conducted in this manner because the experimental
errors appear to be more significant when the ρ^2 dispersion law is
considered. The dispersion laws in the ρ^2 plane will be shown to
aid any future studies that may be conducted along these lines.

The remainder of this chapter will be divided into four parts.
The first part will deal with the continuous mode analysis. The pure
moderator and one fuel rod pulsed experiments will then be analyzed
and finally a lattice of fuel rods will be considered.

Continuous Mode Analysis

The continuous mode data serve three purposes:

1) it offers a standard for comparison with the zero
   frequency component of the thermal neutron pulse

2) it provides a standard for normalization of minor
   anomalies in the pulsed data due to source or count-
   ing system variations

3) it establishes a standard for comparison with previous
   and subsequent experiments.

It becomes apparent that the continuous mode data are the key to the reproducibility of the experiment.

At each data position the thermal ratio, TR, is computed from the relation

$$TR = \left(\dfrac{N_{mov}}{N_{ref}} \right)_{bare} - \left(\dfrac{N_{mov}}{N_{ref}} \right)_{cd}$$

where

N   = the resolution corrected scaler counts

mov   = the movable detector system

ref   = the reference detector system

bare = the bare run data

cd   = the cadmium run data.

TR, as a function of distance was fitted to an exponential function using the least squares technique. The logarithmic decay constants for each experiment are given in Table 3.

TABLE 3.

CONTINUOUS MODE DECAY CONSTANTS

Experiment	Asymptotic Range	Alpha (cm^{-1})
Heavy Water	50-75 cms	- 0.0371
Heavy Water-One Fuel Rod	50-75 cms	- 0.0385

As will be seen, there was no normalization required for anomalies in the data. In this case the continuous mode data are used only for comparative purposes.

Heavy Water Pulsed Experiment

The thermal neutron pulses obtained in the heavy water only experiment are shown in Figure 8. The last 512 channels contain few or no counts. These are insignificant compared to the peak counts of approximately 43,000 counts and are not plotted. The pulses are normalized to the 50 cm pulse. Each channel represents 50 microseconds. These pulses are the ones that were numerically Fourier Transformed.

The Fourier Transformed fluxes and the least squares fit to the amplitudes and phases are shown in Figures 9. and 10. The maximum deviations of points included in the least squares fit from the least squares fit are 4% in α and 1% in ξ. Theoretical values of α and ξ computed from equation [2.12] are listed in Table 4. while the resulting experimental values are listed in Table 5. Theoretical and experimental values of α are illustrated in Figure 11. A maximum deviation of 2.1% occurs at 300 cps. The smaller deviations at higher frequencies is fortuitous. Statistical deviations at these higher frequencies are too significant to allow valid analyses.

An illustration of ξ, similar to the one of α, is given in Figure 12. In this case the experimental data agree with theory within 1.5%.

The heavy water dispersion laws are shown in Figures 13. and 14. The former shows the experimental and theoretical dispersion laws of this work and the latter shows a comparison of this work with that of Dunlap (6). Both comparisons are reasonably good. The better high frequency content of these data over that of Dunlap's (6) is demon-
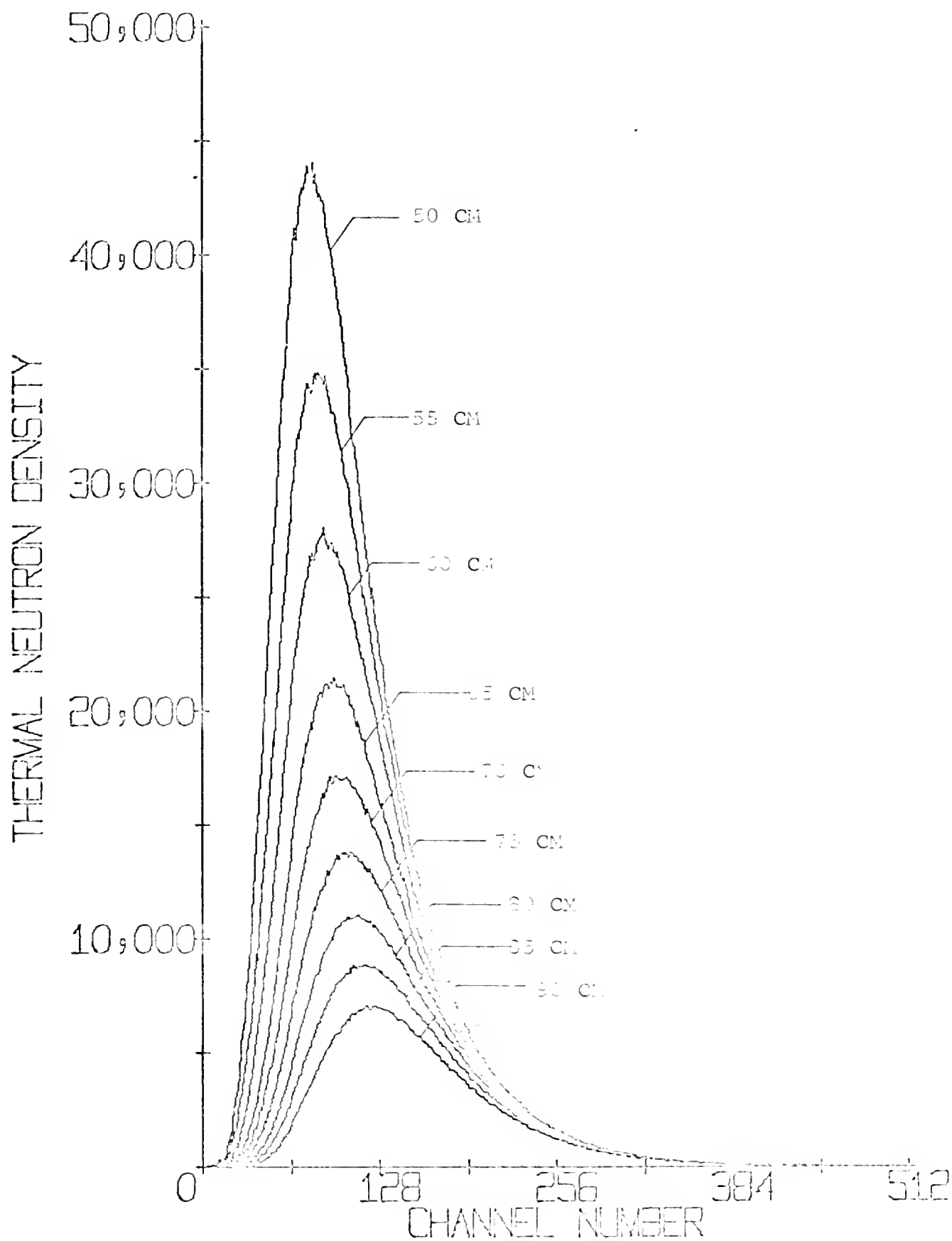
FIGURE 9.

NORMALIZED NEUTRON PULSES IN HEAVY WATER
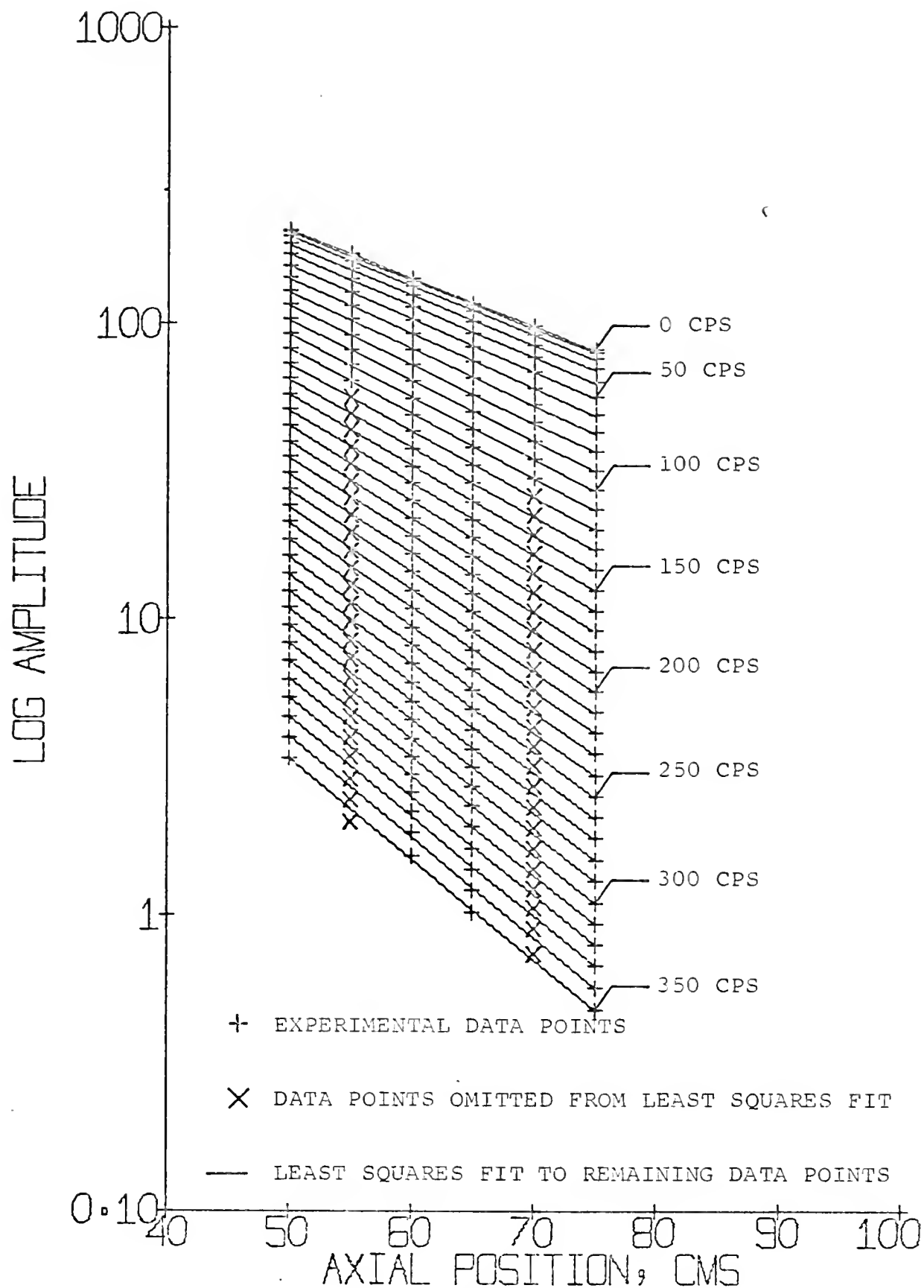
FIGURE 9.
EXPERIMENTAL AMPLITUDES
FOR HEAVY WATER
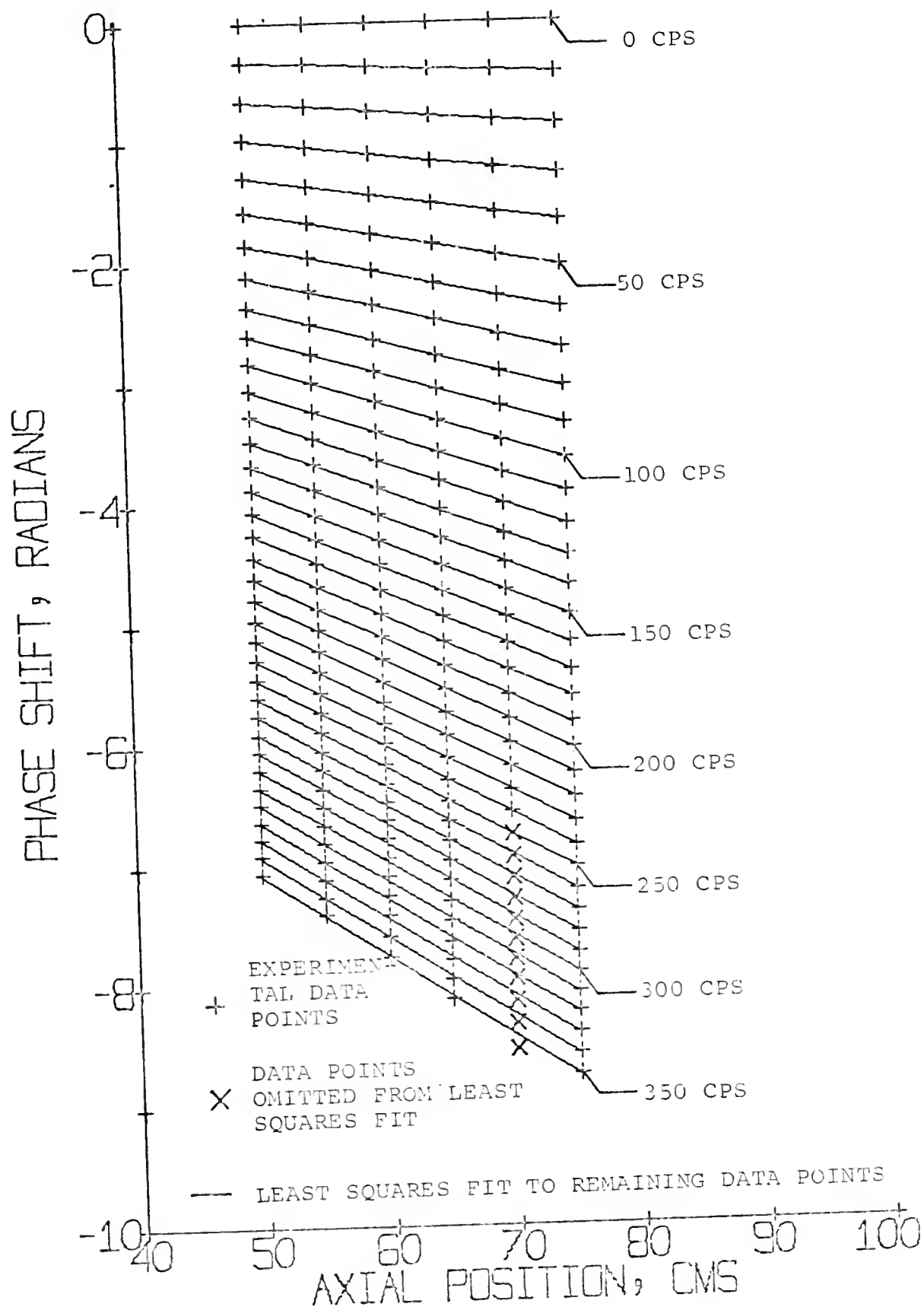
FIGURE 10.

EXPERIMENTAL PHASES FOR HEAVY WATER

TABLE 4.

THEORETICAL VALUES OF ALPHA AND XI
FOR HEAVY WATER

FREQUENCY(CPS)	ALPHA(1/CM)	XI(1/CM)
0.	-0.0375	0.0000
10.	-0.0377	-0.0041
20.	-0.0384	-0.0081
30.	-0.0393	-0.0118
40.	-0.0405	-0.0153
50.	-0.0419	-0.0186
60.	-0.0433	-0.0215
70.	-0.0447	-0.0243
80.	-0.0462	-0.0269
90.	-0.0477	-0.0294
100.	-0.0491	-0.0317
110.	-0.0506	-0.0339
120.	-0.0520	-0.0359
130.	-0.0534	-0.0379
140.	-0.0547	-0.0398
150.	-0.0561	-0.0416
160.	-0.0574	-0.0434
170.	-0.0587	-0.0451
180.	-0.0600	-0.0467
190.	-0.0612	-0.0483
200.	-0.0624	-0.0499
210.	-0.0636	-0.0514
220.	-0.0648	-0.0528
230.	-0.0660	-0.0543
240.	-0.0671	-0.0557
250.	-0.0683	-0.0570
260.	-0.0694	-0.0584
270.	-0.0705	-0.0597
280.	-0.0716	-0.0609
290.	-0.0726	-0.0622
300.	-0.0737	-0.0634
310.	-0.0747	-0.0646
320.	-0.0758	-0.0658
330.	-0.0768	-0.0670
340.	-0.0778	-0.0681
350.	-0.0788	-0.0692

TABLE 5.

EXPERIMENTAL VALUES OF ALPHA AND XI
FOR HEAVY WATER

.

FREQUENCY(CPS)	ALPHA(1/CM)	XI(1/CM)
0.	-0.0376	0.0000
10.	-0.0378	-0.0040
20.	-0.0383	-0.0079
30.	-0.0391	-0.0117
40.	-0.0402	-0.0153
50.	-0.0414	-0.0187
60.	-0.0428	-0.0218
70.	-0.0443	-0.0247
80.	-0.0458	-0.0275
90.	-0.0473	-0.0300
100.	-0.0488	-0.0324
110.	-0.0503	-0.0347
120.	-0.0519	-0.0368
130.	-0.0534	-0.0388
140.	-0.0549	-0.0407
150.	-0.0564	-0.0425
160.	-0.0578	-0.0442
170.	-0.0593	-0.0458
180.	-0.0606	-0.0473
190.	-0.0619	-0.0488
200.	-0.0631	-0.0503
210.	-0.0643	-0.0519
220.	-0.0655	-0.0533
230.	-0.0669	-0.0547
240.	-0.0682	-0.0561
250.	-0.0696	-0.0572
260.	-0.0708	-0.0582
270.	-0.0719	-0.0592
280.	-0.0730	-0.0603
290.	-0.0741	-0.0613
300.	-0.0753	-0.0623
310.	-0.0762	-0.0631
320.	-0.0769	-0.0641
330.	-0.0776	-0.0652
340.	-0.0782	-0.0664
350.	-0.0786	-0.0677
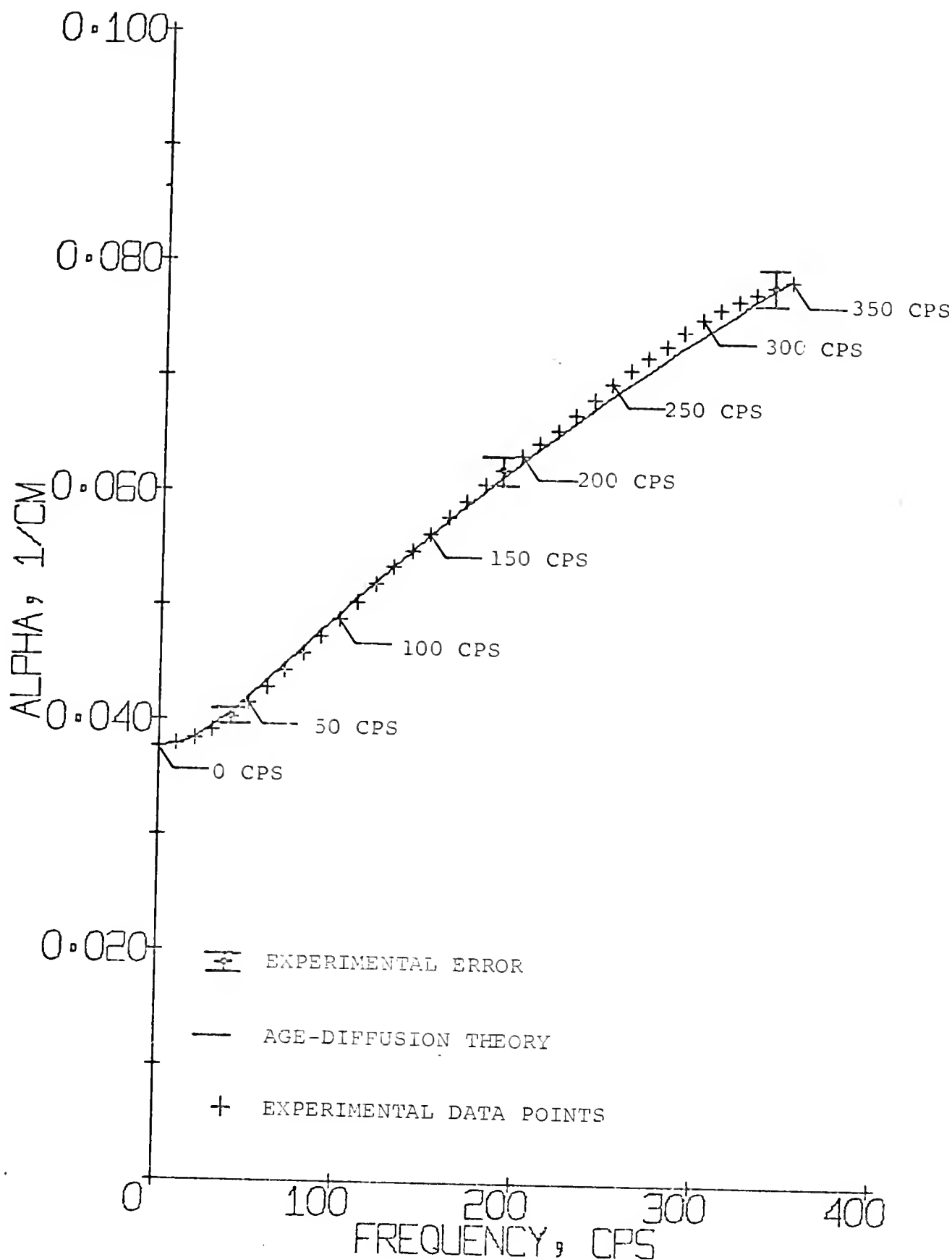
FIGURE 11.

EXPERIMENTAL AND THEORETICAL
VALUES OF ALPHA FOR HEAVY WATER
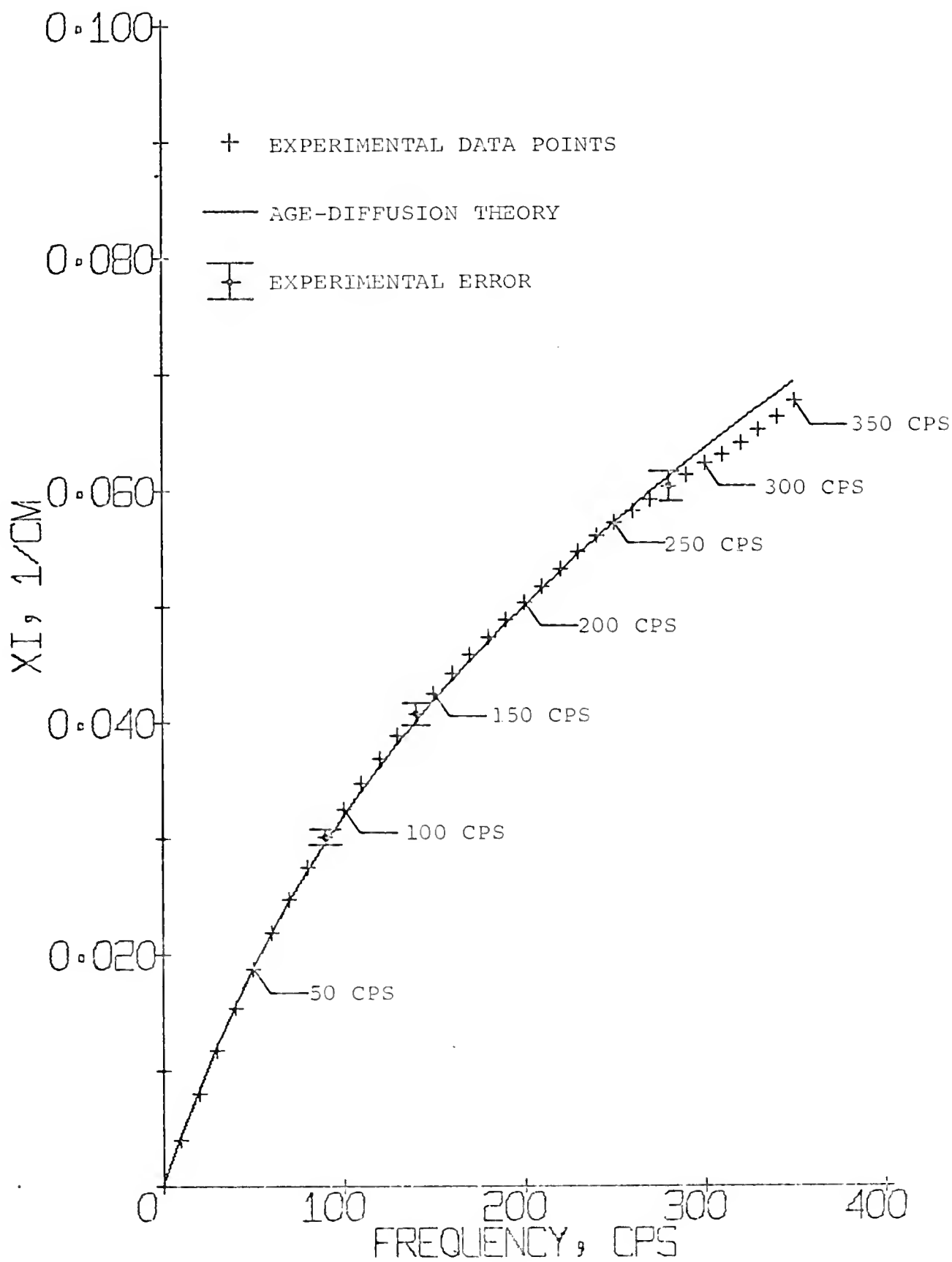
FIGURE 12.

EXPERIMENTAL AND THEORETICAL
VALUES OF XI FOR HEAVY WATER
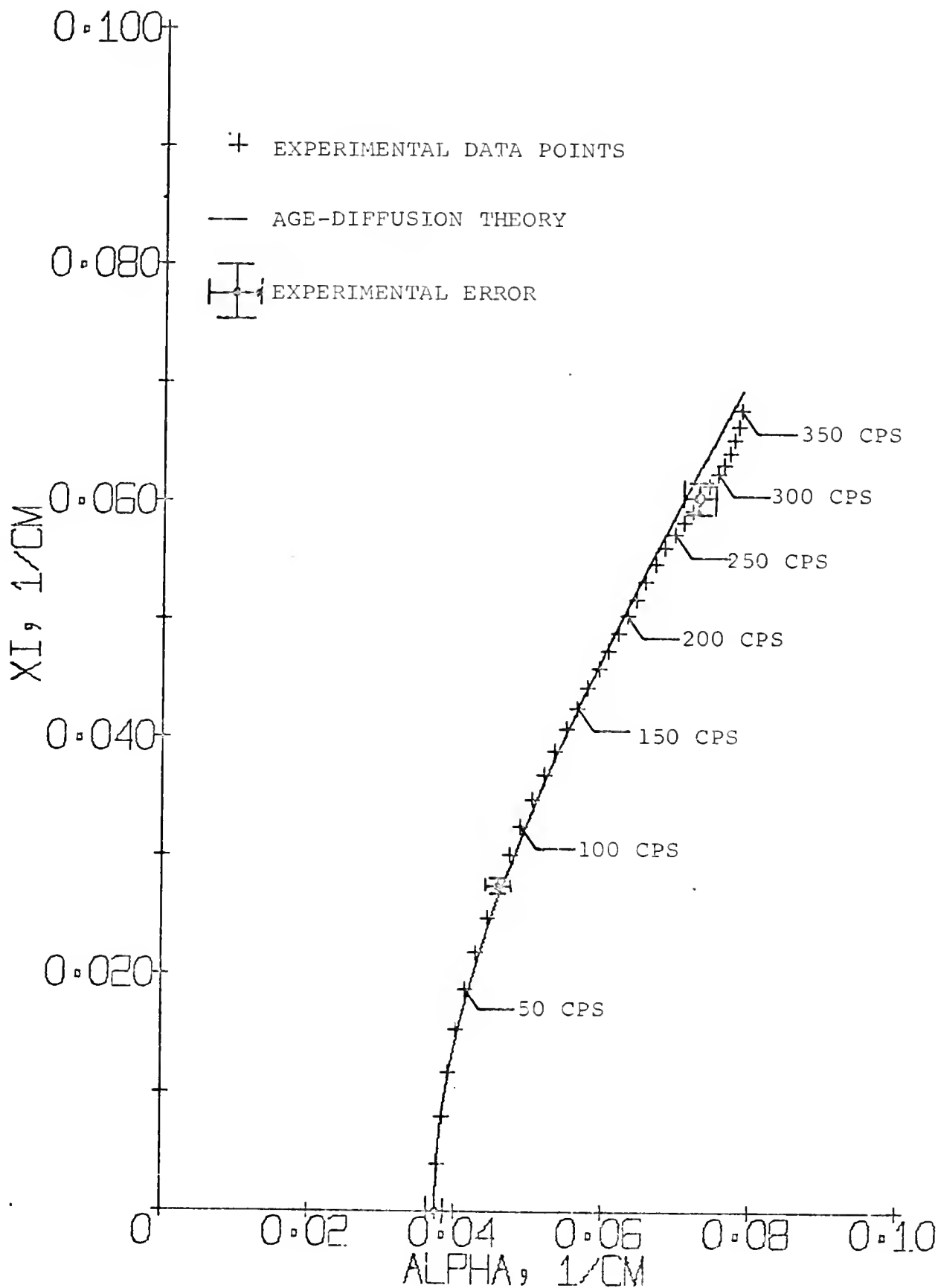
FIGURE 13.

EXPERIMENTAL AND THEORETICAL DISPERSION
LAWS IN RHO PLANE FOR HEAVY WATER
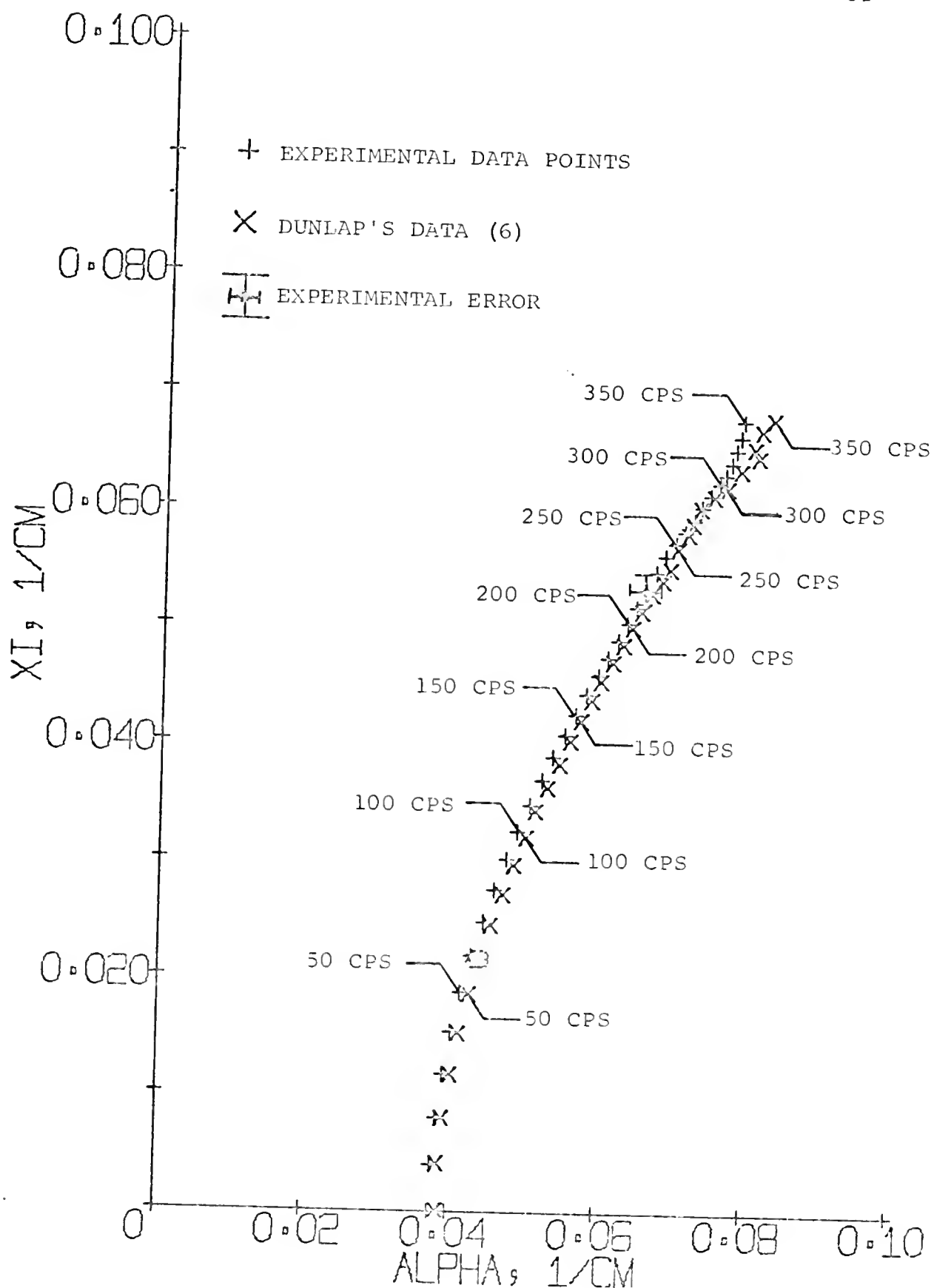
FIGURE 14.

COMPARISON OF EXPERIMENTAL DISPERSION LAWS
IN RHO PLANE FOR HEAVY WATER

strated by the more consistent results in the 240-310 cps range. Results of the two experiments differ by 3.2% in α, a phenomenon attributable to a difference in heavy water purity.

The imaginary and real components of ρ^2 are shown in Figures 15. and 16. respectively. The polynomial fits are included in each plot. Values obtained for the expansion coefficients are listed in Table 6. Resultant values for the thermalization and diffusion parameters are included. Values obtained by Dunlap (6) are also listed. P_0 and P_1 agree within 7.1% and 1.2% respectively but the other coefficients differ radically in magnitude and sign. An examination of Figure 16. shows that the real component of ρ^2 is erratic, exhibiting oscillations and increasing less rapidly than Dunlap's results (6). The experimental values of the real and imaginary components of ρ^2 are listed in Table 7. The experimental and theoretical dispersion laws for heavy water in the ρ^2 plane are shown in Figure 17. The vertical line result of Age-Diffusion Theory is due to the neglect of thermalization effects. The experimental dispersion law obtained by Dunlap (6) is also shown. The theoretical dispersion law obtained by Perez, Ohanian and Dunlap (19) is also included. The latter includes thermalization effects. Apart from the shift in α due to a difference in heavy water purity, the two sets agree relatively well at low frequencies but pronounced differences occur at high frequencies. The anomalous behavior of the heavy water data in this experiment is more apparent here.

In the heterogeneous analysis the dispersion law in the ρ plane is required. This agrees reasonably well with both theory and Dunlap's data (6).
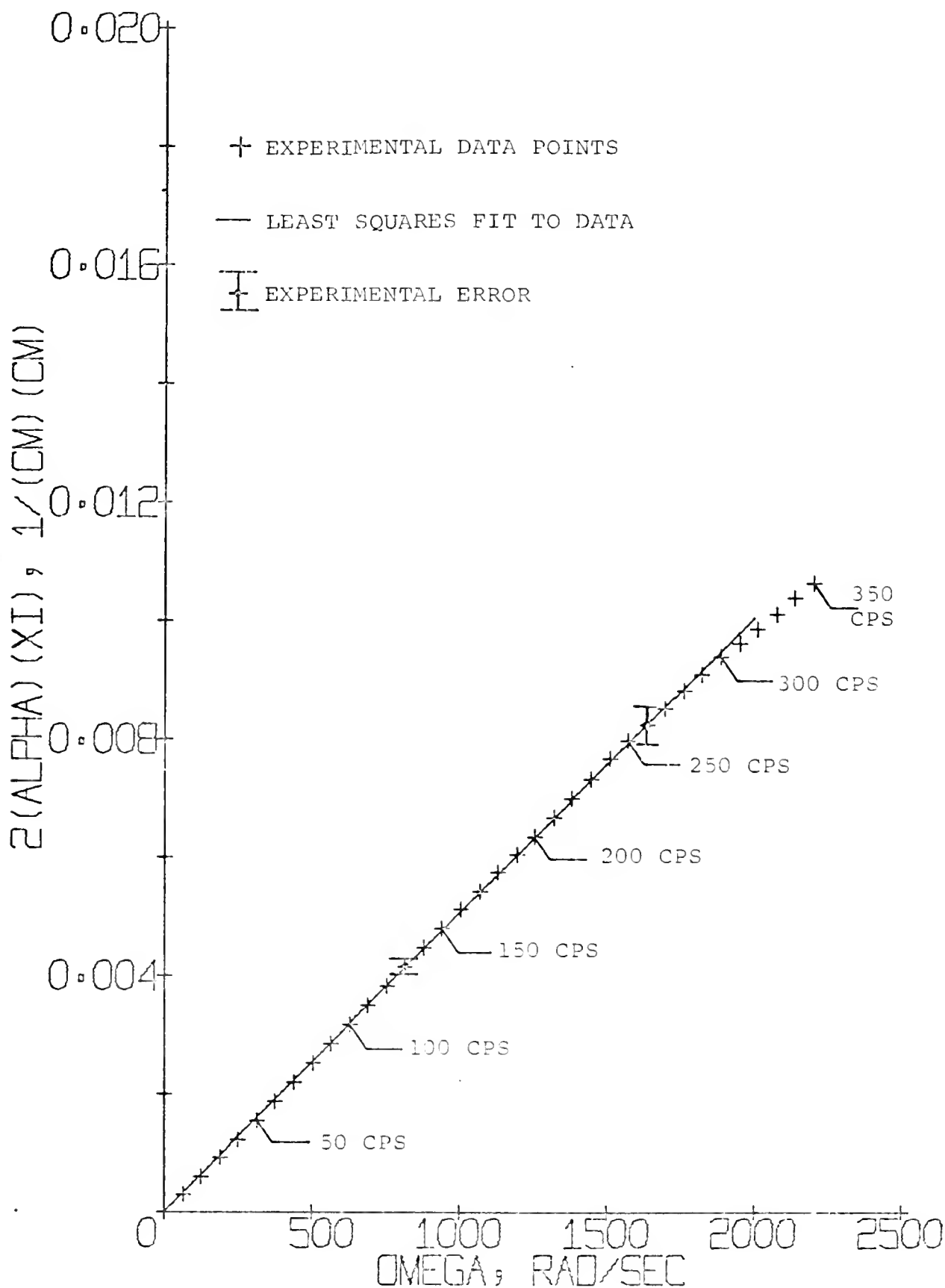
FIGURE 15.

IMAGINARY COMPONENT OF RHO
SQUARED FOR HEAVY WATER
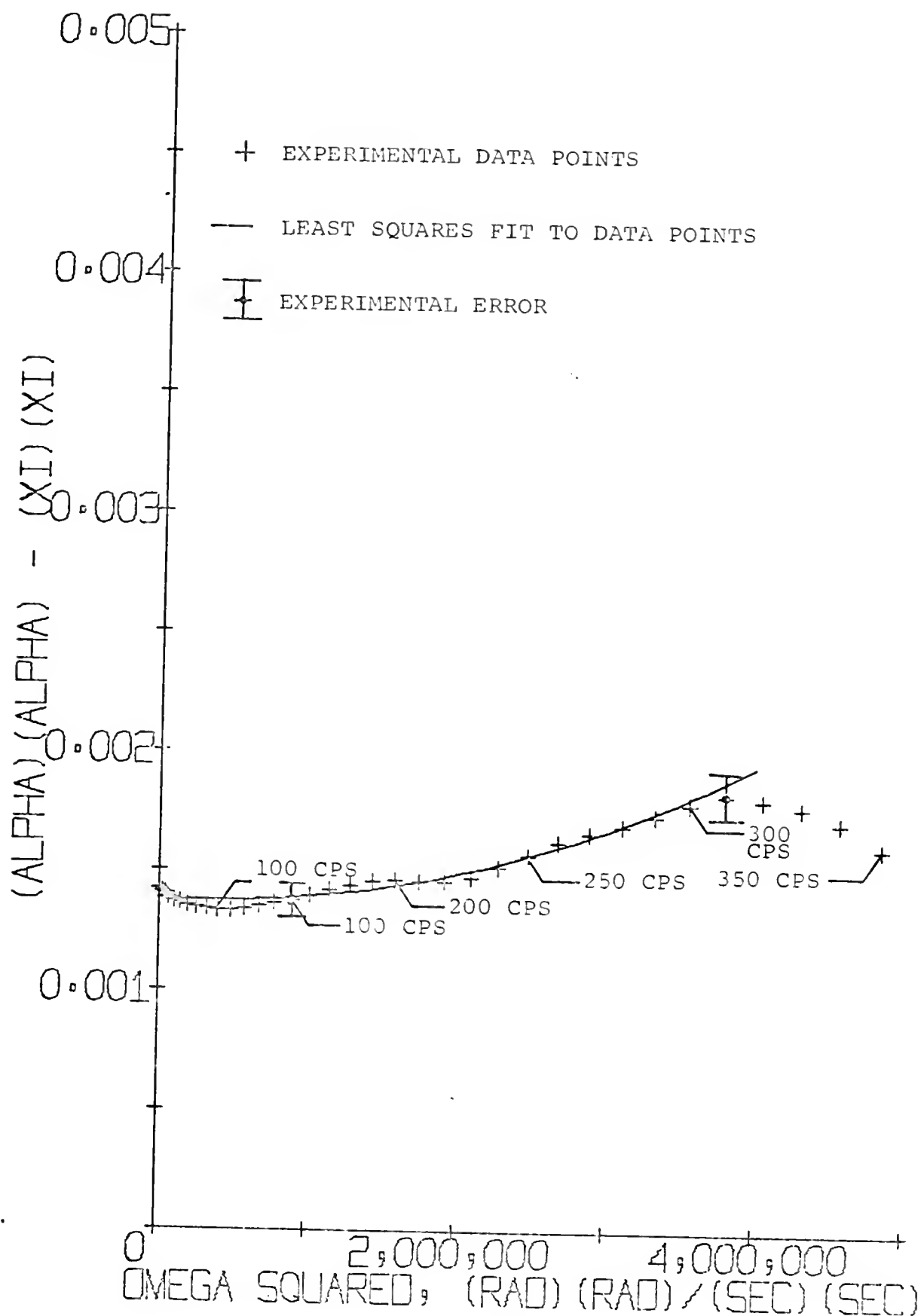
FIGURE 16.

REAL COMPONENT OF RHO
SQUARED FOR HEAVY WATER

TABLE 6.

EXPANSION COEFFICIENTS OF RHO SQUARED AND THERMALIZATION AND DIFFUSION PARAMETERS FOR HEAVY WATER

QUANTITY	EXPERIMENTAL VALUE	EXPERIMENTAL VALUE OF DUNLAP (16, 19)
P_0 [cm^{-2}]	1.3746×10^{-3}	1.4713×10^{-3}
P_1 [cm^{-2} sec]	5.0613×10^{-6}	5.0083×10^{-6}
P_2 [cm^{-2} sec^2]	-3.1374×10^{-11}	3.9684×10^{-11}
P_3 [cm^{-2} sec^3]	8.443×10^{-15}	1.8026×10^{-14}
P_4 [cm^{-2} sec^4]	4.3259×10^{-17}	2.5045×10^{-17}
α_0 [sec^{-1}]	20	20
D_0 [cm^2 sec^{-1}]	1.976×10^5	1.996×10^5
C_0 [cm^4 sec^{-1}]	***	3.73×10^5

*** Lack of high frequency content of the heavy water data prevented a suitable determination of C_0.

TABLE 7.

EXPERIMENTAL VALUES OF REAL AND IMAGINARY COMPONENTS OF RHO SQUARED FOR HEAVY WATER

OMEGA(RAD/SEC)	OMEGA SQUARED	REAL	IMAGINARY
0.000	0.0	0.0014189	0.0000000
62.831	3947.8	0.0014159	0.0003043
125.663	15791.3	0.0014083	0.0006109
188.495	35530.5	0.0013970	0.0009211
251.327	63165.3	0.0013841	0.0012354
314.159	98695.8	0.0013714	0.0015536
376.990	142122.0	0.0013600	0.0018746
439.822	193443.3	0.0013500	0.0021977
502.654	252661.3	0.0013421	0.0025221
565.486	319774.6	0.0013362	0.0028471
628.318	394783.4	0.0013325	0.0031728
691.140	477687.9	0.0013315	0.0034982
753.931	568488.1	0.0013401	0.0038270
816.313	667183.9	0.0013484	0.0041510
879.645	773775.4	0.0013593	0.0044734
942.476	888262.6	0.0013746	0.0047949
1005.308	1010645.4	0.0013932	0.0051153
1068.140	1140924.2	0.0014168	0.0054360
1130.972	1279098.4	0.0014403	0.0057505
1193.804	1425168.1	0.0014554	0.0060573
1256.636	1579133.7	0.0014597	0.0063602
1319.468	1740994.7	0.0014553	0.0066659
1382.299	1910751.7	0.0014557	0.0069836
1445.131	2088404.1	0.0014764	0.0073278
1507.963	2273952.7	0.0015166	0.0076626
1570.795	2467396.0	0.0015690	0.0079712
1633.626	2668735.9	0.0016250	0.0082580
1696.458	2877971.1	0.0016602	0.0085311
1759.290	3095101.9	0.0016927	0.0088207
1822.122	3320128.4	0.0017350	0.0091095
1884.953	3553050.7	0.0017877	0.0093906
1947.785	3793868.0	0.0018256	0.0096284
2010.617	4042581.6	0.0018043	0.0098742
2073.449	4299190.4	0.0017778	0.0101361
2136.281	4563696.3	0.0017149	0.0103992
2199.113	4836098.9	0.0016073	0.0106566
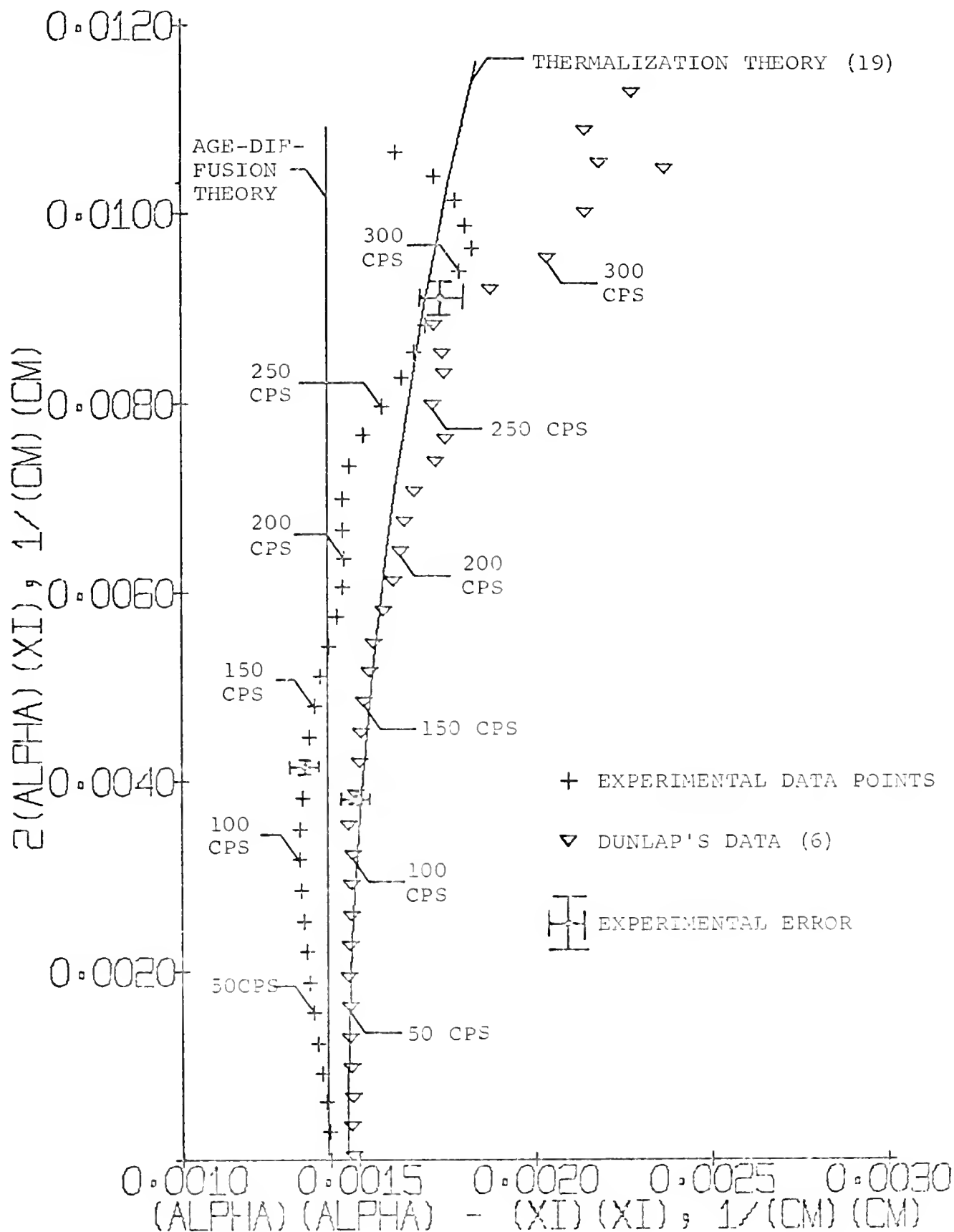
FIGURE 17.

EXPERIMENTAL AND THEORETICAL DISPERSION
LAWS IN RHO SQUARED PLANE FOR HEAVY WATER

One Fuel Rod Pulsed Experiment

In Figure 18. the thermal neutron pulses are shown for the various axial positions. Again, the last 512 channels are not shown and each channel represents 50 microseconds. All pulses are normalized to the pulse at 50 cm.

Figures 19. and 20. show the Fourier transformed fluxes. At each position considered in the final analysis, the amplitude and phase of the frequency components are shown. Included are the least squares fits to the data. Deviations between the least squares fit and the data points considered in the least square fit are small, the largest being less than 3% in amplitude and less than 1% in phase. The theoretical results for α and ξ are given in Table 8. and the experimental results are given in Table 9. The results of both are illustrated in Figures 21. and 22. The deviations at high frequencies caused by the neglect of thermalization effects, are seen in the illustrations. Theory under estimates α and over estimates ξ at high frequencies. Maximum deviations, however, are less than 5.5% in α and 6.5% in ξ. These deviations occur at 310 cps and 320 cps respectively. The closer agreement between theory and experiment at higher frequencies is again fortuitous. In the subsequent analyses data above 300 cps, where maximum deviations were 5.1% in α and 4.9% in ξ, were excluded.

Both the experimental and theoretical dispersion laws are shown in Figure 23. The theoretical dispersion law is obtained from equation [2.12] with $\gamma = 0.25$. This value of γ gave agreement at zero frequency with the experimental data and the resulting
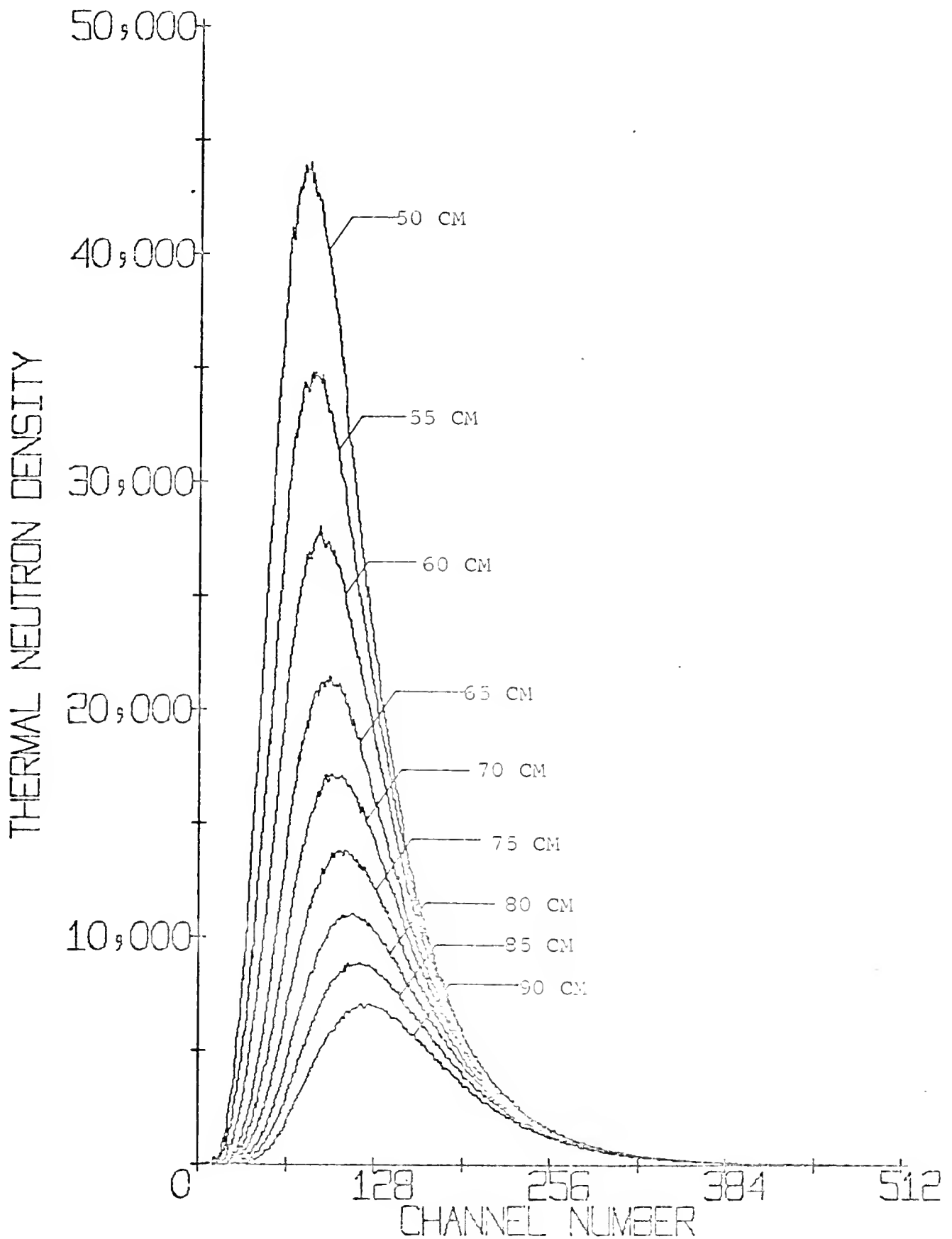
FIGURE 18.

NORMALIZED THERMAL NEUTRON PULSES FOR
HEAVY WATER--ONE FUEL ROD SYSTEM

60
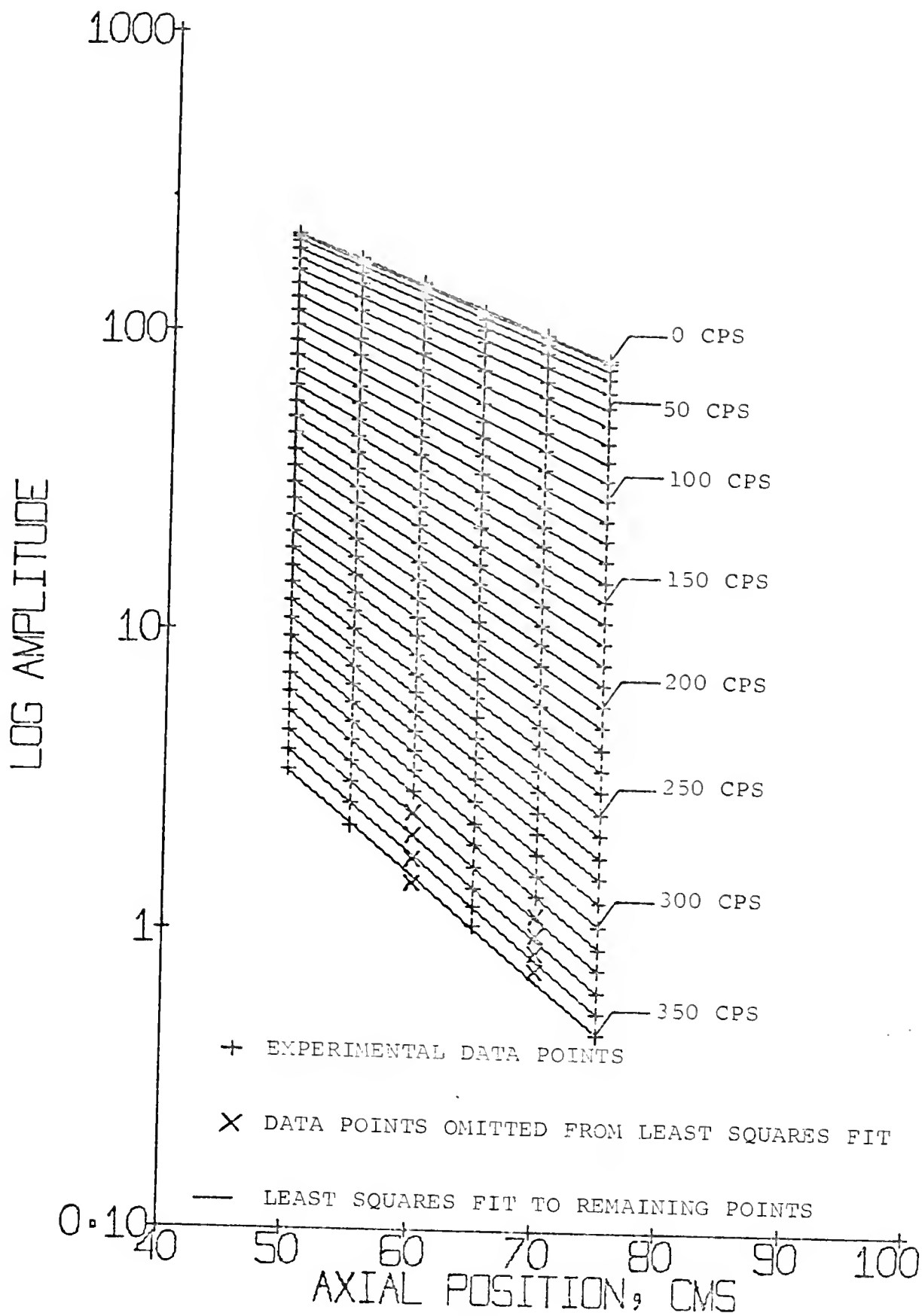
FIGURE 19.

EXPERIMENTAL AMPLITUDES FOR
HEAVY WATER-ONE FUEL ROD SYSTEM
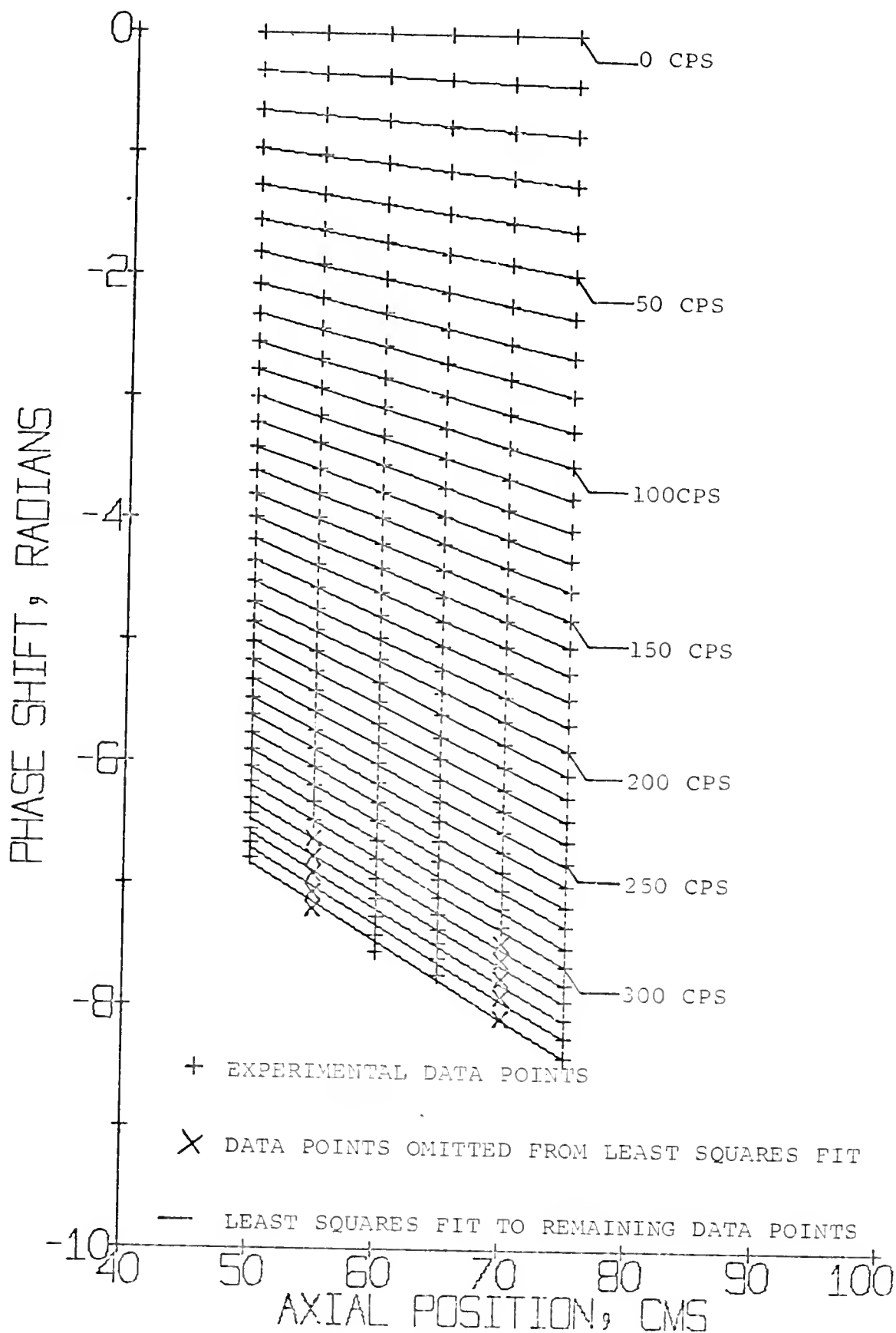
FIGURE 20.

EXPERIMENTAL PHASES FOR HEAVY
WATER-ONE FUEL ROD SYSTEM

TABLE 8.

THEORETICAL VALUES OF ALPHA AND XI
FOR HEAVY WATER-ONE FUEL ROD SYSTEM

FREQUENCY(CPS)	ALPHA(1/CM)	XI(1/CM)
0.	-0.0379	0.0000
10.	-0.0381	-0.0040
20.	-0.0387	-0.0078
30.	-0.0397	-0.0115
40.	-0.0408	-0.0149
50.	-0.0421	-0.0181
60.	-0.0434	-0.0211
70.	-0.0449	-0.0238
80.	-0.0463	-0.0264
90.	-0.0477	-0.0288
100.	-0.0492	-0.0311
110.	-0.0506	-0.0332
120.	-0.0520	-0.0353
130.	-0.0533	-0.0373
140.	-0.0547	-0.0391
150.	-0.0560	-0.0409
160.	-0.0573	-0.0427
170.	-0.0586	-0.0444
180.	-0.0599	-0.0460
190.	-0.0611	-0.0476
200.	-0.0624	-0.0491
210.	-0.0636	-0.0506
220.	-0.0648	-0.0520
230.	-0.0659	-0.0534
240.	-0.0671	-0.0548
250.	-0.0682	-0.0562
260.	-0.0693	-0.0575
270.	-0.0704	-0.0588
280.	-0.0715	-0.0600
290.	-0.0726	-0.0613
300.	-0.0737	-0.0625
310.	-0.0747	-0.0637
320.	-0.0757	-0.0648
330.	-0.0768	-0.0660
340.	-0.0778	-0.0671
350.	-0.0788	-0.0682

TABLE 9.

EXPERIMENTAL VALUES OF ALPHA AND XI
FOR HEAVY WATER-ONE FUEL ROD SYSTEM

FREQUENCY(CPS)	ALPHA(1/CM)	XI(1/CM)
0.	-0.0380	0.0000
10.	-0.0382	-0.0038
20.	-0.0387	-0.0076
30.	-0.0395	-0.0112
40.	-0.0405	-0.0147
50.	-0.0418	-0.0179
60.	-0.0431	-0.0209
70.	-0.0446	-0.0236
80.	-0.0461	-0.0262
90.	-0.0476	-0.0286
100.	-0.0491	-0.0309
110.	-0.0505	-0.0330
120.	-0.0520	-0.0351
130.	-0.0535	-0.0370
140.	-0.0549	-0.0388
150.	-0.0564	-0.0406
160.	-0.0579	-0.0422
170.	-0.0593	-0.0437
180.	-0.0606	-0.0452
190.	-0.0619	-0.0467
200.	-0.0632	-0.0482
210.	-0.0646	-0.0496
220.	-0.0660	-0.0510
230.	-0.0674	-0.0522
240.	-0.0688	-0.0534
250.	-0.0701	-0.0544
260.	-0.0714	-0.0555
270.	-0.0728	-0.0566
280.	-0.0741	-0.0576
290.	-0.0755	-0.0586
300.	-0.0771	-0.0592
310.	-0.0783	-0.0599
320.	-0.0791	-0.0604
330.	-0.0796	-0.0616
340.	-0.0799	-0.0628
350.	-0.0800	-0.0651
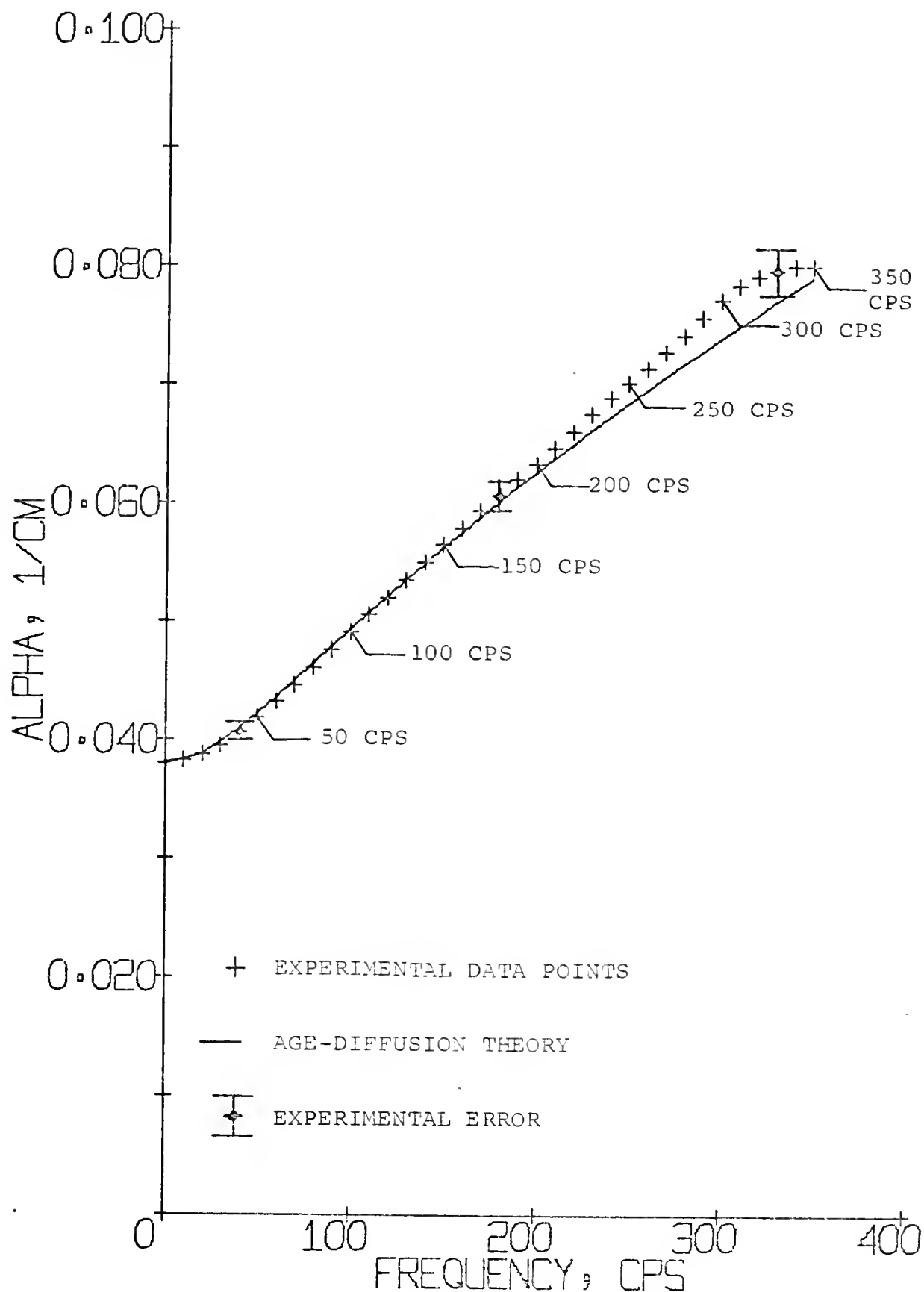
FIGURE 21.

EXPERIMENTAL AND THEORETICAL VALUES OF
ALPHA FOR HEAVY WATER-ONE FUEL ROD SYSTEM
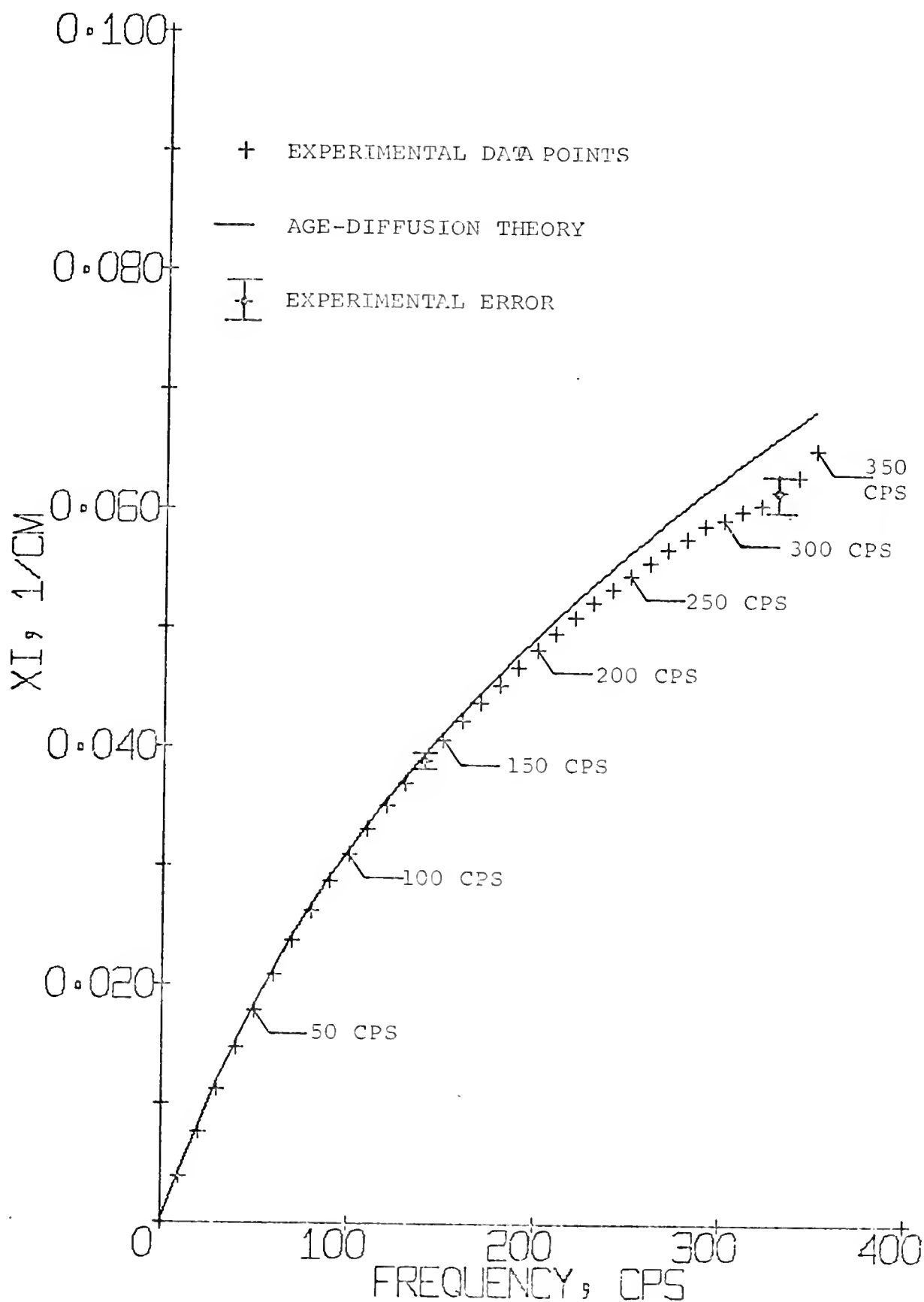
FIGURE 22.

EXPERIMENTAL AND THEORETICAL VALUES OF
XI FOR HEAVY WATER-ONE FUEL ROD SYSTEM
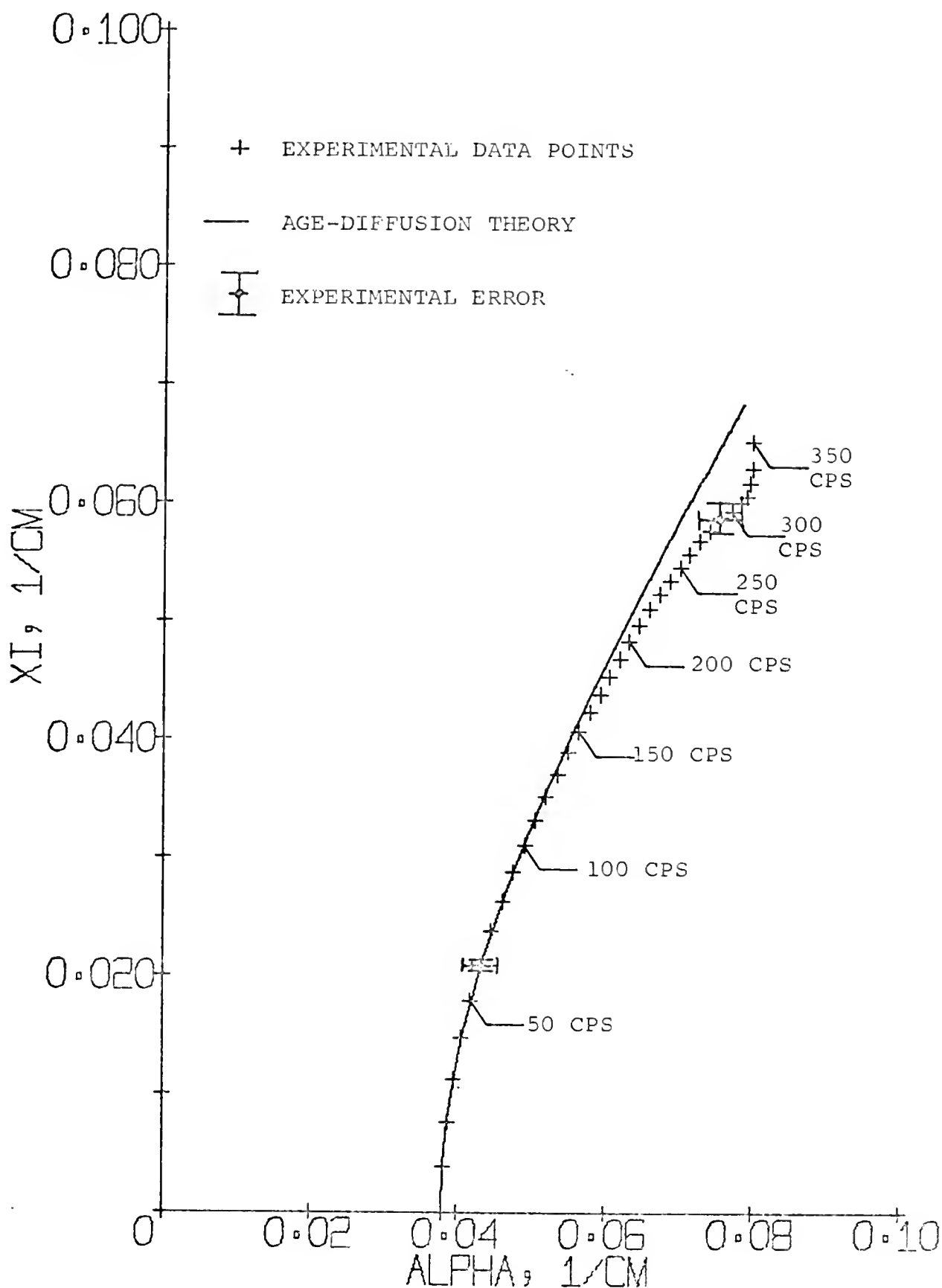
FIGURE 23.

EXPERIMENTAL AND THEORETICAL DISPERSION LAWS IN
RHO PLANE FOR HEAVY WATER-ONE FUEL ROD SYSTEM

dispersion law is shown. Again, the deviation at high frequency is seen. Since the determination of γ is based on the zero frequency data where theory and experiment better agree, the high frequency deviation has no significant effect on the experimental value.

The sensitivity of the fit to γ was determined by computing the dispersion law for several values of γ. It was found that

$$\delta \gamma = 22 \; \delta \; \alpha'$$

where α' is the zero frequency α. Assuming that α is accurate to $\pm$ 0.0008 (2.1% error) this sensitivity allows the determination of γ to $\pm$ 0.02. The feasibility of using the neutron wave technique to measure γ based on the dispersion law is demonstrated.

Attention is now turned to the polynomial expansion of ρ^2 in powers ω. The expansion coefficients obtained from the UFNLLS Code (20) are listed in Table 10.

TABLE 10.

EXPANSION COEFFICIENTS OF RHO SQUARED
FOR HEAVY WATER - ONE FUEL ROD SYSTEM

COEFFICIENTS	UFNLLS RESULT
P_0 [cm^{-2}]	1.4285×10^{-3}
P_1 [cm^{-2}sec]	4.8545×10^{-6}
P_2 [cm^{-2}sec^2]	6.6175×10^{-11}
P_3 [cm^{-2}sec^3]	1.2051×10^{-14}
P_4 [cm^{-2}sec^4]	5.8555×10^{-17}

Figures 24. and 25. show the experimental data and the least squares fit

for the imaginary and real parts of ρ^2 respectively. The $2\alpha\xi$ fit has

a maximum deviation of 1.5% from the experimental data at 300 cps while

$\alpha^2 - \xi^2$ has a maximum deviation of 2.5% at 300 cps. Experimental

results for $2\alpha\xi$ and $\alpha^2 - \xi^2$ are listed in Table 11.

In Chapter II P_0 and P_1 were related to γ. Using these relations,

equations [2.13] and [2.14], γ was computed to be 0.29 in terms of P_0

and 0.31 in terms of P_1. The difference of these values from the 0.25

value obtained in the dispersion law fit are now discussed individually.

The P_0 value of γ is based principally on zero frequency data, P_0

being the zero frequency intercept of $\alpha^2 - \xi^2$. It follows that fairly

good agreement should exist between the two values of γ, 0.25 and 0.29,

both being determined from zero frequency data. Nonetheless, a 16%

difference exists in γ. This discrepancy is explained by recalling

that P_0, the zero frequency intercept, was a computed parameter in the

least squares fit to the experimental data. This value is less than

the observed intercept, a phenomenon which is caused by the minimum

occurring in the $\alpha^2 - \xi^2$ data at approximately 50 cps. The minimum

has yet to be explained, there being no established theoretical basis

for its existence. It may be the result of some systematic error. Con-

sequently, the experimental value of P_0 is in question. It is noted

that if the value of the observed intercept is used, γ is computed to

be 0.24 and this agrees within 4% with the dispersion law result.

The greater deviation of the P_1 value of γ has two causes. First,

the relation derived for γ in terms of P_1 is dependent on the full fre-

quency range, P_1 being the first derivative of the $2\alpha\xi$ function. A

more accurate model would predict a lower value of P_1. A lower value
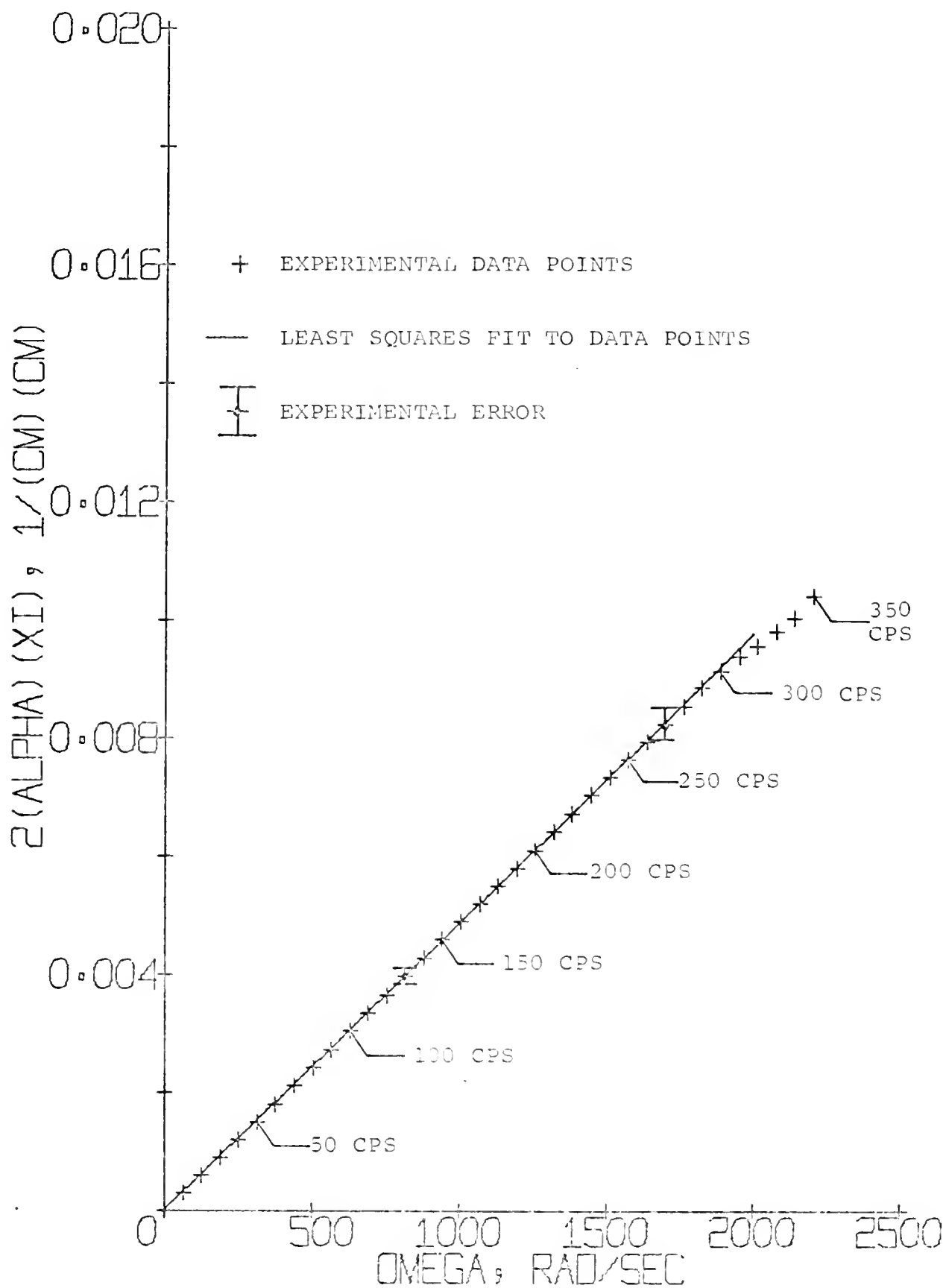
FIGURE 24.

IMAGINARY COMPONENT OF RHO SQUARED
FOR HEAVY WATER-ONE FUEL ROD SYSTEM
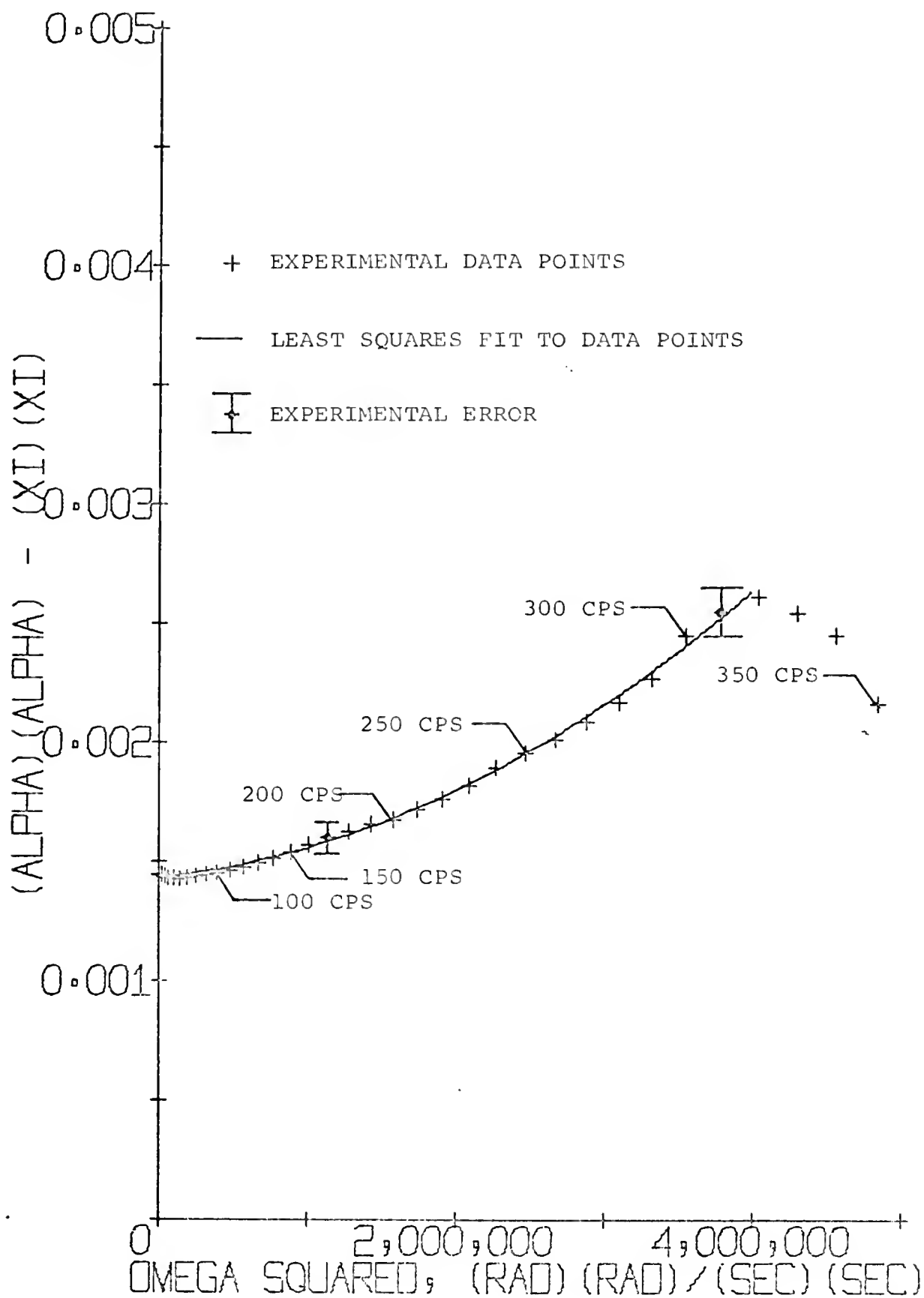
FIGURE 25.

REAL COMPONENT OF RHO SQUARED FOR
HEAVY WATER-ONE FUEL ROD SYSTEM

TABLE 11.

EXPERIMENTAL VALUES OF REAL AND IMAGINARY COMPONENTS OF RHO SQUARED FOR HEAVY WATER—ONE FUEL ROD SYSTEM

OMEGA(RAD/SEC)	OMEGA SQUARED	REAL	IMAGINARY
0.000	0.0	0.0014468	0.0000000
62.831	3947.8	0.0014455	0.0002949
125.663	15791.3	0.0014415	0.0005913
188.495	35530.5	0.0014363	0.0008908
251.327	63165.3	0.0014315	0.0011934
314.159	98695.8	0.0014282	0.0014990
376.990	142122.0	0.0014281	0.0018065
439.822	193443.8	0.0014304	0.0021147
502.654	252661.3	0.0014354	0.0024241
565.486	319774.6	0.0014438	0.0027320
628.318	394783.4	0.0014526	0.0030399
691.149	477687.9	0.0014643	0.0033485
753.981	568488.1	0.0014774	0.0036562
816.813	667183.9	0.0014921	0.0039662
879.645	773775.4	0.0015112	0.0042771
942.476	888262.6	0.0015348	0.0045890
1005.308	1010645.4	0.0015676	0.0048986
1068.140	1140924.2	0.0016016	0.0051967
1130.972	1279093.4	0.0016280	0.0054947
1193.804	1425168.1	0.0016544	0.0057953
1256.636	1579133.7	0.0016773	0.0061051
1319.468	1740994.7	0.0017161	0.0064234
1382.299	1910751.7	0.0017604	0.0067375
1445.131	2088404.1	0.0018203	0.0070574
1507.963	2273952.7	0.0018927	0.0073565
1570.795	2467396.0	0.0019571	0.0076470
1633.626	2668735.9	0.0020113	0.0079417
1696.458	2877971.1	0.0020863	0.0082558
1759.290	3095101.9	0.0021691	0.0085456
1822.122	3320128.4	0.0022690	0.0088723
1884.953	3553050.7	0.0024522	0.0091399
1947.785	3793868.0	0.0025514	0.0094011
2010.617	4042581.6	0.0026108	0.0095808
2073.449	4299190.4	0.0025451	0.0098191
2136.281	4563696.8	0.0024460	0.0100510
2199.113	4836095.9	0.0021829	0.0104173

of P_1 produces a lower value of γ. γ computed from the P_1 relation was found to be very sensitive to the value used for v_{th}. 2,480 m/sec and 2,490 m/sec yielded results of $\gamma = 0.27$ and $\gamma = 0.22$ respectively. The 2,470 m/sec is the average thermal neutron velocity in heavy water. Insertion of the fuel rod would tend to increase the average velocity because of preferential absorption of lower energy neutrons and production of fast neutrons in the fuel rod. Consequently, the correct value of v_{th} should be somewhat larger than that for the moderator, resulting in a more consistent value of γ.

For the present, $\gamma = 0.25 \pm .02$ obtained from the dispersion law, is considered the most accurate value. Assuming that Diffusion Theory holds in the rod, γ was computed to be 0.3227 by Cain (13).

The experimental and theoretical dispersion laws in the ρ^2 plane are shown in Figure 26. The high frequency difference is amplified.

The next analysis deals with the intersection of the dispersion laws of the heavy water only and heavy water-one fuel rod systems. This analysis is hampered somewhat by the difference in heavy water purity that existed between the two sets of data. This difference was taken into account by reducing the α of the one fuel rod data 0.00157 to compensate for absorptions of the additional 0.5% light water. This correction was obtained by computing the zero frequency α at the two concentrations of heavy water from equation [2.12]. The intersection is then based on a 99.5% heavy water purity. The dispersion law intersection is shown in Figure 27. where both the experimental and theoretical intersections are shown. Theoretically the intersection occurs at 310.4 cps, a value much higher than the experimental intersection at 138 cps which was obtained by plotting
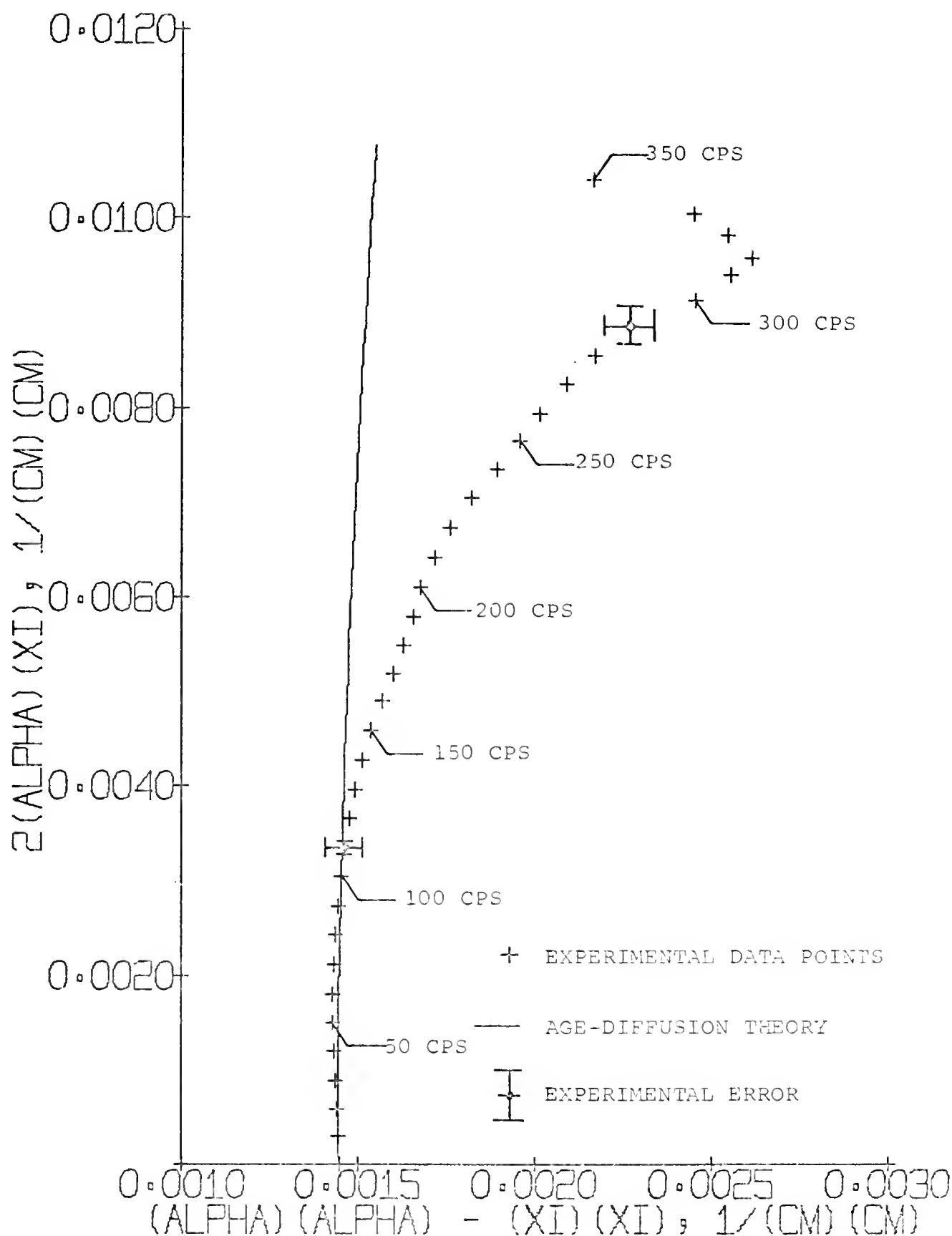
FIGURE 26.

EXPERIMENTAL AND THEORETICAL DISPERSION LAWS IN RHO
SQUARED PLANE FOR HEAVY WATER-ONE FUEL ROD SYSTEM
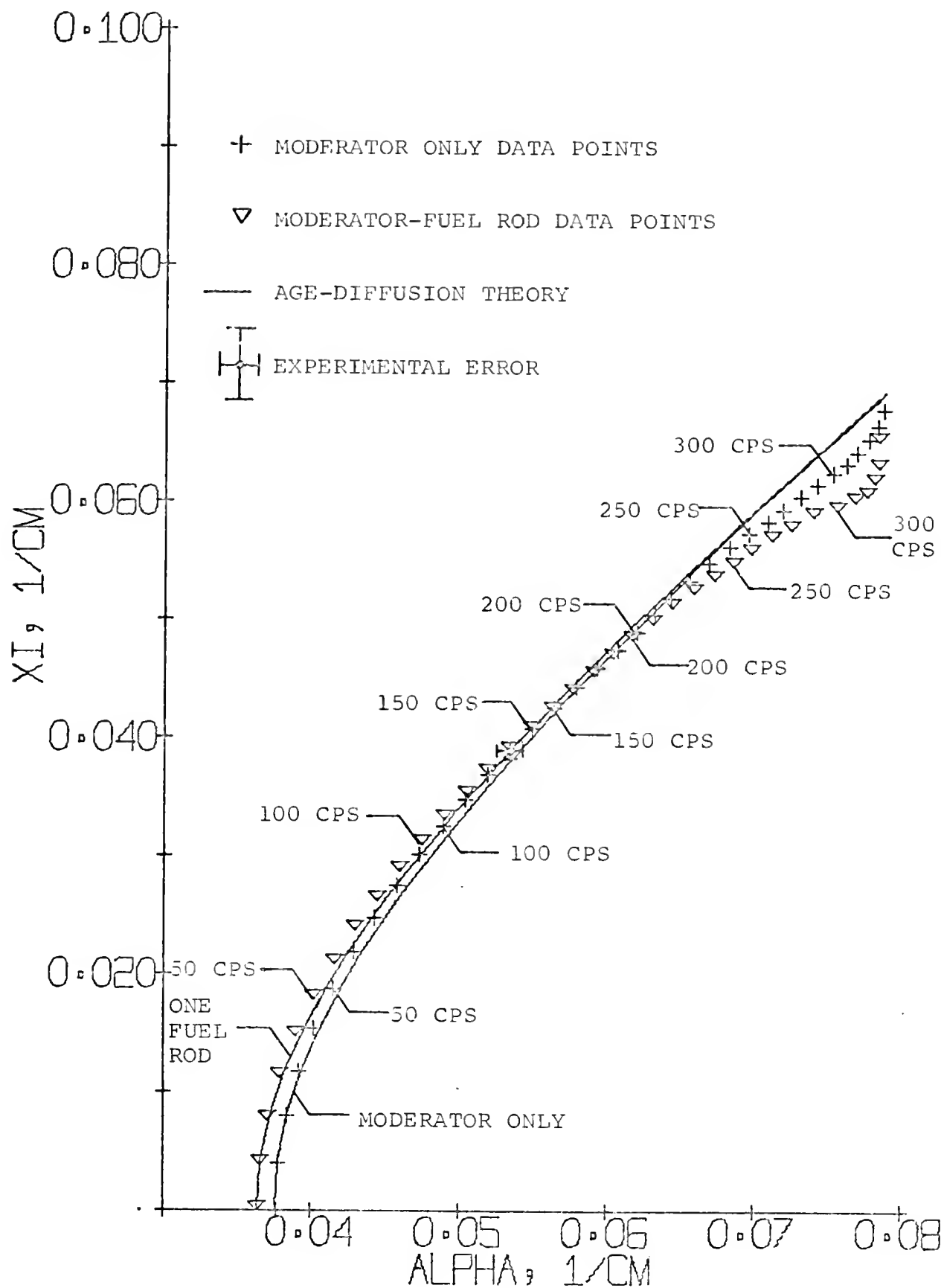
FIGURE 27.

EXPERIMENTAL AND THEORETICAL INTERSECTION
OF DISPERSION LAWS IN RHO PLANE

the observed dispersion laws for the heavy water only and heavy water-one fuel rod systems. This discrepancy is due to the experimental error and the inadequacy of the Age-Diffusion Model. The dominant experimental error is caused by the uncertainty of the heavy water purity for it was found that

$$\delta \omega_c \sim 7,000 \; \delta C$$

where C is the correction term applied for the purity difference between the two experiments. C is approximate and introduces significant deviations. More accurate results would have been obtained if the experiments had been conducted at the same heavy water purity. On the other hand, an improved theoretical model would predict a smaller value of ω_c thereby producing better agreement between the theoretical and experimental intersection. The intersection in the ρ^2 plane is shown in Figure 23. Uncertainty in the heavy water results obscure this analysis but a more distinct intersection may occur.

The combination of theoretical and experimental uncertainties prevent the accurate determination of heterogeneous parameters based on the intersection of the dispersion laws. This is readily apparent in Table 12, where the experimental and predicted parameters are given. A more accurate experiment and theoretical model are needed for proper analysis of the dispersion law intersection.

A Lattice of Fuel Rods

γ has been measured for a one fuel rod system. Will the value of γ change when a lattice of fuel rods is considered? It is not possible at this time to answer this question resolutely but the work of
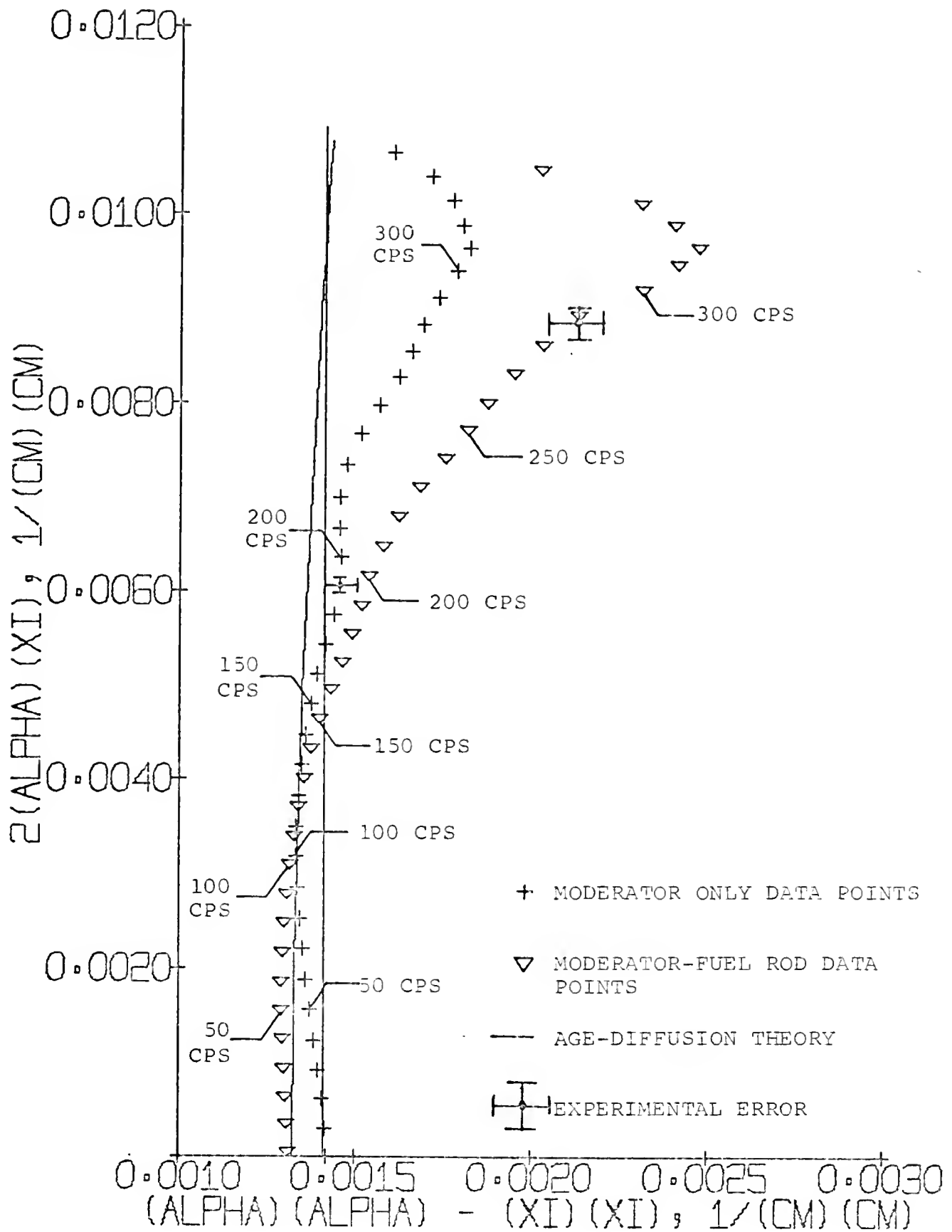
FIGURE 28.

EXPERIMENTAL AND THEORETICAL INTERSECTION
OF DISPERSION LAWS IN RHO SQUARED PLANE

TABLE 12.

HETEROGENEOUS PARAMETERS BASED ON
INTERSECTION OF DISPERSION LAWS

VARIABLE	EXPERIMENTAL VALUE	PREDICTED VALUE
$\alpha_c [cm^{-1}]$	-0.05315	-0.07478[1]
$\xi_c [cm^{-1}]$	-0.03855	-0.06375[1]
$\omega_c [cps]$	130.8	310.0[1]
$\omega_r [cps]$	120.9	310.4[1]
$\tau_{th} [cm^2]$	332.3	118.8[2]
p	> 1	.999[2]

1 These values were obtained from the Age-Diffusion Model.

2 These values were obtained from N. J. Diaz by private communication.

Dunlap (6) does offer a clue to the answer. His study included the calculation of cell parameters of a lattice of fuel rods of the same type as the one considered in this experiment. The calculated parameters yielded a theoretical dispersion law which agreed reasonably well with the experimental one. The agreement leads one to believe that the calculated and true values of the parameters are nearly the same. The value of L^2 for the lattice will now be considered.

L^2 of the lattice is related to γ and L^2 of the moderator (15) and is very sensitive to γ in that

$$\delta L^2 \sim 1.6 \text{ X } 10^4 \, \delta\gamma.$$

Using Dunlap's data and $\gamma = 0.25$, L^2 was computed to be 92.2 cm^2. This compares within 0.6% of the 91.68 cm^2 value computed by Dunlap (6). The close agreement in L^2 and the agreement obtained by Dunlap between the theoretical and experimental dispersion law indicate that the γ measured for one fuel rod may be applicable to a simple lattice of fuel rods.

CHAPTER V

CONCLUSIONS AND RECOMMENDATIONS FOR FUTURE WORK

Conclusions

The neutron wave technique has been used to study a heterogeneous system. γ has been determined using the experimental and theoretical dispersion laws and the expansion coefficients of ρ^2 in a power series of $(i\omega)$. The intersection of the experimental dispersion laws of the heavy water only and the heavy water-one fuel rod systems made possible the determination of two other heterogeneous parameters. Heterogeneous parameters have been extracted from the neutron wave data. These parameters are sufficiently sensitive to neutron wave parameters to allow their determination by this technique. Accuracy of this technique has been partially established in that γ can be determined through the dispersion law fit to two significant digits. Further investigation of accuracy was precluded because of the theoretical model and/or experimental phenomena.

The extension of the results obtained for γ to a lattice has been investigated for the case of a single lattice. The diffusion length squared for the lattice was computed based on the measured value of γ and it was found to agree very well with previous results. The fact that the correct value of the diffusion length squared can be computed from the measured value of γ is very significant.

The experimental technique has been tested under the most adverse

conditions in that a minimum of fuel was used. With larger amounts of natural uranium or with enriched uranium more pronounced characteristics will be exhibited. In these systems improved results should be obtained.

Recommendations

The most important recommendation is the development of a more accurate theoretical model. Better accuracy at high frequencies would improve the technique, predicting more accurate values for the appropriate parameters.

Future studies should be conducted to determine interaction and shadowing effects on the heterogeneous parameters. These studies can be accomplished by a study equivalent to this one where two, three or more fuel rods are inserted at various locations in the assembly. An interesting and useful study would be the determination of heterogenous parameters as a function of the number of fuel rods in the assembly. Still another approach would be the study of the heterogeneous parameters as a function of the center line separation of the fuel rods.

The analysis of future experiments may be modified in the following way. Let the parametric fit in γ of the theoretical to the experimental dispersion laws be the method of determining γ. Then, in the evaluation of the expansion coefficients, eqs. (2.13) and (2.14), γ is known and two other parameters can be determined.

The dispersion laws intersection was not studied in the ρ^2 plane. It may be worthwhile to do so in the future. It appears that a more distinct intersection may occur.

Remaining recommendations are concerned with the experimental procedure. An accurate and reliable method of determining the resolution

time of the counting system is needed. The method described in Appendix A may serve as a starting point for the development of a suitable method. It is important to determine the resolution time accurately to 0.01 seconds because the experimental value of α and ξ are dependent on the resolution time used. A more accurate resolution time yields a more accurate experimental values of α and ξ and the other neutron wave parameters.

Determination of heavy water purity proved to be a difficulty in this experiment. Should heavy water or some other moderator with variable properties be used in future experiments, the physical properties must be accurately determined and verified. Efforts should be made to conduct the moderator only and moderator-fuel experiments under the same conditions when such moderators are used. The error in determining the physical properties must be minimized to improve the validity of the data analysis.

APPENDIX A

MEASUREMENT OF RESOLUTION TIME USING A PULSED

NEUTRON SOURCE

The method presented here for determination of the resolution time was found to be inadequate when performed in the manner described herein. The method, however, is believed to be sound and with one improvement good results should be obtained.

The difficulty concerns the rectangular shape of the neutron pulse at the detector. The asymptotic decay constant of the thermalizing apparatus was such that the individual pulses at the detector are not sharp and the decay time consumes a great percentage of the time between pulses. Consequently, an "effective" time between pulses exists rather than the time between the end of one pulse and the beginning of the subsequent one which was measured at the source. An improved procedure to overcome this difficulty is discussed at the end of this Appendix.

Resolution time is defined as the minimum time between successive neutron interaction events such that both events are registered by the counting system. The definition is not changed if, instead of a single neutron, a burst of neutrons, as shown in Figure 29, is used. Assuming that the neutron bursts from the neutron generator are:

(a) the same

and

(b) near a square wave at the detector

a method for determining the resolution time of the counting systems was developed which used the neutron generator. The major advantage of this method is that the resolution time of the counting system in its operating condition is determined.

The method is illustrated graphically in Figure 29. It is seen
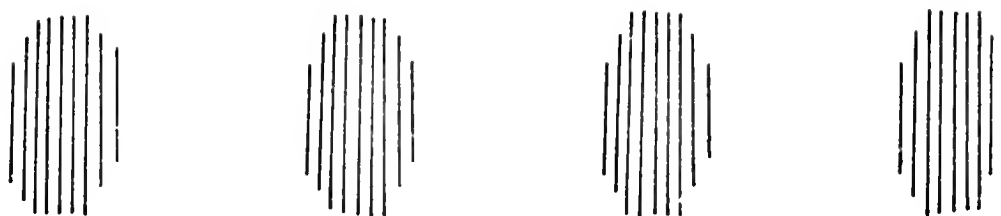
(A) EFFECTIVE NUMBER OF COUNTS
REGISTERED PER BURST

(B) LESS-THAN EFFECTIVE NUMBER OF COUNTS
REGISTERED PER BURST

FIGURE 29.

ILLUSTRATION OF RESOLUTION TIME AND TIME
BETWEEN BURSTS ON COUNT RATE

that when the time between the end of one burst and the beginning of the next is less than the resolution time, τ, of the system the effective number of neutrons counted per burst is less, because some of the leading neutrons of the burst are not counted. Otherwise the effective number of counts per burst is constant.

To verify assumption (a) the target current was monitored with a Type 547 Tecktronix Oscilloscope with a 1A1 Plug-in PreAmplifier unit. This PreAmplifier unit permitted double amplification of the input signal by cascading the two channels of the PreAmplifier. This monitoring method presented a trace of the target current which could be monitored accurately enough for assurance of constant target current and hence a constant burst of neutrons.

Since moderation will spread the neutron burst, the detector was placed as near the source as practical. In this case, the detector was placed in the reference detector position shown in Figure 3. This arrangement was the optimum position for obtaining nearly square pulses of thermal neutrons at the detector.

The resolution time of the system was believed to be of the order of several microseconds. For this reason data were taken using a 10 microsecond target pulse initially separated by an 8 microsecond time interval. The time intervals were measured by observing the terminating and initiating signals for the neutron pulses on an oscilloscope. The time interval of separation was decreased until a nonlinear deviation was observed.

The integral number of counts were recorded by the detector system. If the time interval of pulse separation is greater than the resolution time, the counts should increase linearly with decreasing time separa-

tion (increasing repetition rate). When the time separation is less than the resolution time there should be a nonlinear deviation in the scaler counts. Representative data are given in Table 13. and illustrated in Figure 30.

In order to overcome the difficulty of pulse spreading the generator should be withdrawn from the thermalizing assembly and a small amount, for example several inches, of moderator placed between the target and the detector. Although the sharpness of the detector pulse has not been completely verified, a later experiment indicates that this procedure will yield suitable results for the resolution time.

TABLE 13.

DATA FOR RESOLUTION TIME DETERMINATION

TIME BETWEEN BURSTS (MICROSECONDS)	AVERAGE COUNTS FOR ONE MINUTE
2	340,792
3	344,665
4	343,681
6	318,507
8	301,070
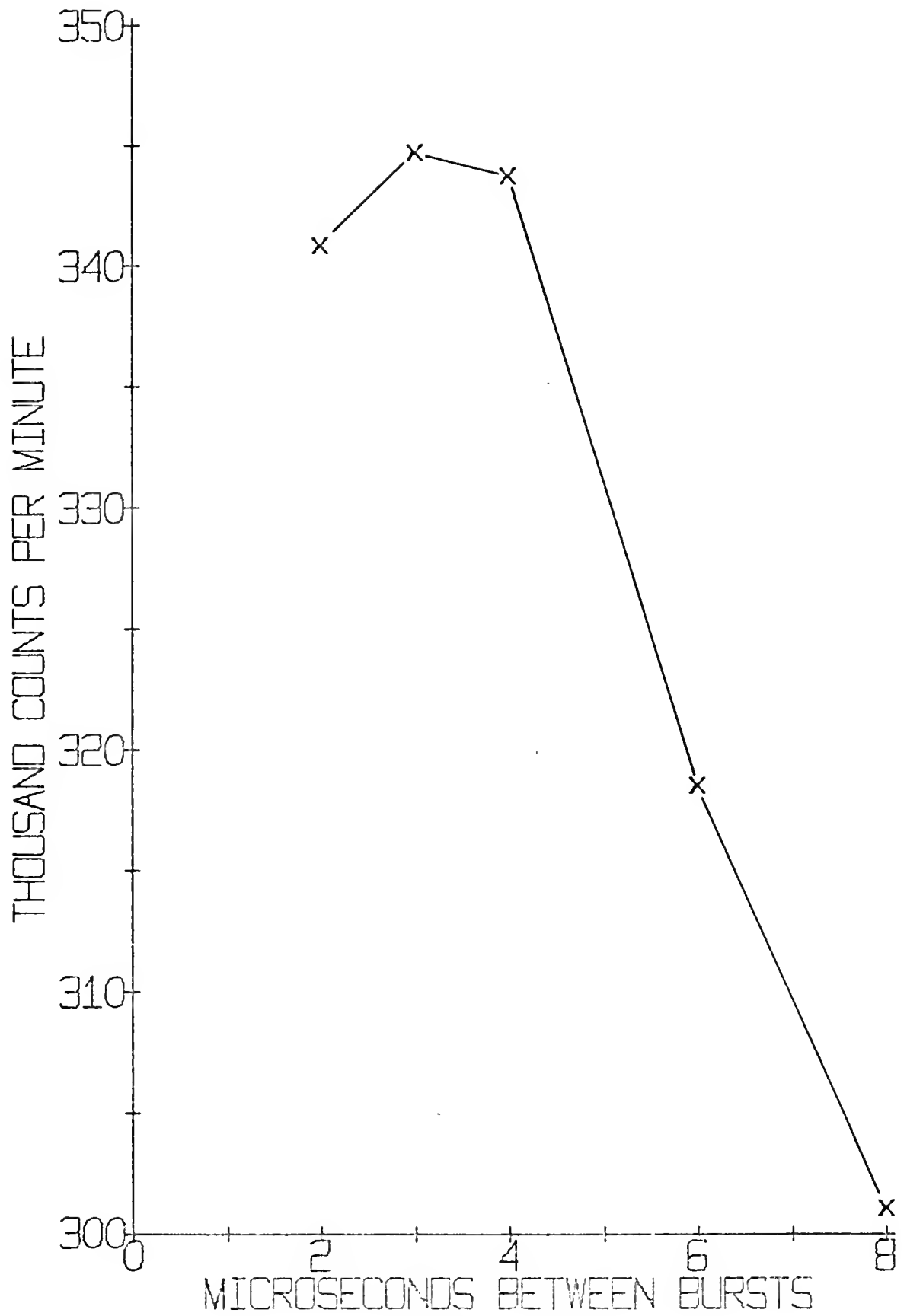
FIGURE 30.

COUNT RATE VERSUS TIME BETWEEN BURSTS

APPENDIX B

DETERMINATION OF TARGET CURRENT PULSE WIDTH AND

MULTICHANNEL ANALYZER CHANNEL WIDTH

Operation in the pulsed neutron mode requires a mutual compatability between the current pulse width at target, the time sweep of the multichannel analyzer and the thermal neutron decay constant for the system being pulsed. Since one would like to have pulses with the ratio of high frequency to low frequency contents as high as possible, a minimal current pulse width at target is dictated. However, one also needs to obtain good statistics so the minimal pulse width will be longer depending on the amount of time one wishes to devote to the accumulation of data. For this set of experiments a pulse width on target of 2.0 milliseconds was selected as the practical compromise between these two conditions.

The multichannel analyzer time sweep must be long enough to describe fully the decay to background of the neutron population. This is most important since the data analysis assumes that the neutron pulse decays to zero in the last channels of time. The buildup, decay and background levels must be recorded by the multichannel analyzer.

For the experiments performed here the channel width selected was 40 microseconds. This yielded a multichannel analyzer time sweep of 51.2 milliseconds. The cutoff was found to be in the background region in all cases.

Now that the multichannel analyzer time sweep is established a repetition rate for the neutron gun is determined. Proper operation requires that a trigger signal initiates the sweep of the multichannel analyzer and operation of the neutron generator simultaneously. Two milliseconds later (the width of the pulse on target) the neutron generator's operation is terminated by the final pulse. 51.2 milliseconds later the multichannel analyzer completes its sweep. The

time for the next initiating trigger signal can be any time after

51.2 milliseconds. It should be close to 51.2 milliseconds in order to

minimize the lost time between cycles of operation.

APPENDIX C

EXPERIMENTAL CHECKS

Introduction

As soon as the data are recorded certain checks, auxillary measurements and computations can be made to insure that the data are valid. Each one is described and the reasons for it are given. The only equipment needed is a desk calculator. Since they are extremely simple it would be poor judgement not to perform them.

Effective Counting Fraction

The effective counting fraction is the ratio of the detection system counting time in a cycle to the total cycle time. The effective counting time is needed in order to make proper resolution corrections which should be based on the actual count rate rather than the count rate averaged over the complete cycle. During the neutron pulse the count rate is at a maximum value. But the pulse only lasts for approximately 10% of the cycle. After the decay of the pulse the count rate is essentially zero. Therefore, an averaged count rate is approximately 10% of the effective count rate and resolution corrections based on the averaged count rate would be too small. The effective counting fraction allows one to determine the actual count rate.

The input to the main amplifier furnishes a suitable oscilloscope display for determination of the effective counting fraction. A representative display is shown in Figure 31. The counting time is the width of the pulse packet. The cycle time is the time between the leading edges of two succeeding packets. The effective counting
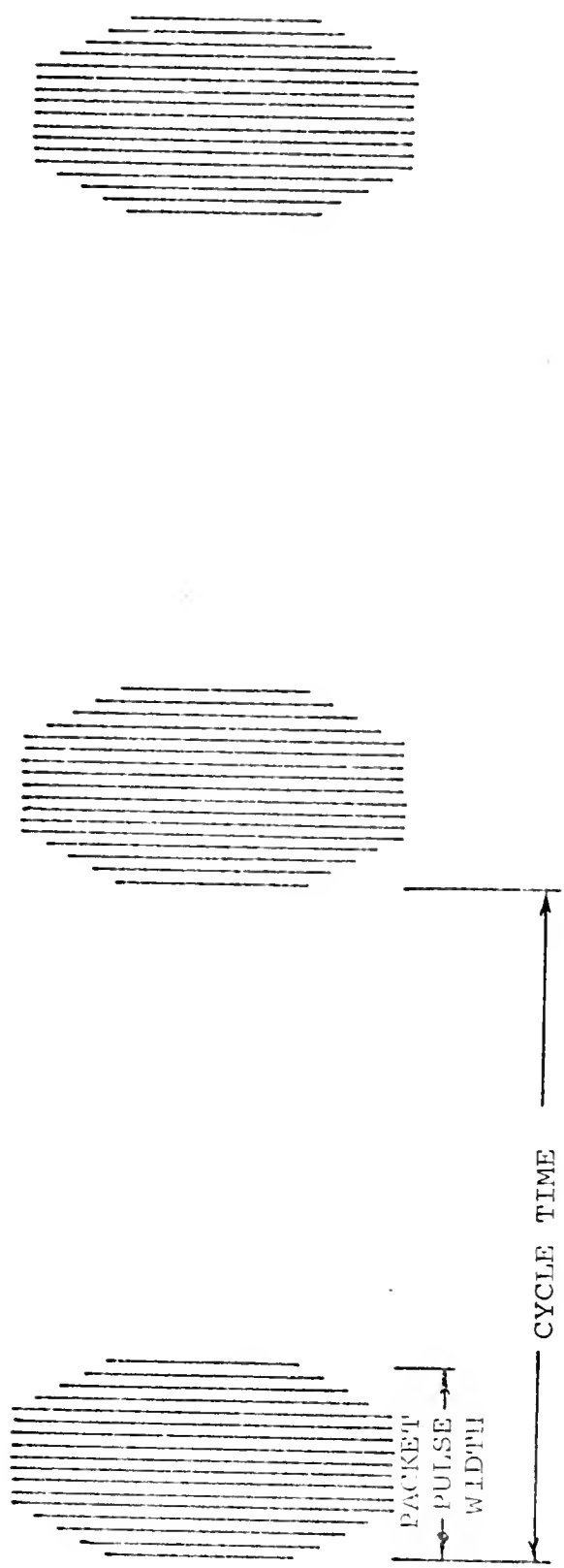
FIGURE 31.

REPRESENTATIVE DISPLAY OF COUNTING PATTERN

fraction F is defined by the equation

$$F = \frac{\text{time width of pulse packet}}{\text{cycle time}}.$$

Resolution corrections are then computed by the relation

$$N = \frac{n\tau}{1 - \frac{n\tau}{TF}}$$

where

N = resolution corrected counts

n = observed counts

T = total run time

τ = resolution time.

The resolution correction of all pulsed data was computed in this manner.

The effective counting fraction changes with position because the neutron pulse becomes wider as distance from the source is increased. Therefore, the fraction must be measured for the movable detector system at each axial position. The reference detector is fixed so its fraction has to be measured only once. Note that the fractions will change if the neutron generator target current pulse width is changed. The effective counting fraction for the reference detector was 0.07 while the movable detector's fraction varied from 0.24 at $z=50$ cm to 0.31 at $z=75$ cm.

Peak to Background Ratio

A pulse neutron experiment should be conducted with a high peak to background ratio, 1,000/1 being a minimum ratio. The background

was obtained by averaging over the last 100 channels. The peak to background ratio varied from 65,000 and 4,000 at z=50 cm to 24,000 and 2,500 at z=75 cm in the moderator only and moderator-fuel rod experiments respectively.

Time Per Trigger

The run time represents the time between each initial trigger of the system. This number should be greater than the multichannel analyzer time sweep and equal to the measured time between trigger pulses. Some variation occurs due to drift in the time between triggers and loss of trigger signals in the electronic system. Variations of greater than 1.0% are indicative of system malfunction. In this series of experiments the time per trigger was 51.63 ± .40 or 51.63 ± 0.8% sec.

Thermal Ratio of Movable Dector Scaler Counts to

Reference Detector Scaler Counts

The resolution corrected counts computed as described in the second section of this Appendix are used in this step. The thermal ratio is computed in the manner as the continuous mode thermal ratio was computed in Chapter IV.

The thermal ratio computed here is compared with the one obtained from the continuous mode data. The two should be comparable, and as a function of distance, the thermal ratios should possess the same linear slope on a semi-log plot. The more significant part of this check is the comparision of the slopes. If, at a given position, the thermal ratios do not reasonably compare (within ~ 25%) in magnitude and the slopes differ by more than a few percent, the run should be repeated. The slopes differed by 1.6% in the moderator only experiment and by 1.3% in the moderator-one fuel rod experiment. The thermal

ratios differed by as much as 12%

Ratio of Movable Detector System Multichannel Analyzer Counts
to Scaler Counts

The movable detector system counts are measured by both the scaler and the multichannel analyzer. However, the multichannel analyzer counts for a fraction of the cycle time due to dead time between channels and dead time between the last channel and the beginning of the next cycle. The multichannel analyzer counting time (channel width times the number of channels) divided by the time between triggers, described above, should equal the ratio of multichannel analyzer integral counts to the movable detector system observed scaler counts. Some variation will occur because of the differing resolution times of the multichannel analyzer and the scaler. However, the ratio should not vary more than a few tenths of a percent. In this series of experiments the ratio was found to be $0.8106 \pm .0020$ or $0.8106 \pm 0.25\%$.

APPENDIX D

COMPUTER PROGRAMS

General

A set of computer programs to be used in the analysis of neutron wave propagation data has been written for the IBM-1800. This computer has a paper tape reader which allows the paper tape output of the multichannel analyzer to be read in directly. The 1800 programs, as well as those used on the IBM 360/50, are now described. Each description includes a brief synopsis of the program, the input/output and any special control features utilized. Additional comments are made at the end of the sections. All programs are written in FORTRAN IV.

An extensive number of plots are among the output of the various programs. The size of the axes has been set at five inches along the horizontal and eight inches along the vertical directions. This can be changed by adjusting the appropriate scaling factor and recompiling the program. Any type or size of paper can be used as long as one dimension does not exceed 11 inches.

TAPRD

Synopsis

This 1800 program reads the paper tape output of the multichannel analyzer and stores the content of each channel on magnetic disk. After the tape is read the channel content is printed out for comparison with the printed output of the multichannel analyzer. If the tape has been read correctly, it is stored on disk. Otherwise,

another attempt can be made to read the tape. A bare data tape is read first, followed by a cadmium data tape. The data are stored on disk in groups of 256 channels. Each group is assigned a file number.

Input

The following data are read from the keyboard in FORMAT (314):

L = first storage file number, usually an odd 3 digit number

MAX = number of runs, each run having a bare and cadmium data tape

N = number of channels per data tape.

Output

To identify the storage files the initial file number is printed The channel number and content of every 50th channel are then printed After all data tape sets have been read, the next available file number is printed.

Special Controls

PAUSE 1111.-- This pause occurs so that the first (bare) data tape can be readied in the tape reader. When readied, press START to begin the reading process.

PAUSE 4444.-- This pause occurs after the printout of each data tape and allows one to verify that the tape has read correctly. If an error has occurred, turn SENSE SWITCH 0 on and press START to return the program to PAUSE 1111. If the tape has read correctly, press START to store the data on disk.

PAUSE 2222.-- This pause occurs so that the second (cadmium) data tape can be readied in the tape reader. When readied, press START.

PAUSE 4444.-- This pause is the same as the previous PAUSE 4444

except that turning SENSE SWITCH 0 on and pressing START returns
the program to PAUSE 2222.

PAUSE 3333.-- This pause occurs when all the data sets,
specified by MAX, have been read. Pressing START returns the program
to the initial reading of the keyboard input data.

Comment

Approximately 15 seconds are required to read a 1,024 channel tape.

THERM

Synopsis

This 1800 program computes the corrected and normalized thermal
neutron pulse from the bare and cadmium data stored on disk. Each
channel of the bare and cadmium data is corrected for resolution
losses. The number of thermal neutrons per channel is then computed,
background is subtracted and normalization is performed. Due to the
limited core capacity of the 1800 the computations are made in groups
of 256 channels. The complete normalized pulse is stored on disk in
one file after each group of computations.

Input

Input data is read from cards. One initial set of two cards is
required for each set of runs   A second set of two cards is required
for each run within the set. The initial cards contain the following
data in FORMAT (4E10.4, 2E13.7/6I4):

TAU = resolution time of movable detector system in microseconds

CTAU = resolution time of reference detector system divided by
          the effective counting fraction of the reference detector
          system (See Appendix D)

TMCCH = channel width of multichannel analyzer in microseconds

TMCDT = deadtime between channels in microseconds

STREF = observed reference detector system counts for bare run
to which the data are normalized

TIMER = run time for which STREF counts were observed

NCHAN = number of channels of data

NSKIP = print control parameter, every NSKIPth channel is
printed beginning with channel #1

MRUNS = maximum number of runs in the set

L1 = initial file number of the bare data of the first run for
which the thermal pulse is to be computed

L2 = the file number for storing the first thermal pulse com-
puted in the set, usually a 4 digit number ending in 1

IBKGD = the number of final channels over which the average
background is computed.

The run data cards contain the following numbers in FORMAT (6E13.7/3I4):

REF1 = observed reference detector system counts for bare run

REF2 = observed reference detector system counts for cadmium run

TIME1 = time for bare run

TIME2 = time for cadmium run

TRIG1 = number of triggers for bare run

TRIG2 = number of triggers for cadmium run

NRUN = run number

NZPOS = axial position

NRAD = radial position.

Output

The observed bare counts, resolution corrected bare counts, observed cadmium counts and resolution corrected cadmium counts, are printed out for every NSKIPth channel. Then the normalized and background corrected thermal neutron pulse is printed out for every NSKIPth channel. The last portion of the printout is the background per channel of the bare, cadmium and thermal pulses. After all pulses have been computed the next available file number is printed.

Special Controls

PAUSE 3333.-- This pause occurs when the thermal neutron pulses have been computed for MRUNS runs. Pressing START returns the program to the reading of the initial set of data cards.

Comments

The logic of the file numbering system can now be explained. Assume that one has 10 sets of 1,024 channel data tapes and that L = 101 in the TAPRD input. Four files will be required to store each data tape (4 X 256 = 1,024). The first bare data tape will be stored in files #101, #103, #105, and #107. The first cadmium data tapes will be stored in files #102, #104, #106, and #108. Files #101 and #102 contain the bare and cadmium data for channels 1 through 256. Succeeding data are stored in the same fashion in higher file numbers. If L2 = 1001 in the THERM input then the normalized pulses will be stored in files #1001 through #1010 inclusive. Subsequent sets can be identified by using 201 and 2001, 301 and 3001, etc., for L1 and L2 respectively. Thus, the leading digit can be used to identify the different data sets.

PLOT1

Synopsis

This 1800 program plots the thermal neutron pulses which were computed and stored by THERM. Scaling and labeling is based on the first pulse plotted (the LMINth file) which is usually of maximum amplitude.

Input

The following data are read from the keyboard in FORMAT (13I4):

LMIN = file number of first pulse to be plotted

LMAX = file number of final pulse to be plotted

NCHAN = number of channels to be plotted

LBAD = file number of pulses to be omitted in plotting, a maximum of 10, leave blank if none.

Output

The thermal neutron pulses are plotted, superimposed on the same axes.

Special Control

PAUSE 3333.--This pause occurs after all plots are made. Pressing START returns the program to the reading of the keyboard input data.

Comments

The x axis is labeled at five points including zero. To obtain integer numbers, NCHAN should be divisible by four. The plotter and paper should be readied before the keyboard input data are read.

FORTX

Synopsis

This 1800 program computes the Fourier Transform of the thermal neutron pulse stored on disk by THERM. The integration scheme used is Simpson's Rule, with the initial channel contribution being computed by the trapezoidal rule. The summation increment is greater than the channel width by an amount equal to the deadtime between channels. The midpoint of the summation increment coincides with the midpoint of the channel. The frequency range and interval are specified in the input data. The frequency, amplitude and phase are punched on paper tape and printed.

Input

The following data are read from a card in FORMAT (3I4, 5E10.4):

   LMIN = file number of first pulse

   LMAX = file number of last pulse

   NCHAN = number of channels

   TMCCH = multichannel analyzer channel width in microseconds

   TMCUT = deadtime between channels in microseconds

   FRMIN = initial frequency (cps) of Fourier analysis

   FRMAX = final frequency (cps) of Fourier analysis

   DELTA = frequency interval (cps).

Output

The printed output includes, at each frequency, the real and imaginary components of the transformed pulse, the amplitude and the phase. The paper tape output includes only the frequency, amplitude and phase.

Special Controls

PAUSE 3333.-- This pause occurs when the analysis of the specified pulses has been completed. Pressing START returns the program to the reading of the data input card.

Comments

The paper tape output is punched for input into the ALPHA and XI Codes which will be described next. One frequency analysis requires approximately 20 seconds when 1,024 channels of data are used.

ALPHA

Synopsis

This 1800 program plots the experimental values of the amplitudes as a function of distance for each frequency on a semilog scale. A rough plot for even frequencies only is given so that a check can be made for asymptotic decay and bad data points. A second plot is then made which plots the data points for all frequencies, computes a semilog least squares fit of the form

$$F(z) = ae^{bz}$$

where a and b are fitting parameters and $F(z)$ is the experimental data and draws the least squares fit through the data points. The experimental points to be included in the computation are fixed from 1 to MAX or can be varied by using the sense switches and data input.

Input

The output tape of FORTX is required input. 51 frequency data are read for each data position (0-500 cps, in steps of 10 cps). The following data are read from the keyboard in FORMAT (F4.0, 16I4):

YMIN = minimum value to be plotted (should be an integer
        power of 10)

NCYCL = number of cycles to be used along vertical axis

IMIN = 1

IMAX = number of data runs to be included in the least
        squares fitting

MAXFR = one plus the number of frequencies to be analyzed
        (frequencies are incremented by 10 cps)

ILLFR = the number of the frequency at which data elimination
        is to begin

ISTEP = minimum number of data points to be considered in the
        progressive scanning of the data

IBAD = data run numbers to be omitted, maximum of 10, leave
        blank if none.

Output

If the data are being scanned the printed output includes the
initial and final data positions, the asymptotic decay constant, the
zero value and the deviation of each from the previous computation.
Any omitted data poistions are also listed. If the data are not being
scanned, the deviations are not printed.

When there is no scanning and the ILLFRth frequency is about to
be computed a message is printed to input the initial, final and
intermediate data positions to be omitted at the keyboard. This pro-
vision allows the omission of any run from the computations.

The minimum number of data runs allowed is three. If less than
three are being considered, the computation is omitted and the next
frequency computation is made. A "NO ASYMPTOTIC DECAY" and frequency

identification message is printed in this case.

The frequency and symptotic decay constants are punched on paper tape at the end of the program. This tape is an input to the PLOT2 program which will be described.

Special Controls

SENSE SWITCH 0.--If SENSE SWITCH 0 is turned on, no plots are made.

SENSE SWITCH 1.--If SENSE SWITCH 1 is turned on, no printed output is obtained.

SENSE SWITCH 3.--If SENSE SWITCH 3 is on the data points are scanned. The scanning procedure is such that α is computed and printed for the first ISTEP+1 data points. The group of ISTEP+1 points is then shifted over one data position and α is computed again. These processes, computing, printing and shifting, are continued until the last ISTEP+1 data points are considered. This completes one scan of the data. The next scan is made with ISTEP increased by one. Additional scans are made until the group of data points considered equals the total number of data points

PAUSE 2222.--This pause occurs so that the paper on the plotter may be changed between the rough and final plots.

PAUSE 1111.--This pause occurs at the completion of the computations. Pressing START returns the program to the initial reading of the keyboard input data.

Comments

Several runs of ALPHA may be necessary to obtain the proper asymptotic region and to determine which data points are to be eliminated. For these runs the tape output can be suppressed by turning the paper tape punch off.

XI

Synopsis

This 1800 program is very similar in logic to the ALPHA program. However, a linear least squares fit is made to the corrected phase shifts as a function of frequency. The correction is required because the range of arguments for inverse angles is from $-\pi/2$ to $+\pi/2$. Arguments less than $-\pi/2$ must be corrected by subtracting the appropriate multiple of π. This correction is performed by XI. A tape of the frequencies and corrected phases can be obtained.

Input

The data output tape of FORTX is also read by XI. The following numbers are read from the keyboard in FORMAT (F4.0,15I4):

YMAX = the maximum phase shift (lag) to be plotted

IMIN = 1

IMAX = the number of data runs

MAXFR = one plus the number of frequencies to be analyzed
        (frequencies are incremented by 10 cps)

ILLFR = the first frequency number at which data elimination
        is to begin

ISTEP = initial number of points considered in the scanning
        of the data positions

IBAD = the data runs to be omitted, maximum of 10, leave
        blank if none.

Output

The output of XI is identical to the output of ALPHA.

Special Controls

SENSE SWITCH 2.--If SENSE SWITCH 2 is turned on, the corrected

phases are punched on paper tape.

Comments

The comments for ALPHA are applicable. Generally ALPHA and XI

are run successively. If several runs of XI are required, the paper

tape punch can be turned off until the final run. Then a continuous

tape input to PLOT2, to be described next, is obtained.

PLOT2

Synopsis

PLOT2 is an 1800 program which plots α versus frequency (cps), ξ

versus frequency (cps), ξ versus α, $2\alpha\xi$ versus ω (rad/sec), and α^2 -

ξ^2 versus ω^2. $2\alpha\xi$ and $\alpha^2 - \xi^2$ are computed and printed as well as

plotted.

Input

The ALP-XI tape which is the ALPHA and XI Codes output is read at

the tape reader. The following data are read from card in FORMAT

($2F4.0$, $3I4$):

XMAX = maximum value of horizontal axis

YMAX = maximum value of vertical axis

MAXFR = maximum number of frequencies

NO   = point plot symbol control and run number for UFNLLS

ICARD = card punch option; if 0, no cards punched; if 1, $2\alpha\xi$

and $\alpha^2 - \xi^2$ are punched out for input to UFNLLS Code.

Output

The value of $2\alpha\xi$ and $\alpha^2 - \xi^2$ are printed. Depending on the value
of ICARD, cards are punched for UFNLLS input. The independent variable
on the $\alpha^2 - \xi^2$ cards is ω^2 rather than ω. The five plots mentioned
in the synopsis are also obtained.

Special Controls

PAUSE 1111.--This pause occurs so that the ALP tape output of
ALPHA can be readied at the tape reader. When readied, press START
to read the tape.

PAUSE 2222.--This pause occurs after the reading of the ALP tape.
It occurs so that the XI tape output can be readied at the tape reader.
When readied, press START to read the tape.

PAUSE 2222.--These pauses occur between the plots to allow the
paper on the plotter to be readied for the succeeding plots. When
readied, press START to continue the plots.

PAUSE 3333.--This pause occurs when all plots have been made.
Pressing START returns the program to the reading of the data input
card.

Comments

The maximum values read in for the vertical and horizontal axes
apply only to the x and ξ axes. The maximum on the frequency axis is
400 cps. The maxima on the vertical axes for $2\alpha\xi$ and $\alpha^2 - \xi^2$ are
0.02 and 0.005 respectively. ω and ω^2 maxima are set at 2.5×10^3 and
5.0×10^6 respectively. Should it be desired to change any of these
latter values, the appropriate scaling factors must be changed and the
program recompiled.

PLOT3

Synopsis

This 1800 program plots and prints the theoretical values of α and ξ. The FERVE2 Code punches the value of frequency, α and ξ on cards for input to PLOT3. The theoretical values can be point or line plotted. Options are available for obtaining theoretical plots which are drawn over the experimental point plots obtained from the PLOT2 Code.

Input

The following data are read from card in FORMAT (5I4):

MAX = number of frequencies

NO = point plot symbol control

NRUN = axis drawing and labeling control; if 0 axes are drawn and labeled, if not 0 only the theoretical values are plotted

LORPT = line or point plot control; 1 = line, 2 = point plots

NDUN = plot control; if = 1, ξ versus α is plotted; if = 2, α versus frequency, ξ versus frequency as well as ξ versus α are plotted.

Frequency, α and ξ are read from card in FORMAT (3E12.5). MAX cards are read.

Output

In addition to the graphs the theoretical values of α and ξ are printed, depending on SENSE SWITCH 1.

Special Control

PAUSE 1111.--This pause occurs so that the plotter may be readied
for the α versus frequency plot. Push START when readied to obtain
plot.

PAUSE 2222.--Same as PAUSE 1111 except that ξ versus frequency
is plotted.

PAUSE 3333.--Same as Pause 1111 except that ξ versus α is plotted.

PAUSE 4444.--This pause occurs so that the printer may be readied.
When readied press START to continue.

PAUSE 5555.--Press START to continue.

SENSE SWITCH 1.--If SENSE SWITCH 1 is turned on the listing of
theoretical values of α and ξ will not be made.

Comments

If only the listing is desired it can be obtained by setting
NDUN = 1 and turning SENSE SWITCH 0 on.

The axes of the α versus frequency and ξ versus frequency plots
can not be drawn or labeled by PLOT3. These are drawn by PLOT2 and
are positioned on the plotter so that the theoretical plots are made
over the experimental plots. The plots are positioned by taping the
plots on the drum and placing the alignment reticle over the origin.
The same holds true for the ξ versus α plots in that the reticle must
be placed over the origin of the PLOT2 plot if the plots are to be
superimposed. The PLOT2 plots and PLOT3 plots are offset by one inch
in the horizontal direction.

FERVE2

Synopsis

This 360/50 program computes the theoretical values of α and ξ

from equation [2.12] with n,p = 1 and 2. The Newton-Raphson itera-
tion technique is used to obtain solutions. At each frequency, initial
estimates for α and ξ are read.

Input

The first card read is a title card, FORMAT (12A6). Three
initial data input cards are read for each set of computations. The
following data are read in FORMAT (6E12.6):

BTSQ1 = fundamental transverse buckling squared

BTSQ2 = first higher transverse buckling squared

SQLO = diffusion length squared

TAU   = age to thermal

DTH   = diffusion constant

VTH   = thermal velocity

SL   = slowing down time

AO   = alpha zero

CI   = cooling index

GAMMA = Feinberg-Galanin constant

PESCP = resonance escape probability

ETA   = fast neutrons produced per thermal neutron absorption

JONE = $J_o(B_1 *RTOT)$ where B_1 = BTSQ1

JTWO = $J_o(B_2 *RTOT)$ where B_2 = BTSQ2

RTOT = R, extrapolated radius of assembly

RZERO = radius of fuel rod

Next, the following data are read in FORMAT (I4,E12.6):

MAXIT = maximum number of interations

. E   = tolerance of computing α and ξ

The last set of cards read contain the following date in FORMAT (3F12.6, 2I4):

ω = frequency (cps)

ALPHA = initial estimate of α

PSI   = initial estimate of ξ

ILAST = 0, for last card in the set

      = 1, for all other cards in the set

ISENT = 0, for last card in the last set

      = 1, for all other cards

Succeeding sets must have each of the above cards included.

Output

The title card, initial input data and the frequency analysis at each frequency is printed out. Cards of frequency, α and ξ are punched for input to PLOT3.

APPENDIX E

EXPERIMENTAL AMPLITUDES AND PHASES

HEAVY WATER

Z = 50. CMS AXIAL POSITION

FREQ(CPS)	AMPLITUDE	PHASE(RADIANS)
0.	0.207609E 03	0.000000E 00
10.	0.204843E 03	0.335188E 00
20.	0.197036E 03	0.663727E 00
30.	0.185625E 03	0.980767E 00
40.	0.171963E 03	0.128374E 01
50.	0.157391E 03	-0.156949E 01
60.	0.142818E 03	-0.129513E 01
70.	0.128813E 03	-0.103356E 01
80.	0.115678E 03	-0.783382E 00
90.	0.103541E 03	-0.543342E 00
100.	0.924402E 02	-0.312389E 00
110.	0.823584E 02	-0.896399E-01
120.	0.732505E 02	0.125704E 00
130.	0.650437E 02	0.334251E 00
140.	0.576913E 02	0.536404E 00
150.	0.511135E 02	0.732852E 00
160.	0.452345E 02	0.923384E 00
170.	0.400039E 02	0.110935E 01
180.	0.353537E 02	0.129144E 01
190.	0.312251E 02	0.146912E 01
200.	0.275499E 02	-0.149783E 01
210.	0.242628E 02	-0.132640E 01
220.	0.213231E 02	-0.115832E 01
230.	0.186967E 02	-0.994906E 00
240.	0.163613E 02	-0.834229E 00
250.	0.143035E 02	-0.679043E 00
260.	0.125163E 02	-0.527124E 00
270.	0.109454E 02	-0.376865E 00
280.	0.955673E 01	-0.227308E 00
290.	0.852300E 01	-0.799290E-01
300.	0.722436E 01	0.655821E-01
310.	0.625999E 01	0.203637E 00
320.	0.541012E 01	0.351241E 00
330.	0.465742E 01	0.493317E 00
340.	0.398737E 01	0.635024E 00
350.	0.330133E 01	0.775390E 00

HEAVY WATER

Z = 55. CMS AXIAL POSITION

FREQ(CPS)	AMPLITUDE	PHASE(RADIANS)
0.	0.172123E 03	0.000000E 00
10.	0.169669E 03	0.355192E 00
20.	0.162780E 03	0.703325E 00
30.	0.152622E 03	0.103916E 01
40.	0.140562E 03	0.135987E 01
50.	0.127774E 03	-0.147631E 01
60.	0.115068E 03	-0.118701E 01
70.	0.102941E 03	-0.911173E 00
80.	0.916693E 02	-0.647927E 00
90.	0.813702E 02	-0.395821E 00
100.	0.720602E 02	-0.153443E 00
110.	0.636926E 02	0.803920E-01
120.	0.561970E 02	0.306621E 00
130.	0.494948E 02	0.525944E 00
140.	0.435133E 02	0.733741E 00
150.	0.381881E 02	0.945144E 00
160.	0.334738E 02	0.114530E 01
170.	0.293160E 02	0.133907E 01
180.	0.256545E 02	0.152960E 01
190.	0.224321E 02	-0.142653E 01
200.	0.195853E 02	-0.124511E 01
210.	0.170731E 02	-0.106765E 01
220.	0.148553E 02	-0.894670E 00
230.	0.129172E 02	-0.726173E 00
240.	0.112249E 02	-0.561106E 00
250.	0.974999E 01	-0.398038E 00
260.	0.845716E 01	-0.238421E 00
270.	0.732084E 01	-0.802304E-01
280.	0.652367E 01	0.763901E-01
290.	0.544424E 01	0.230392E 00
300.	0.467342E 01	0.383256E 00
310.	0.399380E 01	0.533261E 00
320.	0.341302E 01	0.681547E 00
330.	0.289937E 01	0.830042E 00
340.	0.244303E 01	0.976200E 00
350.	0.205553E 01	0.111958E 01

HEAVY WATER

Z = 60. CMS AXIAL POSITION

FREQ(CPS)	AMPLITUDE	PHASE(RADIANS)
0.	0.140965E 03	0.000000E 00
10.	0.138830E 03	0.375748E 00
20.	0.132839E 03	0.744057E 00
30.	0.124019E 03	0.109919E 01
40.	0.113592E 03	0.143809E 01
50.	0.102590E 03	-0.138167E 01
60.	0.917449E 02	-0.107641E 01
70.	0.814994E 02	-0.786362E 00
80.	0.720714E 02	-0.509835E 00
90.	0.635330E 02	-0.245224E 00
100.	0.558752E 02	0.887002E-02
110.	0.490492E 02	0.253668E 00
120.	0.429838E 02	0.480054E 00
130.	0.376205E 02	0.718389E 00
140.	0.328867E 02	0.939609E 00
150.	0.287200E 02	0.115402E 01
160.	0.250803E 02	0.136275E 01
170.	0.213745E 02	0.156609E 01
180.	0.190570E 02	-0.137600E 01
190.	0.165751E 02	-0.113344E 01
200.	0.143959E 02	-0.995042E 00
210.	0.124855E 02	-0.811054E 00
220.	0.108234E 02	-0.634405E 00
230.	0.938435E 01	-0.461325E 00
240.	0.813592E 01	-0.291457E 00
250.	0.704153E 01	-0.125053E 00
260.	0.608784E 01	0.363151E-01
270.	0.526087E 01	0.194276E 00
280.	0.455035E 01	0.347208E 00
290.	0.394502E 01	0.497608E 00
300.	0.342835E 01	0.648100E 00
310.	0.298131E 01	0.801075E 00
320.	0.258847E 01	0.960259E 00
330.	0.223621E 01	0.112608E 01
340.	0.190270E 01	0.130225E 01
350.	0.158554E 01	0.147623E 01

HEAVY WATER
Z = 65. CMS AXIAL POSITION

FREQ(CPS)	AMPLITUDE	PHASE(RADIANS)
0.	0.116225E 03	0.000000E 00
10.	0.114369E 03	0.395917E 00
20.	0.109154E 03	0.784036E 00
30.	0.101494E 03	0.115820E 01
40.	0.924778E 02	0.151509E 01
50.	0.830168E 02	-0.128777E 01
60.	0.737502E 02	-0.966694E 00
70.	0.650569E 02	-0.661756E 00
80.	0.571045E 02	-0.371212E 00
90.	0.499500E 02	-0.937076E-01
100.	0.435947E 02	0.172258E 00
110.	0.379823E 02	0.428135E 00
120.	0.330455E 02	0.674842E 00
130.	0.287173E 02	0.913193E 00
140.	0.249322E 02	0.114378E 01
150.	0.216349E 02	0.136715E 01
160.	0.187703E 02	-0.155729E 01
170.	0.162792E 02	-0.134553E 01
180.	0.141105E 02	-0.113852E 01
190.	0.122145E 02	-0.935876E 00
200.	0.105605E 02	-0.737652E 00
210.	0.911463E 01	-0.543425E 00
220.	0.785329E 01	-0.353527E 00
230.	0.675034E 01	-0.167240E 00
240.	0.573238E 01	0.135545E-01
250.	0.494569E 01	0.187146E 00
260.	0.423032E 01	0.353568E 00
270.	0.364441E 01	0.515979E 00
280.	0.314741E 01	0.679239E 00
290.	0.271543E 01	0.846652E 00
300.	0.233118E 01	0.101526E 01
310.	0.199019E 01	0.118435E 01
320.	0.168645E 01	0.134367E 01
330.	0.143023E 01	0.150813E 01
340.	0.121013E 01	-0.147371E 01
350.	0.102560E 01	-0.131650E 01

HEAVY WATER

Z = 70. CMS AXIAL POSITION

FREQ(CPS)	AMPLITUDE	PHASE(RADIANS)
0.	0.974131E 02	0.000000E 00
10.	0.957731E 02	0.416627E 00
20.	0.911814E 02	0.824981E 00
30.	0.844534E 02	0.121874E 01
40.	0.765640E 02	-0.154729E 01
50.	0.683255E 02	-0.119108E 01
60.	0.603079E 02	-0.853607E 00
70.	0.523364E 02	-0.533320E 00
80.	0.460585E 02	-0.228455E 00
90.	0.400101E 02	0.627888E-01
100.	0.346650E 02	0.341890E 00
110.	0.299733E 02	0.609923E 00
120.	0.253783E 02	0.867746E 00
130.	0.223220E 02	0.111622E 01
140.	0.192400E 02	0.135616E 01
150.	0.165776E 02	-0.155372E 01
160.	0.142925E 02	-0.132050E 01
170.	0.123344E 02	-0.111003E 01
180.	0.106424E 02	-0.896937E 00
190.	0.917352E 01	-0.687352E 00
200.	0.789240E 01	-0.482426E 00
210.	0.677961E 01	-0.283670E 00
220.	0.582571E 01	-0.906446E-01
230.	0.500935E 01	0.980685E-01
240.	0.430379E 01	0.233727E 00
250.	0.370748E 01	0.467345E 00
260.	0.318437E 01	0.650234E 00
270.	0.272442E 01	0.831759E 00
280.	0.231884E 01	0.100906E 01
290.	0.196802E 01	0.117001E 01
300.	0.167422E 01	0.134500E 01
310.	0.142861E 01	0.150472E 01
320.	0.122801E 01	-0.147282E 01
330.	0.105714E 01	-0.129514E 01
340.	0.893121E 00	-0.109401E 01
350.	0.730783E 00	-0.883923E 00

HEAVY WATER

Z = 75. CMS AXIAL POSITION

FREQ(CPS)	AMPLITUDE	PHASE(RADIANS)
0.	0.812410E 02	0.000000E 00
10.	0.798048E 02	0.435019E 00
20.	0.757911E 02	0.861442E 00
30.	0.699291E 02	0.127263E 01
40.	0.630740E 02	-0.147668E 01
50.	0.559402E 02	-0.110448E 01
60.	0.490253E 02	-0.751889E 00
70.	0.426163E 02	-0.417502E 00
80.	0.368401E 02	-0.995358E-01
90.	0.317294E 02	0.203796E 00
100.	0.272572E 02	0.494222E 00
110.	0.233701E 02	0.773114E 00
120.	0.200071E 02	0.104155E 01
130.	0.171079E 02	0.130032E 01
140.	0.146185E 02	0.155032E 01
150.	0.124819E 02	-0.134926E 01
160.	0.106497E 02	-0.111482E 01
170.	0.908025E 01	-0.838017E 00
180.	0.774738E 01	-0.668395E 00
190.	0.662309E 01	-0.455430E 00
200.	0.566938E 01	-0.245470E 00
210.	0.485076E 01	-0.372878E-01
220.	0.413533E 01	0.163793E 00
230.	0.350719E 01	0.369441E 00
240.	0.296714E 01	0.561398E 00
250.	0.251233E 01	0.746156E 00
260.	0.213242E 01	0.925343E 00
270.	0.181454E 01	0.110296E 01
280.	0.153958E 01	0.127398E 01
290.	0.130317E 01	0.145240E 01
300.	0.110101E 01	-0.152213E 01
310.	0.934959E 00	-0.136139E 01
320.	0.797162E 00	-0.119455E 01
330.	0.675799E 00	-0.102436E 01
340.	0.570312E 00	-0.852211E 00
350.	0.478250E 00	-0.678563E 00

HEAVY WATER

Z = 80. CMS AXIAL POSITION

FREQ(CPS)	AMPLITUDE	PHASE(RADIANS)
0.	0.671335E 02	0.000000E 00
10.	0.659071E 02	0.453303E 00
20.	0.624739E 02	0.897772E 00
30.	0.574687E 02	0.132655E 01
40.	0.516240E 02	-0.140579E 01
50.	0.455614E 02	-0.101744E 01
60.	0.397096E 02	-0.649577E 00
70.	0.343104E 02	-0.300765E 00
80.	0.294729E 02	0.307864E-01
90.	0.252158E 02	0.346322E 00
100.	0.215122E 02	0.649199E 00
110.	0.183212E 02	0.933070E 00
120.	0.155378E 02	0.121755E 01
130.	0.132506E 02	0.148650E 01
140.	0.112518E 02	-0.139485E 01
150.	0.954090E 01	-0.114352E 01
160.	0.809025E 01	-0.900912E 00
170.	0.686228E 01	-0.665655E 00
180.	0.582559E 01	-0.436736E 00
190.	0.494200E 01	-0.212436E 00
200.	0.419009E 01	0.600451E-02
210.	0.355015E 01	0.220217E 00
220.	0.300210E 01	0.429563E 00
230.	0.253444E 01	0.635164E 00
240.	0.213005E 01	0.835454E 00
250.	0.178445E 01	0.102836E 01
260.	0.148757E 01	0.121273E 01
270.	0.124276E 01	0.138243E 01
280.	0.104642E 01	0.154297E 01
290.	0.890191E 00	-0.144017E 01
300.	0.759523E 00	-0.127905E 01
310.	0.650970E 00	-0.111306E 01
320.	0.558624E 00	-0.948565E 00
330.	0.475525E 00	-0.773342E 00
340.	0.390453E 00	-0.601582E 00
350.	0.335173E 00	-0.445934E 00

HEAVY WATER

Z = 85. CMS AXIAL POSITION

FREQ(CPS)	AMPLITUDE	PHASE(RADIANS)
0.	0.544303E 02	0.000000E 00
10.	0.533918E 02	0.471774E 00
20.	0.504930E 02	0.934366E 00
30.	0.462764E 02	0.138067E 01
40.	0.413689E 02	-0.133496E 01
50.	0.363021E 02	-0.930807E 00
60.	0.314375E 02	-0.548011E 00
70.	0.269763E 02	-0.185107E 00
80.	0.230016E 02	0.159699E 00
90.	0.195284E 02	0.488168E 00
100.	0.165320E 02	0.802060E 00
110.	0.139676E 02	0.110271E 01
120.	0.117885E 02	0.139162E 01
130.	0.994004E 01	-0.147167E 01
140.	0.837901E 01	-0.120301E 01
150.	0.705877E 01	-0.942842E 00
160.	0.594516E 01	-0.691148E 00
170.	0.500749E 01	-0.446332E 00
180.	0.421359E 01	-0.203744E 00
190.	0.354624E 01	0.214168E-01
200.	0.293303E 01	0.244629E 00
210.	0.252534E 01	0.462391E 00
220.	0.213720E 01	0.679657E 00
230.	0.180753E 01	0.894609E 00
240.	0.152640E 01	0.110906E 01
250.	0.128280E 01	0.132152E 01
260.	0.107538E 01	0.153003E 01
270.	0.897415E 00	-0.140362E 01
280.	0.743030E 00	-0.120174E 01
290.	0.612852E 00	-0.100924E 01
300.	0.506404E 00	-0.827912E 00
310.	0.421779E 00	-0.649186E 00
320.	0.352031E 00	-0.470981E 00
330.	0.296195E 00	-0.287025E 00
340.	0.248919E 00	-0.839447E-01
350.	0.202833E 00	0.137280E 00

HEAVY WATER-ONE FUEL ROD

Z = 50. CMS AXIAL POSITION

FREQ(CPS)	AMPLITUDE	PHASE(RADIANS)
0.	0.210294E 03	0.000000E 00
10.	0.207528E 03	0.329788E 00
20.	0.199727E 03	0.653143E 00
30.	0.188175E 03	0.965078E 00
40.	0.174396E 03	0.126314E 01
50.	0.159662E 03	0.154668E 01
60.	0.144930E 03	-0.132527E 01
70.	0.130743E 03	-0.106817E 01
80.	0.117410E 03	-0.822559E 00
90.	0.105034E 03	-0.586925F 00
100.	0.937802E 02	-0.360461E 00
110.	0.835136E 02	-0.142274E 00
120.	0.742154E 02	0.682784E-01
130.	0.658604E 02	0.271654E 00
140.	0.583813E 02	0.463826E 00
150.	0.516928E 02	0.659834E 00
160.	0.457371E 02	0.845734E 00
170.	0.404229E 02	0.102698E 01
180.	0.356761E 02	0.120390E 01
190.	0.314372E 02	0.137622E 01
200.	0.276633E 02	0.154385E 01
210.	0.243321E 02	-0.143466E 01
220.	0.213820E 02	-0.127461E 01
230.	0.187673E 02	-0.111855E 01
240.	0.164564E 02	-0.964521E 00
250.	0.143779E 02	-0.814495E 00
260.	0.125616E 02	-0.660060E 00
270.	0.109594E 02	-0.526073E 00
280.	0.955173E 01	-0.385101E 00
290.	0.828188E 01	-0.246320E 00
300.	0.718113E 01	-0.115467E 00
310.	0.621699E 01	0.167236E-01
320.	0.535539E 01	0.142795E 00
330.	0.461482E 01	0.265057E 00
340.	0.397064E 01	0.382011E 00
350.	0.342236E 01	0.500465E 00

HEAVY WATER--ONE FUEL ROD

Z = 55. CMS AXIAL POSITION

FREQ(CPS)	AMPLITUDE	PHASE(RADIANS)
0.	0.176123E 03	0.000000E 00
10.	0.173650E 03	0.348163E 00
20.	0.166643E 03	0.689599E 00
30.	0.156278E 03	0.101866E 01
40.	0.143989E 03	0.133271E 01
50.	0.130930E 03	-0.151046E 01
60.	0.117960E 03	-0.122721E 01
70.	0.105584E 03	-0.957719E 00
80.	0.940776E 02	-0.700690E 00
90.	0.835560E 02	-0.454359E 00
100.	0.740009E 02	-0.217693E 00
110.	0.654003E 02	0.101936E-01
120.	0.577068E 02	0.230425E 00
130.	0.503315E 02	0.443309E 00
140.	0.447122E 02	0.649774E 00
150.	0.392822E 02	0.849810E 00
160.	0.344836E 02	0.104471E 01
170.	0.302275E 02	0.123464E 01
180.	0.264693E 02	0.141976E 01
190.	0.231256E 02	-0.154090E 01
200.	0.201823E 02	-0.136590E 01
210.	0.176019E 02	-0.119440E 01
220.	0.153256E 02	-0.102814E 01
230.	0.133546E 02	-0.865671E 00
240.	0.116226E 02	-0.705625E 00
250.	0.100983E 02	-0.543401E 00
260.	0.875374E 01	-0.395098E 00
270.	0.760166E 01	-0.247294E 00
280.	0.659130E 01	-0.393772E-01
290.	0.572342E 01	0.443227E-01
300.	0.496940E 01	0.191857E 00
310.	0.429173E 01	0.341043E 00
320.	0.367940E 01	0.489396E 00
330.	0.313815E 01	0.633517E 00
340.	0.266154E 01	0.775927E 00
350.	0.224260E 01	0.913330E 00

HEAVY WATER-ONE FUEL ROD

Z = 60. CMS AXIAL POSITION

FREQ(CPS)	AMPLITUDE	PHASE(RADIANS)
0.	0.146374E 03	0.000000E 00
10.	0.144165E 03	0.367907E 00
20.	0.137981E 03	0.728379E 00
30.	0.128878E 03	0.107594E 01
40.	0.118086E 03	0.140748E 01
50.	0.106693E 03	-0.141952E 01
60.	0.954437E 02	-0.112117E 01
70.	0.847998E 02	-0.837884E 00
80.	0.749858E 02	-0.563002E 00
90.	0.660865E 02	-0.310074E 00
100.	0.581121E 02	-0.625468E-01
110.	0.509924E 02	0.175876E 00
120.	0.446719E 02	0.405372E 00
130.	0.390710E 02	0.623480E 00
140.	0.341210E 02	0.843692E 00
150.	0.297752E 02	0.105253E 01
160.	0.259472E 02	0.125575E 01
170.	0.225777E 02	0.145330E 01
180.	0.196221E 02	-0.140654E 01
190.	0.170431E 02	-0.130963E 01
200.	0.147779E 02	-0.112759E 01
210.	0.128138E 02	-0.950871E 00
220.	0.111013E 02	-0.777296E 00
230.	0.961083E 01	-0.603560E 00
240.	0.831860E 01	-0.441681E 00
250.	0.718039E 01	-0.279546E 00
260.	0.621502E 01	-0.120307E 00
270.	0.536257E 01	0.399536E-01
280.	0.461741E 01	0.195610E 00
290.	0.397693E 01	0.350621E 00
300.	0.342449E 01	0.506518E 00
310.	0.293166E 01	0.669156E 00
320.	0.247711E 01	0.323590E 00
330.	0.208316E 01	0.983026E 00
340.	0.173589E 01	0.113315E 01
350.	0.144232E 01	0.127171E 01

HEAVY WATER-ONE FUEL ROD

Z = 65. CMS AXIAL POSITION

FREQ(CPS)	AMPLITUDE	PHASE(RADIANS)
0.	0.117520E 03	0.000000E 00
10.	0.115648E 03	0.388979E 00
20.	0.110427E 03	0.770023E 00
30.	0.102767E 03	0.113741E 01
40.	0.937297E 02	0.148767E 01
50.	0.842464E 02	-0.132164E 01
60.	0.749378E 02	-0.100665E 01
70.	0.661804E 02	-0.707799E 00
80.	0.581679E 02	-0.423405E 00
90.	0.509578E 02	-0.151815E 00
100.	0.445375E 02	0.108424E 00
110.	0.388603E 02	0.358500E 00
120.	0.338650E 02	0.590584E 00
130.	0.294773E 02	0.832646E 00
140.	0.256277E 02	0.105826E 01
150.	0.222616E 02	0.127686E 01
160.	0.193173E 02	0.148956E 01
170.	0.167347E 02	-0.144560E 01
180.	0.144836E 02	-0.124526E 01
190.	0.125204E 02	-0.105119E 01
200.	0.108297E 02	-0.863063E 00
210.	0.937138E 01	-0.673924E 00
220.	0.810917E 01	-0.497766E 00
230.	0.700415E 01	-0.313777E 00
240.	0.603452E 01	-0.142161E 00
250.	0.516766E 01	0.305983E-01
260.	0.442166E 01	0.194212E 00
270.	0.378505E 01	0.357697E 00
280.	0.321976E 01	0.515667E 00
290.	0.273707E 01	0.670484E 00
300.	0.230182E 01	0.817938E 00
310.	0.194348E 01	0.950405E 00
320.	0.163995E 01	0.107906E 01
330.	0.139686E 01	0.113342E 01
340.	0.121813E 01	0.131100F 01
350.	0.105133E 01	0.144797E 01

HEAVY WATER-ONE FUEL ROD

Z = 70. CMS AXIAL POSITION

FREQ(CPS)	AMPLITUDE	PHASE(RADIANS)
0.	0.989173E 02	0.000000E 00
10.	0.972562E 02	0.407242E 00
20.	0.926077E 02	0.806277E 00
30.	0.857998E 02	0.119086E 01
40.	0.778036E 02	0.155736E 01
50.	0.694506E 02	-0.123671E 01
60.	0.613063E 02	-0.907707E 00
70.	0.537035E 02	-0.595735E 00
80.	0.468050E 02	-0.298978E 00
90.	0.406386E 02	-0.158363E-01
100.	0.351924E 02	0.255221E 00
110.	0.304167E 02	0.515486E 00
120.	0.262508E 02	0.765955E 00
130.	0.226307E 02	0.100797E 01
140.	0.194776E 02	0.124205E 01
150.	0.167471E 02	0.146844E 01
160.	0.143735E 02	-0.145390E 01
170.	0.123476E 02	-0.124247E 01
180.	0.106104E 02	-0.103523E 01
190.	0.909923E 01	-0.832850E 00
200.	0.779551E 01	-0.635099E 00
210.	0.666195E 01	-0.442543E 00
220.	0.569325E 01	-0.254790E 00
230.	0.484521E 01	-0.700490E-01
240.	0.411175E 01	0.106941E 00
250.	0.348390E 01	0.277263E 00
260.	0.295708E 01	0.439198E 00
270.	0.251451E 01	0.599040E 00
280.	0.213706E 01	0.752515E 00
290.	0.182494E 01	0.905418E 00
300.	0.154741E 01	0.105818E 01
310.	0.131233E 01	0.119634E 01
320.	0.112930E 01	0.133314E 01
330.	0.974937E 00	0.147499E 01
340.	0.853550E 00	-0.151556E 01
350.	0.737710E 00	-0.133359E 01

HEAVY WATER-ONE FUEL ROD

Z = 75. CMS AXIAL POSITION

FREQ(CPS)	AMPLITUDE	PHASE(RADIANS)
0.	0.820441E 02	0.000000E 00
10.	0.806118E 02	0.425185E 00
20.	0.765943E 02	0.842028E 00
30.	0.707103E 02	0.124378E 01
40.	0.633256E 02	-0.151474E 01
50.	0.566463E 02	-0.115151E 01
60.	0.496807E 02	-0.807876E 00
70.	0.432239E 02	-0.482102E 00
80.	0.373900E 02	-0.172515E 00
90.	0.322265E 02	0.122492E 00
100.	0.277033E 02	0.405058E 00
110.	0.237606E 02	0.676320E 00
120.	0.203443E 02	0.937229E 00
130.	0.173950E 02	0.118382E 01
140.	0.148532E 02	0.143176E 01
150.	0.126639E 02	-0.147520E 01
160.	0.107937E 02	-0.124846E 01
170.	0.920699E 01	-0.102894E 01
180.	0.785106E 01	-0.814663E 00
190.	0.663751E 01	-0.605344E 00
200.	0.568723E 01	-0.400726E 00
210.	0.482502E 01	-0.201890E 00
220.	0.408763E 01	-0.923081E-02
230.	0.346150E 01	0.176200E 00
240.	0.293757E 01	0.357092E 00
250.	0.249547E 01	0.534927E 00
260.	0.211685E 01	0.712695E 00
270.	0.173498E 01	0.886961E 00
280.	0.150774E 01	0.105721E 01
290.	0.125739E 01	0.122650E 01
300.	0.105066E 01	0.137473E 01
310.	0.883812E 00	0.152541E 01
320.	0.745724E 00	-0.147659E 01
330.	0.633670E 00	-0.132416E 01
340.	0.534991E 00	-0.118094E 01
350.	0.455317E 00	-0.101630E 01

HEAVY WATER-ONE FUEL ROD

Z = 80. CMS AXIAL POSITION

FREQ(CPS)	AMPLITUDE	PHASE(RADIANS)
0.	0.677836E 02	0.000000E 00
10.	0.665593E 02	0.444392E 00
20.	0.631157E 02	0.880243E 00
30.	0.580784E 02	0.130056E 01
40.	0.521884E 02	-0.144017E 01
50.	0.460745E 02	-0.106015E 01
60.	0.401696E 02	-0.700509E 00
70.	0.347170E 02	-0.359893E 00
80.	0.293315E 02	-0.365220E-01
90.	0.255322E 02	0.271527E 00
100.	0.217905E 02	0.565960E 00
110.	0.185586E 02	0.847843E 00
120.	0.157887E 02	0.111850E 01
130.	0.134179E 02	0.137399E 01
140.	0.114013E 02	-0.151170E 01
150.	0.968870E 01	-0.126914E 01
160.	0.824146E 01	-0.103367E 01
170.	0.700139E 01	-0.803113E 00
180.	0.594116E 01	-0.580756E 00
190.	0.504773E 01	-0.362635E 00
200.	0.427366E 01	-0.150117E 00
210.	0.362053E 01	0.557071E-01
220.	0.306131E 01	0.256081E 00
230.	0.259400E 01	0.450272E 00
240.	0.219242E 01	0.641409E 00
250.	0.185763E 01	0.824423E 00
260.	0.157258E 01	0.100817E 01
270.	0.133052E 01	0.118205E 01
280.	0.113077E 01	0.135897E 01
290.	0.952901E 00	0.153178E 01
300.	0.801911E 00	-0.144444E 01
310.	0.676259E 00	-0.129336E 01
320.	0.577500E 00	-0.113017E 01
330.	0.488234E 00	-0.993791E 00
340.	0.424673E 00	-0.864031E 00
350.	0.377937E 00	-0.709412E 00

HEAVY WATER-ONE FUEL ROD

Z = 85. CMS AXIAL POSITION

FREQ(CPS)	AMPLITUDE	PHASE(RADIANS)
0.	0.560590E 02	0.000000E 00
10.	0.550024E 02	0.461676E 00
20.	0.520537E 02	0.914350E 00
30.	0.477564E 02	0.135110E 01
40.	0.427444E 02	-0.137367E 01
50.	0.375543E 02	-0.978166E 00
60.	0.325524E 02	-0.603752E 00
70.	0.279568E 02	-0.249117E 00
80.	0.233516E 02	0.876407E-01
90.	0.202574E 02	0.407696E 00
100.	0.171643E 02	0.713204E 00
110.	0.145120E 02	0.100590E 01
120.	0.122575E 02	0.123657E 01
130.	0.103474E 02	0.155734E 01
140.	0.872547E 01	-0.132274E 01
150.	0.735045E 01	-0.106983E 01
160.	0.618387E 01	-0.825840E 00
170.	0.520348E 01	-0.591030E 00
180.	0.438651E 01	-0.363976E 00
190.	0.370426E 01	-0.141777E 00
200.	0.312598E 01	0.757833E-01
210.	0.263876E 01	0.283070E 00
220.	0.222696E 01	0.496999E 00
230.	0.187543E 01	0.701503E 00
240.	0.158147E 01	0.899952E 00
250.	0.133623E 01	0.110122E 01
260.	0.111615E 01	0.130267E 01
270.	0.928116E 00	0.149395E 01
280.	0.767007E 00	-0.146015E 01
290.	0.631610E 00	-0.123990E 01
300.	0.525677E 00	-0.112299E 01
310.	0.435208E 00	-0.955496E 00
320.	0.361311E 00	-0.793715E 00
330.	0.299702E 00	-0.618755E 00
340.	0.240496E 00	-0.433855E 00
350.	0.185072E 00	-0.279607E 00

APPENDIX F

NUMERICAL CONSTANTS

The natural uranium fuel element used in this experiment has been described in detail by Dunlap (6). The fuel rod consisted of six cylindrical slugs contained in an aluminum tube. Numerical values used for other constants were as follows.[1]

Thermal Diffusion Constant (D_{th})................ 0.8154 cm

Diffusion Length Squared (L^2_{th})

     99.0% Heavy Water......................... 3738 cm^2

     99.5% Heavy Water......................... 6751 cm^2

Thermal Velocity (v_{th})......................... 2.47×10^5 cm/sec

Age to Thermal (τ_{th})

     99.0% Heavy Water......................... 118.8 cm^2

     99.5% Heavy Water......................... 119.4 cm^2

Slowing Down Time (L_s)......................... 5.08×10^{-5} sec

Resonance Escape Probability (p)................. .999

Fast Fission Factor (η)......................... 2.07

Fundamental Buckling (B_1^2)...................... 1.263×10^{-3} cm^2

First Order Buckling (B_2^2)...................... 6.642×10^{-3} cm^2

Extrapolated Radius of System (R_{TOT})............ 67.67 cm

Radius of Fuel Rod (r_o)......................... 1.27 cm

---

1. Heavy water parameters were obtained from N. J. Diaz by private communication.

BIBLIOGRAPHY

(1) R. B. Perez and R. E. Uhrig, "Propagation of Neutron Waves in
     Moderating Media," Nuclear Science and Engineering, 17,
     90-100 (1963).

(2) R. S. Booth, "A Theoretical and Experimental Study of Neutron
     Wave Propagation in Moderating Media," Ph.D Dissertation,
     University of Florida (1965).

(3) R. S. Denning, "The Propagation of Neutrons Through A Dis-
     continuity," Master's Thesis, University of Florida (1965).

(4) R. S. Booth and R. B. Perez, "Propagation of Thermal-Neutron
     Waves in Heterogeneous Media," Neutron Noise, Waves and
     Pulse Propagation, USAEC Symposium Series 9, 49-54 (1967).

(5) J. H. Dunlap and R. B. Perez, "Dispersion Law for a Natural-
     Uranium Heavy-Water Subcritical Assembly," Neutron Noise,
     Waves and Pulse Propagation, USAEC Symposium Series 9,
     135-159 (1967).

(6) J. H. Dunlap, "Neutron Wave Propagation In a Heavy Water,
     Natural Uranium, Subcritical Assembly," Ph.D. Dissertation,
     University of Florida (1967).

(7) Q. B. DuBois, "Thermal Neutron Pulse Propagation in a Reflected
     Subcritical Assembly," Master's Thesis, University of
     Florida (1967).

(8) C. Kang, "A Calculational Method For The Space and Energy-
     Dependent Reactor Transfer Function," Master's Thesis,
     University of Florida (1967).

(9) Proceedings of a Symposium, Karlsruhe, 10-14 May 1965,
     "Pulsed Neutron Research," Vol.II, International Atomic
     Energy Agency, Vienna (1965).

(10) "Neutron Noise, Waves and Pulse Propagation," USAEC Symposium
     Series 9, Gainesville, Florida (1967).

(11) Transactions, American Nuclear Society 10. 1, 277-281 (1967).

BIBLIOGRAPHY (continued)

(12) Proceedings of a Symposium, Ann Arbor, Michigan, 17-21, July 1967, "Neutron Thermalization and Reactor Spectra," International Atomic Energy Agency, To be published.

(13) V. R. Cain, "Propagation of Neutron Waves Through Heterogeneous Physics," Consiglio Nazionale Delle Ricerche, Rome, Italy, (1965).

(15) A. D. Galanin, "Thermal Reactor Theory," Pergamon, New York (1960).

(16) R. S. Booth, R. B. Perez and R. G. Hartley, "On the Application of the Neutron-Wave Technique to Thermal-Neutron Systems," Nuclear Science and Engineering, 28, 404-414 (1967).

(17) K. H. Beckurts and K. Wirtz, "Neutron Physics," Springer-Verlag-New York, Inc., (1964).

(18) W. S. Brey, Department of Chemistry, University of Florida, Private Communication.

(19) R. B. Perez, M. J. Ohanian and J. H. Dunlap, "Propagation of Thermal Neutron Waves in Heavy Water," Symposium on Neutron Thermalization and Reactor Spectra sponsored by International Atomic Energy Agency, Ann Arbor, Michigan, (1967).

(20) R. G. Cockrell, "A Description of the UFNLLS, University of Florida Non-Linear Least Squares Code," Internal Report, Nuclear Engineering Department, University of Florida, August, 1965.

(21) EIG4, A Computer Program for Obtaining the Complex Eigenvalues of a Complex Matrix, received from N. J. Diaz, Department of Nuclear Engineering Sciences, University of Florida.
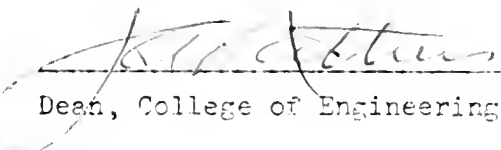
BIOGRAPHICAL SKETCH

Emile Anthony Bernard was born in Brunswick, Georgia, on June 18, 1936. After spending most of his childhood in Waynesville, Georgia, he was graduated from Glynn Academy High School in Brunswick in June 1954. In June 1958 he received a Bachelor of Science Degree with major in Physics from the University of Notre Dame. After graduation he was commissioned a Second Lieutenant in the U. S. Marine Corps Reserve and served two years on active duty and since then has attained the rank of Captain. He then attended the Georgia Institute of Technology from September 1960 to September 1962 and received a Master of Science Degree with major in Nuclear Science (Physics) from there in June 1963. He was employed by the U. S. Atomic Energy Commission from September 1962 until September 1964 at which time he began his PhD studies at the University of Florida. While there he was a graduate assistant in the Department of Nuclear Engineering Sciences and was awarded a U. S. Atomic Energy Commission Traineeship.

Emile Anthony Bernard is married to the former Elizabeth Louise Pastore and is the father of one daughter. He is a member of the American Nuclear Society.

This dissertation was prepared under the direction of the chairman of the candidate's supervisory committee and has been approved by all members of that committee. It was submitted to the Dean of the College of Engineering and to the Graduate Council, and was approved as partial fulfillment of the requirements for the degree of Doctor of Philosophy.
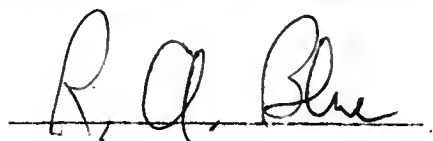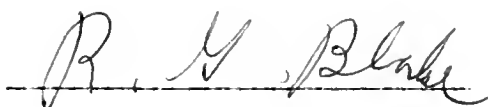
March 1968

_____
Dean, College of Engineering

_____
Dean, Graduate School

Supervisory Committee:

_____
Chairman

_____

_____

_____

_____